NASA CONTRACTOR REPORT

NASA CR-141

NASA CR-1418

GROUND WIND CHARACTERISTICS AT KENNEDY SPACE CENTER

by G. E. McVehil and H. G. Camnitz

Prepared by
CORNELL AERONAUTICAL LABORATORY, INC.
Buffalo, N. Y.
for George C. Marshall Space Flight Center

NATIONAL AERONAUTICS AND SPACE ADMINISTRATION • WASHINGTON, D. C. • SEPTEMBER 1969

NASA CR-1418

GROUND WIND CHARACTERISTICS AT KENNEDY SPACE CENTER

By G. E. McVehil and H. G. Camnitz

Prepared under Contract No. NAS 8-21178 by
CORNELL AERONAUTICAL LABORATORY, INC.
Buffalo, N.Y.

for George C. Marshall Space Flight Center

NATIONAL AERONAUTICS AND SPACE ADMINISTRATION

For sale by the Clearinghouse for Federal Scientific and Technical Information
Springfield, Virginia 22151 – CFSTI price $3.00

ABSTRACT

Wind data from a 150-meter tower at Kennedy Space Center have been analyzed to provide statistical information on mean wind speed, maximum wind speed, gust factor and surface friction velocity. The data have also been utilized for analysis of spectra of the lateral component and for study of gust intensity, duration and acceleration.

Frequency distributions, derived from one year of hourly observations, are presented for mean wind speed, 10-minute and one-hour maximum wind speed, and gust factor for each of six observation heights. Annual statistics are also derived for surface friction velocity u_*, and the exponent in a power-law representation of mean wind profiles. Conditional frequency distributions for each variable, computed for restricted classes of wind direction, wind speed, and stability, are interpreted in terms of the physical relationships between wind parameters.

Lateral turbulence spectra and gust characteristics have been investigated from detailed (10 point per second) wind data. Analysis of lateral spectra show that the low-frequency (F = 0.01 to 0.4) portion is highly sensitive to stability. The spectral intensity decreases with height in neutral stability but is nearly constant with height under unstable conditions. Model spectra are presented which give the lateral spectrum as a function of height for neutral and unstable stratification.

Frequency distributions for gust factor, gust duration and gust acceleration are presented and analyzed. The mean gust factor is proportional to the logarithm of sampling time for times between 3 and 400 seconds. When gust factor is scaled by the mean and variance of wind speed, and sampling time is scaled by turbulence time scale, general relations of the form gust factor = a + b log (ct) where t is sampling time, are shown to apply to the mean and limits of gust factor distributions.

Gust duration distributions are all of similar form after scaling for mean wind, wind variance and time scale. These distributions can be used to calculate the probability of gusts exceeding given wind speeds and durations. Average rate of change of wind speed in gusts is derived from conditional frequency distributions for various initial wind speeds and averaging times. These acceleration distributions can be represented by an empirically modified multivariate Gaussian mathematical model.

ACKNOWLEDGMENT

The authors are indebted to Dr. George H. Fichtl of Marshall Space Flight Center for many valuable discussions during the course of this research. We are also grateful for the opportunities we had to discuss various aspects of the work with Professor Hans Panofsky of Penn State University.

A number of CAL personnel contributed to the performance of the research reported here through data processing, analysis, and preparation of final results. Mr. W.G. Brady provided the summary of vehicle design problems that is included in Appendix A. Applied Physics Department personnel who deserve particular recognition for their contributions include Mr. C.W.C. Rogers, Mr. G.A. Zigrossi, and Mr. R.A. Brown.

TABLE OF CONTENTS

TABLE OF CONTENTS

LIST OF FIGURES

LIST OF FIGURES (Cont.)

LIST OF FIGURES (Cont.)

LIST OF TABLES

I. INTRODUCTION

The objective of this study has been to derive quantitative information on wind and turbulence that will be applicable to the design and operation of launch vehicles. Attention is restricted to the "ground-wind" regime, i.e., winds from the earth's surface to a height of approximately 150 m above the ground. The wind field in this lower layer imposes structural requirements on the launch vehicle, and on the support facilities used to maintain the vehicle before launch. Ground-wind loads must be considered in designing the vehicle and support structure to insure against structural failure before or during launch, and in planning vehicle operations, including launch. A survey of wind effects on vehicles and techniques of utilizing wind inputs in design is presented in Appendix A of this report.

Detailed wind data are collected continuously by NASA from a 150 m meteorological tower on Merritt Island at Cape Kennedy. The tower, instrumentation, and data formats have been described in NASA reports (1, 2). Data from this installation have been used for the present study. Specific wind characteristics which have been investigated include: mean wind speed, peak wind speed, gust factor, gust duration and frequency, turbulence spectra, and correlation between winds at different heights. Tower data supplied by NASA were available in two forms - records of wind speed and direction at 0.1 sec intervals for continuous periods of 30 minutes to over an hour, and hourly values of specific variables (for example, 10 min mean wind, peak gust speed) for all hours of all days. The detailed records were utilized for spectrum analysis and investigation of gust characteristics; hourly data were processed to provide seasonal and annual statistics on mean wind, gust factor, and maximum wind speeds.

The objective throughout this work has been to provide data that will be of maximum use to vehicle designers and engineers. Frequent consultations

were held with Marshall Space Flight Center (MSFC) personnel in order to determine current needs of design engineers in regard to wind inputs, and to insure coordination with MSFC and other contractor studies of wind characteristics. Thus, the emphasis in analysis has been placed on specific wind parameters that currently seem most relevant or that tie in most directly with complementary analyses performed elsewhere for Marshall Space Flight Center.

Attention has been divided evenly between computation of wind statistics that have a direct bearing on design procedures, and analysis directed toward understanding the physical relationships that determine wind structure. Since wind characteristics at any single location such as Cape Kennedy are highly variable in time, it is not always practical to specify one set of parameters that will define the wind environment for design and operational purposes. It is more appropriate to define the relationships between the parameters of direct interest and more conventionally observed meteorological variables, such as mean wind speed and direction or atmospheric stability. Given such relationships, the particular wind characteristics of concern can be specified for a variety of forecast or observed meteorological situations. Thus, while many of the results to be presented in this report are in the form of frequency distributions of observed quantities, an attempt has also been made to generalize these results on the basis of theory or empirical evidence.

Knowledge of the underlying relationships among the various wind and meteorological parameters is particularly valuable because the quantitative results given herein are necessarily preliminary, or first estimates, in many cases. Only one year of tower data were available for analysis, and since any one year is not necessarily typical, climatological inferences from the results must be drawn with caution. The detailed analysis of gust characteristics required extensive data processing and hand analysis, and only a limited number of samples could be treated. Thus, those results represent examples rather than final design models. It is believed that the reported analytical work relating to these results will be useful in extrapolating conclusions to other situations.

The results of these studies are presented in the following chapters, and can be considered to fall into three general subject areas. The first area, reported in Chapter II, includes all statistical results derived from the one year of hourly data. Frequency distributions of various wind parameters are given for the year, and in separate categories of season, stability, wind direction, and mean wind speed. In Chapter III, an analysis of the spectrum of the lateral turbulence component is given. Variations of the turbulence spectrum with stability and height were investigated, and design spectra for neutral and unstable conditions are presented. The third subject area, which is covered in Chapter IV, includes wind properties such as short-period gust factors, gust frequency, wind acceleration in gusts, and correlation between gusts at different heights. These detailed characteristics of wind structure were all analyzed from time-history wind records for individual one-half to one hour periods. Finally, Chapter V of the report briefly summarizes the primary results and conclusions of the entire study.

II. STATISTICS FOR ONE YEAR OF HOURLY WIND DATA

A. Data Processing, Definition of Variables, and Classification of Cases

Wind and temperature from seven heights on the Merritt Island tower are continuously recorded on strip charts. Certain variables are read from the charts for each hour of every day, put on punch cards, and eventually recorded on magnetic tape. One year of these taped data has been used to derive statistics on the wind environment at Kennedy Space Center. The data available for analysis covered the period from December 1965 through November 1966.

The following hourly data, recorded on magnetic tape, were utilized in the analysis:

Mean wind speed for a 10 min period at each height (3, 18, 30, 60, 90, 120, and 150 m),

Mean wind direction for the same period and heights,

Maximum wind speed measured during the 10 min period at each height,

Maximum wind speed measured during the hour at each height,

Temperature difference between the 3m level and the following heights: 18, 60, 120, and 150 m,

Temperature at 3 m height.

It was desired to investigate the following quantities, either given directly or obtainable from the tower data:

Mean wind speed for 10 min period,

Maximum wind speed for 10 min period,

Maximum wind speed for one hour period,

Gust factor (= maximum wind speed/mean wind speed) for 10 min period,

Exponent p in a power-law expression for the 10 min mean wind speed profile ($u_1/u_2 = [z_1/z_2]^p$),

Friction velocity $u_* = (\tau/\rho)^{1/2}$, where τ = surface shearing stress and ρ = density.

In order to classify the observations according to mean (steady-state) meteorological conditions, the following parameters were also required for each hour:

Mean wind direction for 10 min period,

Mean wind speed at 18 m height for 10 min period,

Richardson number = $g/\theta \cdot \frac{\partial\theta}{\partial z} \Big/ \left(\frac{\partial V}{\partial z}\right)^2$, where θ is potential temperature, g is acceleration of gravity, z is height and V is wind speed.

One further classifying parameter was season of the year. For purposes of this analysis, the seasons were defined as winter: Dec to Feb, spring: March to May, summer: June to Aug, and fall: Sept. to Nov.

A computer program was written to compute all desired quantities from the basic data, sort and classify the hourly values, and compute frequency distributions for the variables of interest. The Richardson number was calculated from the equation

$$R_i = \frac{9.8}{T_3} \quad \frac{T_{120} - T_{18} + 1.0}{(V_{120} - V_{18})^2} \quad (102) \qquad (2.1)$$

The subscripts refer to heights in meters. All units in the computations and elswhere in this report are (meters) for height, (meters sec^{-1}) for wind speed, and (degrees Kelvin) for temperature.

Power-law exponents were calculated to fit a power-law profile equation to winds at two pairs of heights. The equations used were

$$P_{60} = (\ln V_{60} - \ln V_{18}) / (\ln 60 - \ln 18)$$
$$P_{120} = (\ln V_{120} - \ln V_{18}) / (\ln 120 - \ln 18) \qquad (2.2)$$

Computation of friction velocity was less straightforward and is explained in detail in Section II E.

The computer program involved reading the taped data for a single hour, converting to proper units, calculating the desired quantities, and then assigning each calculated value to appropriate classification cells. The total number of entries in each cell was tabulated in storage as each new hour of values was processed. After reading each season, and the full year, the totals were read out and means and variances were computed for each distribution.

Table 2.1 lists the frequency distributions that were calculated. A separate distribution was obtained for each variable for each season, and for the entire year. The third column indicates the classifying variables used for conditional distributions; R denotes Richardson number (5 classes), D wind direction (2 classes) and F the 18 m mean wind speed (3 classes). Class limits are shown in Table 2.2. Wind directions were classified to distinguish between sectors with appreciably different roughness as deduced by Fichtl (3).

Table 2.1

Frequency Distributions Computed from KSC Hourly Wind Data

Variable	Heights for which Distributions were obtained	Classifying Variables	Total number of Distributions
10 min mean wind	18, 30, 60, 90, 120, 150	R, D	26
10 min peak gust	18, 60, 150	F	9
one hour peak gust	18, 60, 150	F	9
10 min gust factor	18, 30, 60, 90, 120, 150	F, R, D	38
Power-law exponent	18-60, 18-120	F, R, D	38

Table 2.2

Class Limits for Classifying Variables

Variables	Limits	Description
18 m wind speed, V_{18} (F)	$0.0 \leq V_{18} < 5.0$	F = 1 light
	$5.0 \leq V_{18} < 10.0$	F = 2 moderate
	$10.0 \leq V_{18}$	F = 3 strong
Richardson no., Ri (R)	$Ri \leq -0.15$	R = 1 very unstable
	$-0.15 < Ri \leq -0.05$	R = 2 unstable
	$-0.05 < Ri \leq +0.05$	R = 3 neutral
	$0.05 < Ri \leq 0.15$	R = 4 stable
	$0.15 < Ri$	R = 5 very stable
Wind direction, α (D)	$150^\circ \leq \alpha \leq 179^\circ$ $240^\circ \leq \alpha \leq 299^\circ$	D = 1 rough
	$1^\circ \leq \alpha \leq 149^\circ$ $180^\circ \leq \alpha \leq 239^\circ$ $300^\circ \leq \alpha \leq 360^\circ$	D = 2 smooth

It will frequently be of interest in the discussions to follow to know the relative frequency of occurrence of the various classes of R, D, and F. The observed frequency distributions for these parameters are shown in Figure 2.1. In the next sections, we proceed to discuss the observed distributions of mean wind speed, peak gust, and gust factor.

B. Distribution of Mean Wind Speed

The annual unconditional distributions of 10 min mean wind speed for each of the six heights are shown in Figures 2, 2a through f. Beside each histogram the mean and standard deviation of the distribution are given, along with the total number of hourly observations included. (The maximum number for one year is 8760; the actual number is always less than this due to missing observations.) The percentage of the total number of points

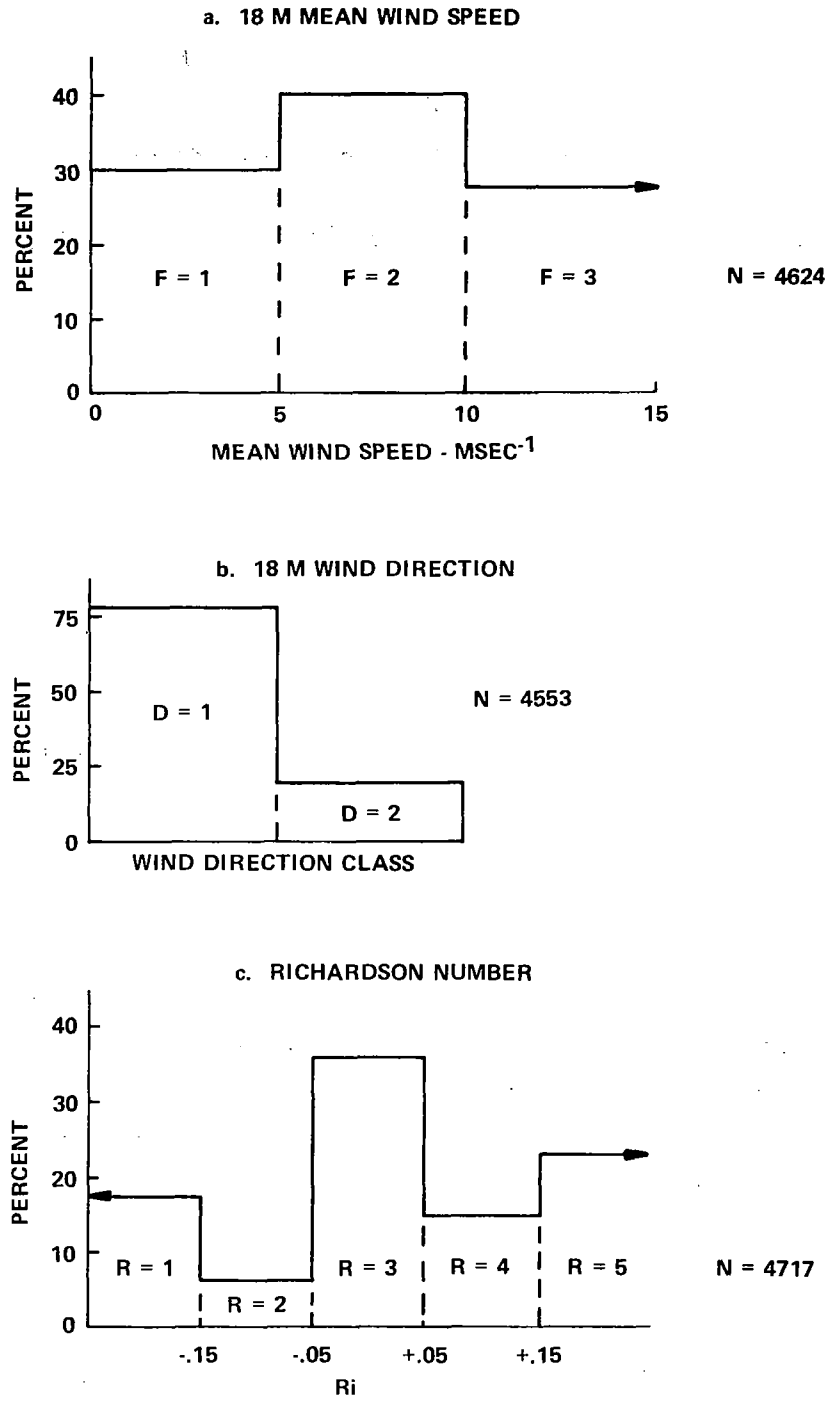

Figure 2.1 FREQUENCY DISTRIBUTIONS OF THE CLASSIFYING PARAMETERS F, D, AND R FROM ONE YEAR OF DATA

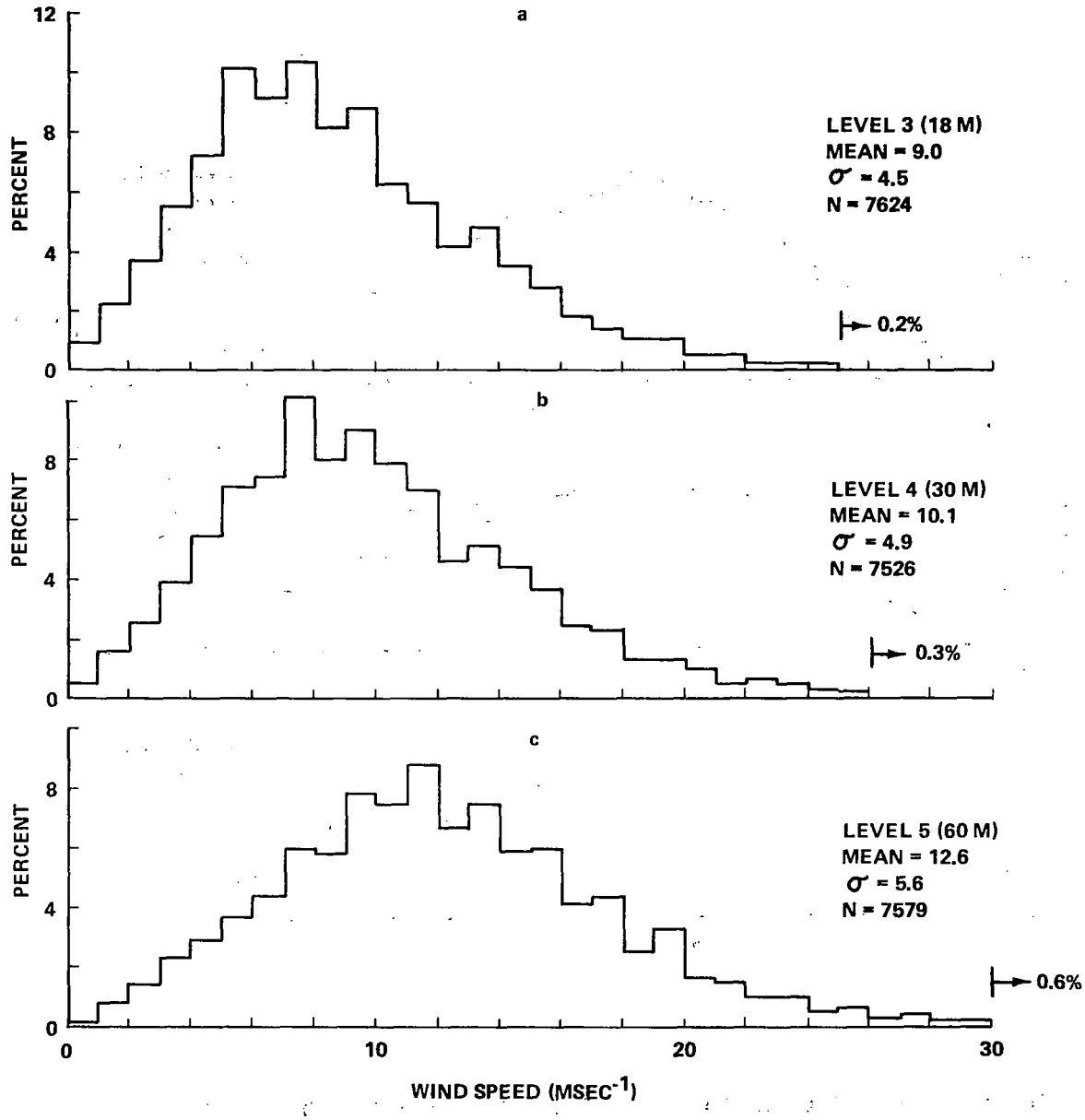

Figure 2.2 a,b,c UNCONDITIONAL FREQUENCY DISTRIBUTIONS OF 10 MIN MEAN WIND SPEED FOR 18, 30 AND 60 M

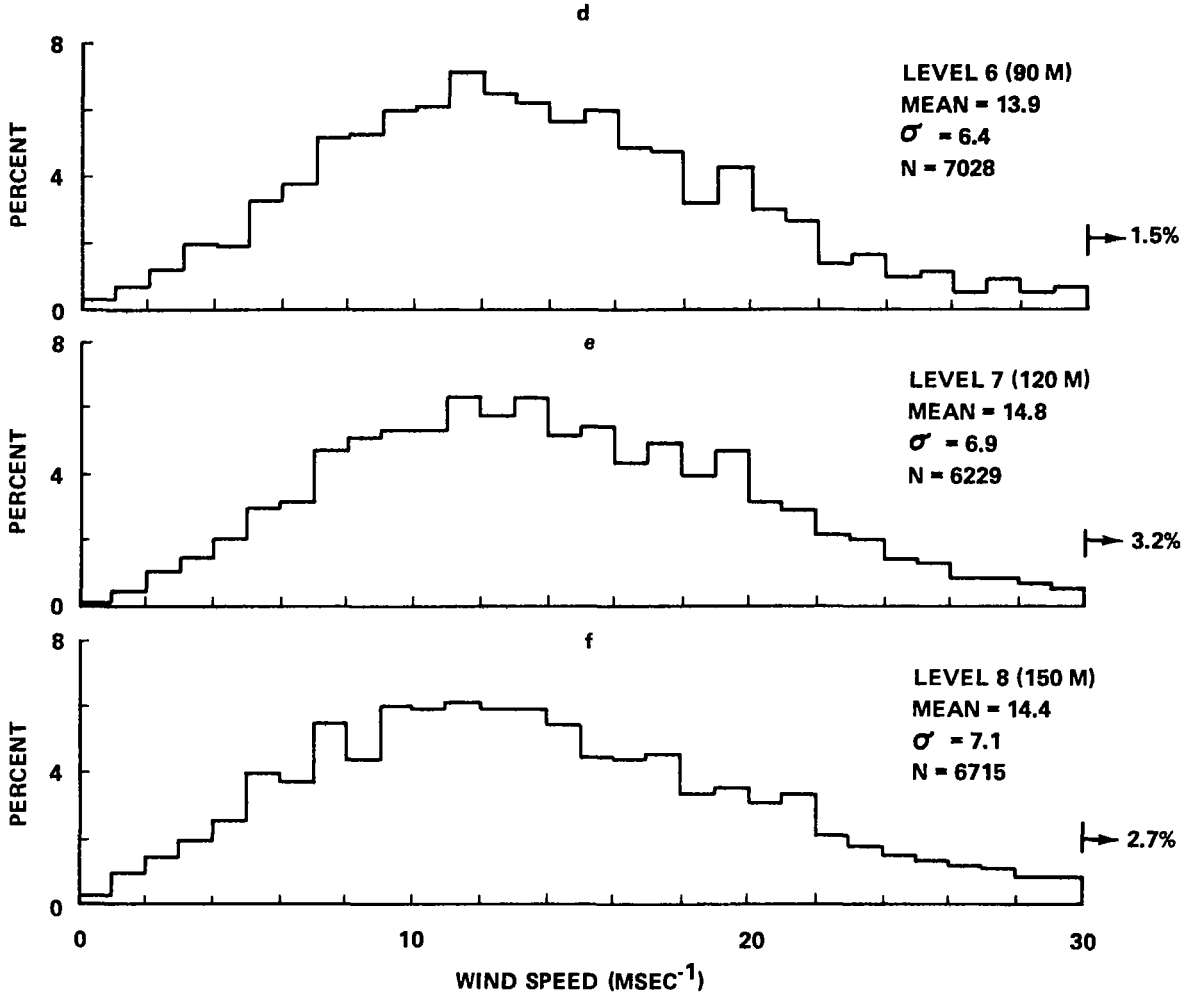

Figure 2.2 d,e,f UNCONDITIONAL FREQUENCY DISTRIBUTIONS OF 10 MIN MEAN WIND SPEED FOR 90, 120, AND 150 M

which fell outside the range of the plotted histogram is shown at the right side of each figure. As expected, both the mean and standard deviation increase with height. The 120m level mean seems high; this may be due to fewer observations than at the levels above and below. However, there are other indications that the 120m anemometer may not have functioned perfectly throughout the year.

The variation of mean wind speed with stability is shown in Figure 2.3. The means of the computed conditional distributions for 18 and 150 m height are plotted for each of the five Richardson number classes. At 18m, both neutral and unstable conditions are associated with higher wind speeds. At 150m, high wind speeds are associated with near-neutral stabilities only; the mean wind is lower for both stable and unstable conditions.

Conditional distributions were computed for the 18m level for separate joint classes of stability and wind direction. The objective was to determine whether the difference in surface roughness in different directions from the tower showed up in the mean wind speed distributions for some stabilities. However, there was no significant difference in the wind speed distributions for the two classes of wind direction.

Seasonal variations in the wind speed distributions are shown in Table 2.3. During the year analyzed, a hurricane was experienced at KSC during August, so the summer season statistics may be slightly biased relative to seasons without an unusually severe storm.

Table 2.3

Variation of 10 min Mean Wind Speed with Season

Season	Mean Wind Speed m sec^{-1}		Standard Deviation of Seasonal Distributions m sec^{-1}	
	18 m	150 m	18 m	150 m
Winter	9.9	16.7	4.9	7.5
Spring	9.9	15.0	4.4	6.2
Summer	7.6	12.1	4.2	6.1
Fall	8.5	13.1	4.1	7.0

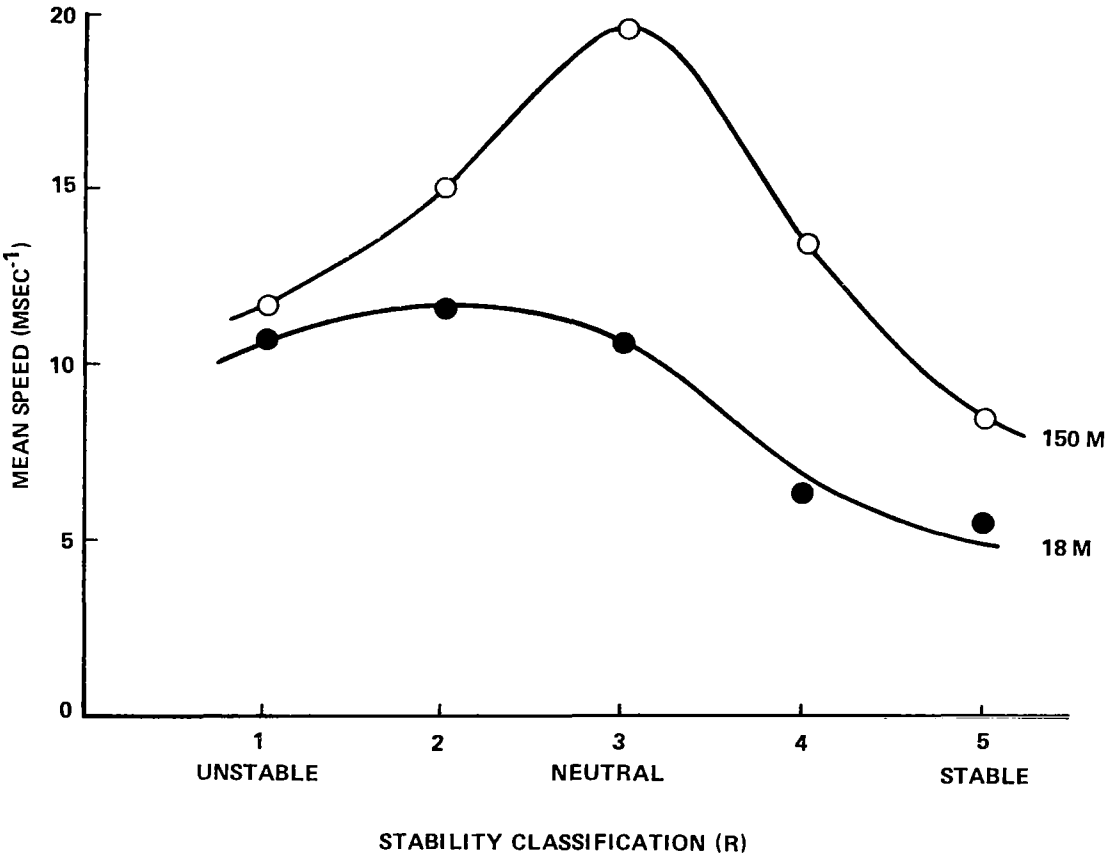

Figure 2.3 MEANS OF CONDITIONAL 10 MIN MEAN WIND SPEED DISTRIBUTIONS VERSUS STABILITY CLASSIFICATION FOR 18 AND 150 M LEVELS

As indicated in Table 2.1, distributions of power-law exponent were derived for many classifications of wind speed, wind direction, and stability. The objective was to characterize the behavior of the mean wind profile as related to steady-state meteorological variables. The computed distributions are, unfortunately, not highly instructive due to very wide scatter in the computed exponents. Most of the distributions are quite broad and contain a significant number of points in the extreme high and low cells. It would clearly be advantageous to compute the exponent by fitting a power-law expression to the entire vertical profile by least-squares, rather than by fitting exactly to winds at two heights.

Because of the scatter the actual exponent distributions are not presented here. However, the mean values of p are tabulated in Table 2.4. The results show that p decreases with increasing wind speed and with height. The exponent increases with increasing stability until the Richardson number exceeds 0.15, beyond which it decreases.

As was the case for mean wind speed, the power-law exponent does not show a significant dependence on wind direction in the joint conditional distributions for which D is a parameter.

C. Distributions of Maximum Wind Speed

Overall distributions of maximum wind speed are not likely to be as useful as distributions that are conditional on the value of mean wind speed for the relevant period. Thus, we have derived distributions of 10 min and one-hour maximum wind, conditional on the 18 m ten-minute mean wind speed. These distributions, for the 18 and 150 m levels and the three classes of 18 m mean speed, are shown in Figures 2.4 through 2.7. All distributions are for the entire year. Since the extreme maximum winds cannot be readily shown in the histograms, 99 and 99.9% values for each of the cumulative distributions are given in Table 2.5.

Table 2.4

Mean Values of Power-law Exponent
(all seasons)

	Wind Speed Class		
	F=1	F=2	F=3
	0.12	0.11	0.08
R = 1	0.09	0.07	0.06
	0.22	0.20	0.14
R = 2	0.21	0.19	0.15
	0.67	0.41	0.26
R = 3	0.62	0.38	0.26
	0.69	0.41	0.27
R = 4	0.60	0.36	0.22
	0.39	0.25	0.17
R = 5	0.33	0.18	0.11

upper number - p from 18 and 60 m data
lower number - p from 18 and 120 m data

Table 2.5

99 and 99.9% Values of Maximum Wind
for Conditional Distributions

(upper figure, 99%, lower figure 99.9%, units m sec^{-1})

	F = 1	F = 2	F = 3
	9.8	16.7	36.4
18 m	11.8	20.5	47.0
10 min max			
	20.9	29.4	44.5
150 m	27.3	35.0	49.7
18 m	15.5	22.8	39.8
	21.5	35.5	49.5
one-hour max			
	25.8	33.1	47.3
150 m	30.4	42.0	> 50

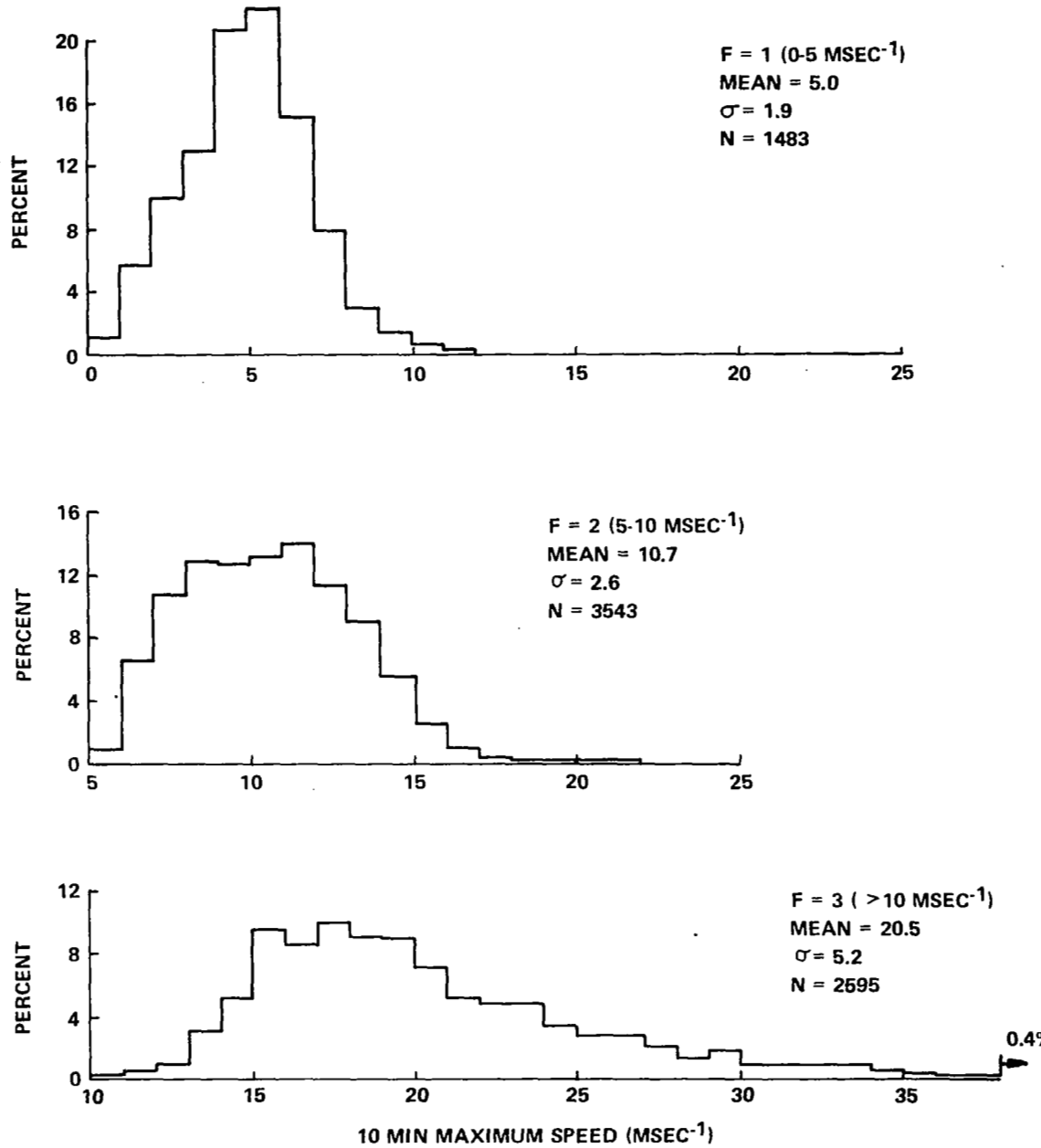

Figure 2.4 CONDITIONAL FREQUENCY DISTRIBUTIONS OF 10 MIN MAXIMUM WIND SPEED AT 18 M HEIGHT. F CLASS DETERMINED BY 18 M MEAN WIND SPEED

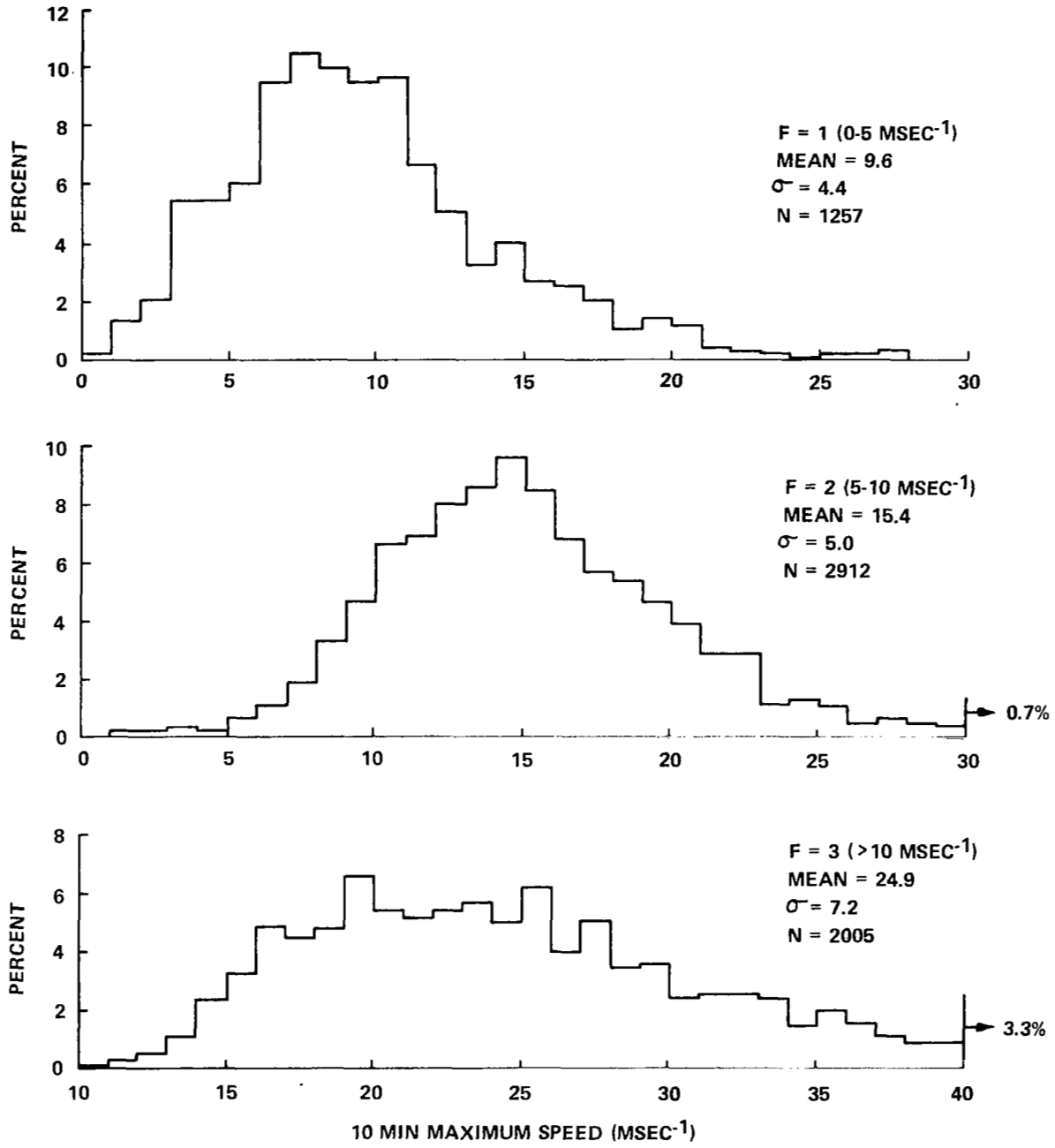

Figure 2.5 CONDITIONAL FREQUENCY DISTRIBUTIONS OF 10 MIN MAXIMUM WIND SPEED AT 150 M HEIGHT. F CLASS DETERMINED BY 18 M MEAN WIND SPEED

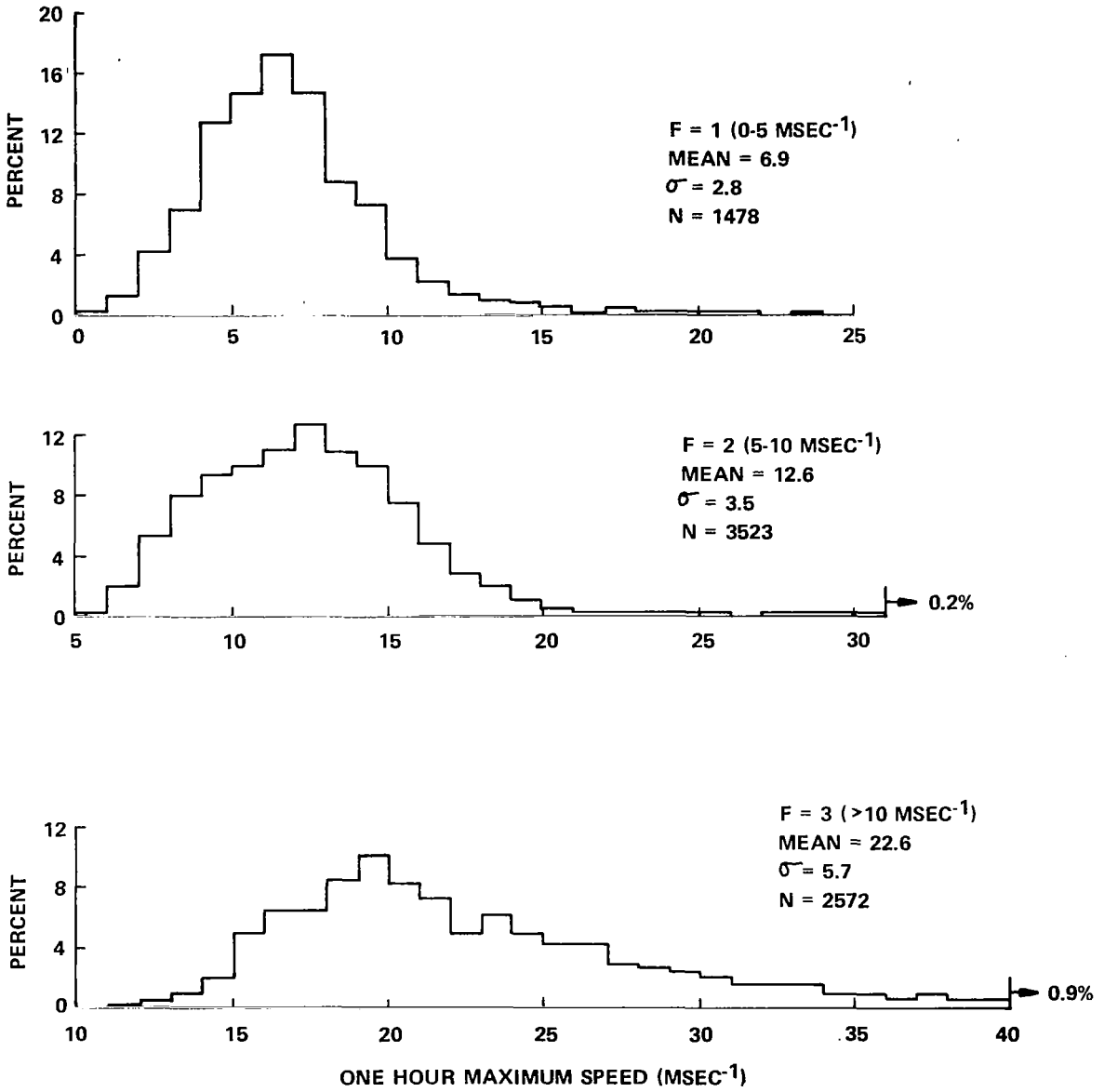

Figure 2.6 CONDITIONAL FREQUENCY DISTRIBUTIONS OF ONE HOUR MAXIMUM WIND SPEED AT 18 M HEIGHT. F CLASS DETERMINED BY 18 M MEAN WIND SPEED

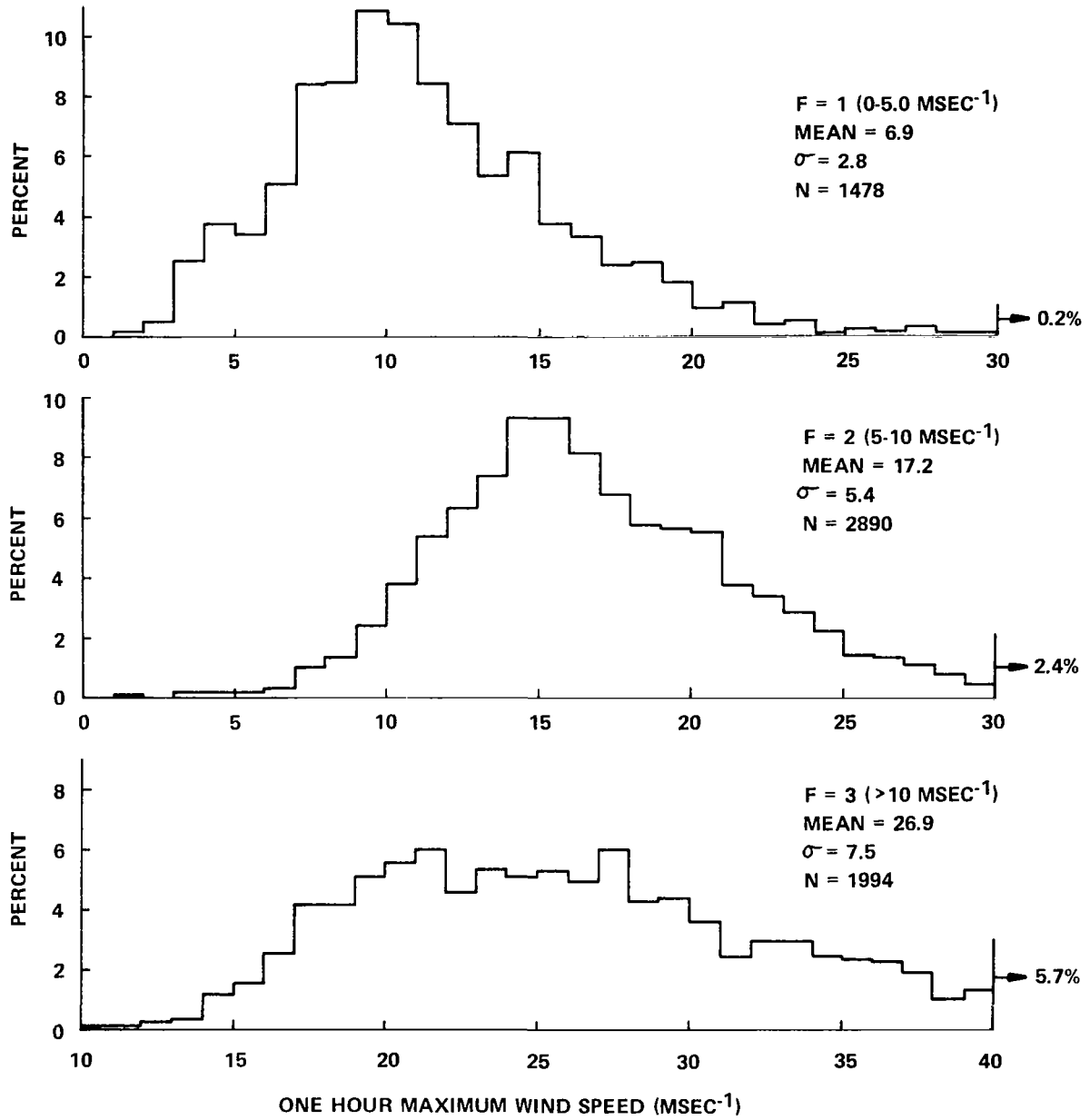

Figure 2.7 CONDITIONAL FREQUENCY DISTRIBUTIONS OF ONE HOUR MAXIMUM WIND SPEED AT 150 M HEIGHT. F CLASS DETERMINED BY 18 M MEAN WIND SPEED

It may be of some interest to consider the ratio of peak wind to the mean for various peak wind sampling times. Table 2.6 shows a comparison of statistics for mean wind and peak wind speed for the three classes of mean wind speed at the 18m level. The ratio of the means for 10 min peak gust to mean wind speed is approximately 1.47 for all three speed classes. The ratio of mean hourly gust to 10 min mean wind speed is approximately 1.65 for Classes 2 and 3, but is 1.90 for Class 1. The higher value for the low wind speed class undoubtedly results from cases where the mean speed for part of the hour was considerably higher than that for the ten-minute sampling period.

Statistics for the overall (unconditional) peak gust distributions are also given in Table 2.6. The overall means for all stabilities and wind speeds, give, for 18 m:

$$\frac{\text{one-hour peak}}{\text{10 min peak}} = 1.23$$

$$\frac{\text{one-hour peak}}{\text{10 min mean}} = 1.66$$

$$\frac{\text{10 min peak}}{\text{10 min mean}} = 1.34 \text{ (gust factor)}$$

Further consideration of the dependence of peak wind on the sampling period is given in Section II D in the discussion of gust factors, and in Section IV B.

Table 2.6

Statistics for Annual Wind Distributions at 18 m Height

Mean Speed Class	10 min Mean Wind ($m\ sec^{-1}$)			10 min Peak Gust ($m\ sec^{-1}$)			Hourly Peak Gust ($m\ sec^{-1}$)		
	Mean	σ	N	Mean	σ	N	Mean	σ	N
F = 1	3.3	1.2	1483	5.0	1.9	1483	6.9	2.8	1478
F = 2	7.4	1.4	3546	10.7	2.6	3543	12.6	3.5	3523
F = 3	13.9	3.2	2595	20.5	5.2	2595	22.6	5.7	2572
All classes combined	9.0	4.5	7624	12.1	8.2	7621	14.9	7.3	7573

D. Distributions of Gust Factor

Gust factor G is defined as the ratio of the maximum instantaneous wind speed observed during a given time interval to the average speed over that interval. The unconditional annual distributions of 10 min gust factor for all heights are shown in Figure 2.8. Table 2.7 lists 99 and 99.9% percentile values for the cumulative distributions. The mean gust factor is largest at the lowest level, and decreases to a steady value in the 90 to 150m height range. The fact that gust factor tends to decrease with height is of course well known from previous analyses at MSFC and studies elsewhere (for example Davis and Newstein (4)).

Examination of the annual distributions at the various tower levels reveals several other interesting characteristics:

a) At 18m the distribution is approximately bell-shaped. The peak is at G = 1.35 and the distribution has slight skewness toward higher values.

b) At progressively higher levels the distributions become less symmetric, with much higher probabilities in the lowest G value category (1.0 to 1.1).

c) The standard deviation becomes smaller at the higher levels as the distributions become narrower. At and above 60m, 70% of all G values are between 1.10 and 1.40.

Table 2.7

99 and 99.9% Values of Gust Factor at Various Heights from Overall Distributions

Height	99%	99.9%
18 m	2.13	3.15
30	2.08	2.99
60	1.99	2.45
90	1.90	2.95
120	1.88	2.30
150	2.05	2.75

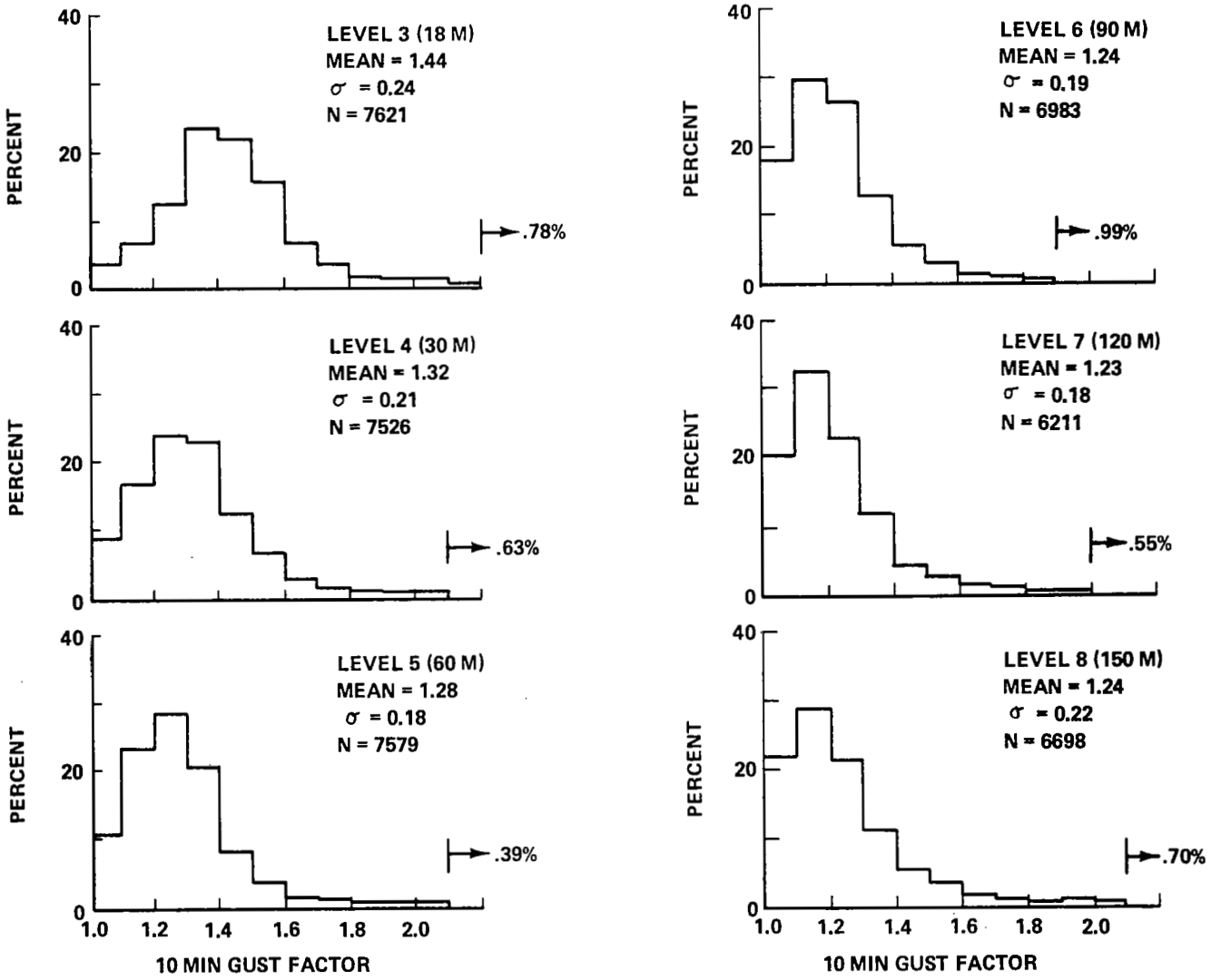

Figure 2.8 UNCONDITIONAL FREQUENCY DISTRIBUTIONS OF 10 MIN GUST FACTOR FOR SIX ANEMOMETER HEIGHTS

The dependence of mean gust factor on wind speed and stability for 18 and 150m is shown in Figures 2.9 and 2.10, respectively. These figures were prepared using the calculated mean gust factors for distributions conditional on R and F. The range of standard deviations computed for various stabilities in each wind speed class is shown on the right-hand side of the figures. There was no significant relationship between standard deviation and Richardson number indicated by the conditional distributions.

In general, mean gust factor decreases with increasing wind speed. Gust factors tend to be larger under unstable conditions at both heights. However, whereas the minimum gust factors at 18 m occur with highest Richardson numbers, the gust factor at 150m is lowest when the bulk Richardson number indicates slightly stable conditions. Also, the highest gust factors at 18 m seem to occur with neutral to slightly unstable lapse rates rather than extremely unstable ones, especially when the wind is strong.

Distributions of gust factor conditional on wind direction appear to show a slight influence of surface roughness. For neutral stability and light winds, the mean gust factor at 18m for direction class D = 1 (smooth) is 1.54. For D = 2 (rougher) the mean gust factor is 1.56. For stronger winds, again in neutral conditions, the corresponding values are 1.47 (directions with small roughness) and 1.57 (directions with greater roughness). At 150m height, the difference with wind direction is smaller, if significant at all.

Most of these trends in gust factor are consistent with the known characteristics of boundary layer turbulence. As an approximation we can assume that gust factor behaves like the ratio of standard deviation of wind speed to mean wind speed, $\sigma_v / \bar{V}$. It is known that $\sigma_v / \bar{V}$ decreases with increasing height, increases with increasing surface roughness, and decreases with increasing stability. However, it is interesting to note that σ_v should be proportional to wind speed for a given height and roughness under neutral conditions (5). Thus, $\sigma_v / \bar{V}$ should not change with wind speed, but the gust factor definitely does increase with increasing $\bar{V}$ in Figures 2.9 and 2.10. A possible explanation is that the observed trend really represents the tendency for conditions to be less steady under light winds. When winds are

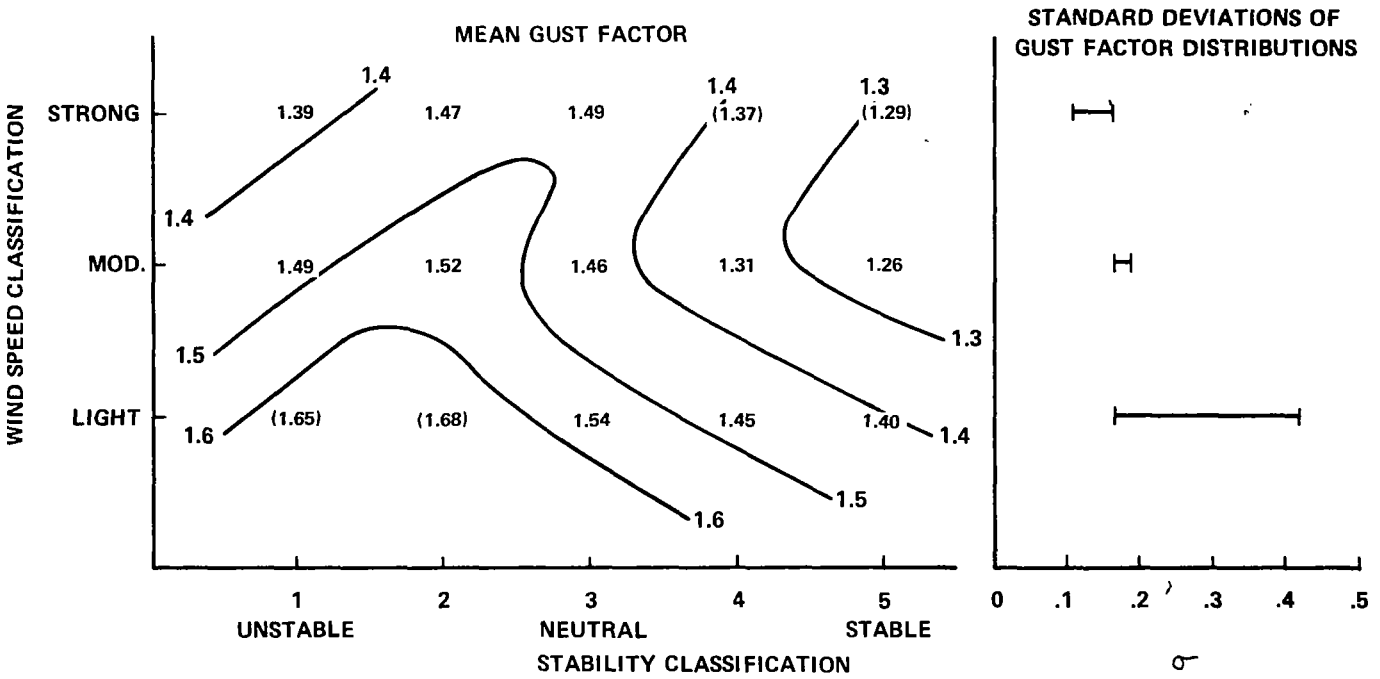

Figure 2.9 MEANS AND STANDARD DEVIATIONS OF CONDITIONAL GUST FACTOR DISTRIBUTIONS AS FUNCTIONS OF MEAN WIND AND STABILITY CLASSIFICATION, 18 M

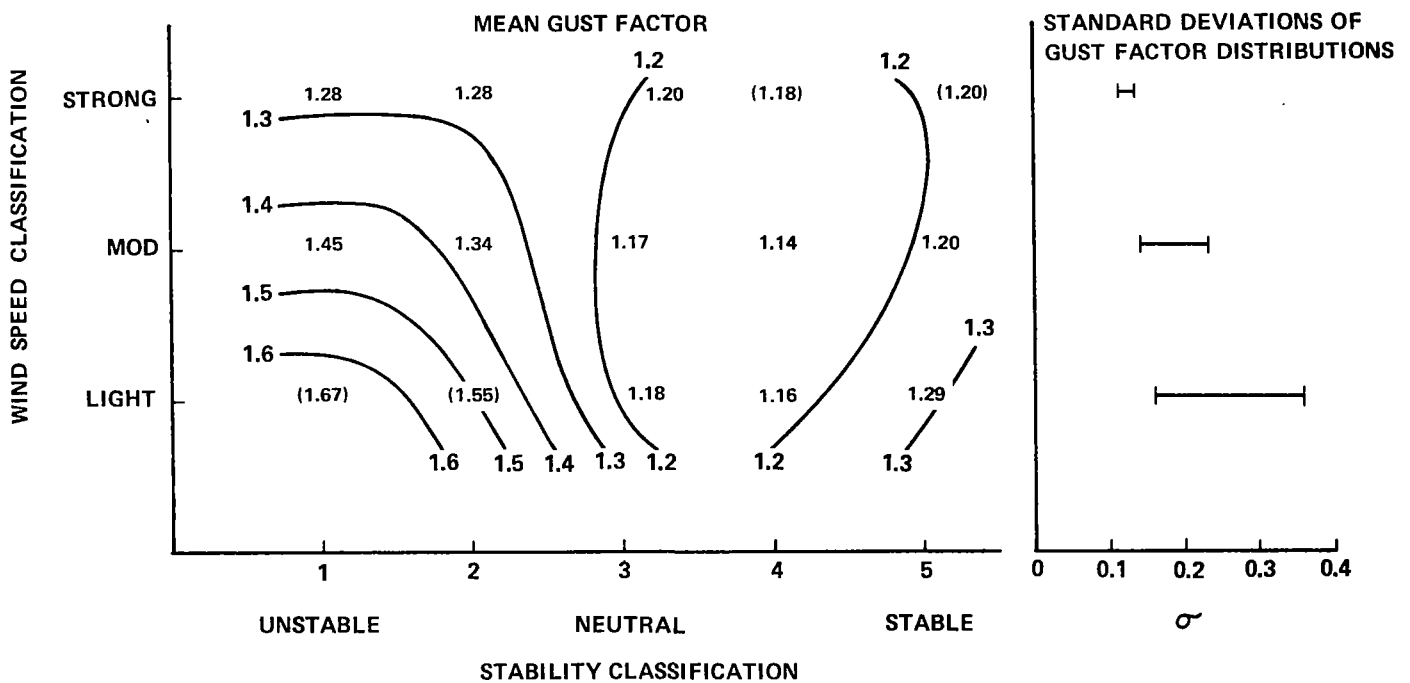

Figure 2.10 MEANS AND STANDARD DEVIATIONS OF CONDITIONAL GUST FACTOR DISTRIBUTIONS AS FUNCTIONS OF MEAN WIND AND STABILITY CLASSIFICATION, 150 M

light there is a greater probability of meso-scale wind shifts or other isolated changes that give rise to large gust factors but do not represent turbulent fluctuations in a steady-state wind field. The parameters that influence gust factor and their relationship to sampling time are discussed further in Chapter IV.

The 18 and 150m gust factor distributions for separate seasons have been examined. It is found that, at 18m:

a) The distributions are approximately bell-shaped for all seasons.

b) The skewness toward higher values noted in the annual distribution arises primarily from the fall distribution (September through November), whose peak occurs at a higher G value than in the annual or other seasonal distributions.

For 150m, in winter and spring the peak of the distributions is at about G = 1.05, whereas in summer and fall the peak is at G = 1.15. The distributions at both 18 and 150m suggest that large gust factors occur more frequently in fall than during the other seasons.

E. The Distribution of Friction Velocity

Friction velocity u_* is a fundamental parameter for the surface layer wind field. It is defined by

$$u_* = \left(\frac{\tau}{\rho}\right)^{1/2} \tag{2.3}$$

where τ is the horizontal shear stress at the surface and ρ is atmospheric density. In addition to being a basic parameter for mean vertical profiles and fluxes in the surface layer, u_* also appears in the quantitative specification of turbulence spectra (Chapter III).

1. Method of Computation

Distributions of friction velocity were calculated indirectly from the mean wind speed distributions. As previously explained, annual distributions of ten-minute mean wind at 18m were calculated for each of five stability classes and two wind direction regimes. Stability classification

was based on the value of bulk Richardson number computed from 18m and 120m data. Wind direction classes were based upon the roughness length in different directions from the tower site. Each of these mean wind speed distributions was converted to a friction velocity distribution through the equation

$$u_* = V_{18}\, k \left[\ell n \frac{z}{z_o} - \psi\left(\frac{z}{L'}\right) \right]^{-1} \qquad (2.4)$$

where V_{18} is the mean wind speed at 18m, k is von Karman's constant (0.40), z_o is roughness length, and $\psi(z/L')$ is a universal function for the stability effect on the wind profile (Lumley and Panofsky, (5) pg. 113).

A separate relationship was determined from Equation (2.4) for each combination of stability class and characteristic roughness length for the site. By use of these relationships, the individual mean wind speed distributions were converted to u_* distributions. The distributions were added to give one distribution for each stability class, and finally an overall annual distribution of u_*.

Utilization of Eq. (2.4) to relate mean wind speed to friction velocity required several preliminary steps. The stability function $\psi(z/L')$ is given by Lumley and Panofsky in graphical form. (The parameter L', a length, is a measure of stability; L' is defined by

$$L' = \frac{u_*^2 T}{kg} \quad \frac{\partial V/\partial z}{\partial \theta/\partial z}$$

where T is mean temperature, g is gravity, and θ is potential temperature.) In order to make use of the Lumley and Panofsky graphs, it was necessary to determine values of z/L' appropriate to 18m height. This was done from the computed Richardson numbers, which apply at a nominal height of 46.5m. Treatment was somewhat different, depending on the stability. The following steps were taken:

a) The mean Richardson number at 46.5m for each of the five stability classes was used to compute a value of z/L' for each class

$$R = 1, 2: \quad \frac{z}{L'} = Ri\,(1 - 18Ri)^{-1/4} \qquad \text{(Reference 5)} \qquad (2.6)$$

$$R = 3: \quad \frac{z}{L'} = Ri \qquad (2.7)$$

$$R = 4, 5: \quad \frac{z}{L'} = \frac{Ri}{1 + 7Ri} \qquad \text{(Reference 6)} \qquad (2.8)$$

b) The z/L' values obtained in a), which apply to 46.5m, were reduced to values appropriate to 18m (assuming L' constant with height).

c) The function $\psi\,(z/L')$ was obtained for 18m height and each stability class.

R = 1, 2: From plot in Lumley & Panofsky

R = 3: $\psi\,(z/L') = \psi(o) = 0$

R = 4, 5: $\psi = -7\,z/L'$ (Ref. 6)

d) Finally, Equation (2.4) was used with the appropriate values of ψ and z_o, providing a relationship between V_{18} and u_* for each conditional distribution. The values of z_o that were used are:*

D = 1: z_o = 58.0 cm

D = 2: z_o = 23.3 cm

The final relationships between V_{18} and u_* are tabulated here.

R	D	u_* =
1	1	$0.098\,V_{18}$
1	2	0.127
2	1	0.095
2	2	0.122
3	1	0.092
3	2	0.117
4	1	0.076
4	2	0.092
5	1	0.051
5	2	0.058

*The z_o values were chosen on the basis of information available from MSFC when these computations were made. There is some recent evidence suggesting that roughness lengths for the site should be revised. If new values are found to be more correct, it will be a relatively simple matter to recompute the u_* distributions.

2. Results

The annual distribution of u_*, obtained by summing the individual conditional distributions, is shown in Figure 2.11. The distribution was derived from all available wind observations for the year, with the exception of three hours of high hurricane winds. Since the passage of a hurricane is a unique event, which significantly alters the wind distribution on the high end, it was felt appropriate to delete those observations that were clearly anomalous and due to the hurricane.

Friction velocity values for selected percentile levels from the cumulative distribution are given in Table 2.8. Also given there are values for the distribution from neutral conditions only (R= 3), within which most of the high wind speed observations occur.

Table 2.8

Cumulative Distributions of Friction Velocity

Percentile	u_* (overall)	u_* (neutral)
10%	0.29 m sec^{-1}	0.48 m sec^{-1}
50	0.81	0.93
75	1.81	1.30
90	1.57	1.67
95	1.80	1.94
99	2.32	2.47
99.9	2.62	2.67

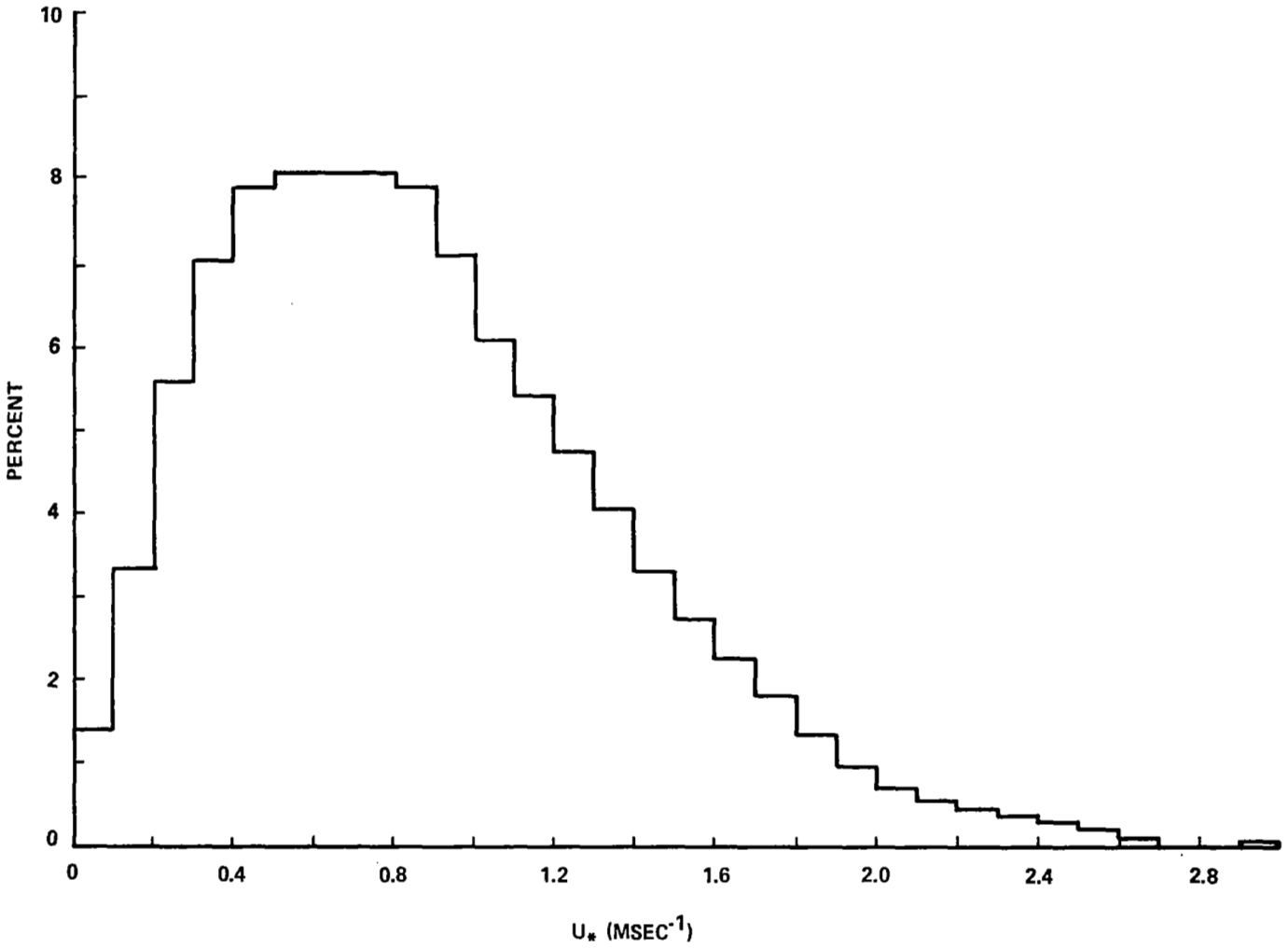

Figure 2.11 UNCONDITIONAL DISTRIBUTION OF FRICTION VELOCITY, U_*, DERIVED FROM ONE YEAR OF 18 M WIND SPEED DATA

III. THE SPECTRUM OF THE LATERAL COMPONENT

The turbulence spectrum is a concise way of presenting much information on the magnitude and frequency of turbulent wind fluctuations. Spectra are used directly as an input in generalized harmonic analysis techniques for computing dynamic response of structures to the wind. Further, considerable research has been done on the subject of atmospheric turbulence spectra; therefore a body of knowledge exists to which new data can be related. A summary of the characteristics of turbulence spectra from Merritt Island is clearly essential for description of the ground-wind environment.

Rather extensive studies of spectra of the longitudinal component of turbulence* have been carried out from Merritt Island data (7). It was decided therefore to restrict attention in the present study to the lateral component. Spectra were supplied for analysis by Marshall Space Flight Center. A total of 31 individual sampling periods was included in the analysis; with a few exceptions spectra were available for each of the six anemometer heights for each case. Data on mean meteorological conditions and sample duration for each case are given in Table 3. 1.

In Table 3. 1 the mean wind speed at 18m height is given along with the Richardson number, Ri_{30} and the friction velocity, u_*. The Richardson number is an average value computed from mean wind and temperature data for 18, 30 and 60m heights. This particular Richardson number was selected in preference to that for a single pair of heights, or an average for all tower

*In accordance with the usual convention, the longitudinal component is that horizontal component of the instantaneous wind vector in the direction of the mean vector wind; the lateral component is perpendicular to this direction in the horizontal plane.

levels, as being perhaps most representative of layer stability for the "constant-stress" layer. Friction velocity values were computed at MSFC on the basis of the mean velocity profile, estimated roughness length, and Richardson number using the wind profile expressions given by Lumley and Panofsky (5). Table 3. 1 also gives the total length of record, T, in seconds, used for spectral computations in each case.

Table 3. 1

Cases Used for Analysis of Lateral Turbulence Spectrum

Case Number	$\overline{V}_{18}$ (m sec^{-1})	Ri_{30}	u_* (m sec^{-1})	T (sec)
150020	4.40	-0.86	0.43	1749
030	9.02	-0.17	0.86	3609
070	6.47	-0.51	0.63	2619
075	5.54	-0.41	0.70	1807
078	6.02	-0.07	0.70	1802
086	3.68	-0.28	0.55	3395
096	6.92	-0.28	0.89	3626
098	5.94	-0.70	0.63	3027
101	3.74	-2.93	0.39	3606
118	4.74	-1.25	0.46	1792
136	3.70	-1.05	0.52	4044
139	3.78	-0.32	0.43	4276
141	3.63	-2.83	0.45	4199
150	5.47	-4.13	0.63	1823
151	2.08	-13.20	0.36	4109
152	1.48	-24.00	0.35	1807
155	2.36	-1.72	0.33	3596
159	3.23	-1.12	0.39	1792
160	3.25	-1.50	0.41	1776
162	3.77	-1.37	0.40	3652
170	3.09	-2.70	0.48	1824
172	4.51	-1.66	0.53	1765
173	3.76	-3.22	0.45	1798
176	2.69	-1.63	0.34	3584
182	4.93	-1.00	0.54	3600
	Cases analyzed but not used for final mean spectra			
091	5.56	-0.29	0.78	3593
133	4.34	+0.55	0.43	3895
142	3.99	+0.14	0.30	4199
156	1.94	+0.37	0.14	3282
165	5.24	-0.26	0.53	3590
174	1.73	-3.55	0.21	1805

As stated, all spectral computations were made at MSFC. Spectra were computed using the standard Tukey Fourier transform methods (8). The original wind records (speed and direction at 0.1-sec intervals) were utilized to compute mean wind speed and direction, from which the lateral and longitudinal components were calculated for each data point. Before spectral analysis the data were block-averaged over 0.5-sec periods and trends were removed by fitting a second order polynomial to the entire record. After averaging and detrending, the lateral component records were spectrum analyzed using the minimum sampling interval of 0.5 sec and 300 lags. Thus, the spectra cover a frequency range from $1/300 = 0.0033$ to 1.0 cycles sec^{-1}. All spectra were corrected for the block-averaging operation.

For conveniece in analysis, a numerical output for the spectrum was provided in similarity coordinates. Thus, for each frequency n the non-dimensional frequency $F = nz/V$ was computed, where z is the height of observation and V is the mean wind speed. (F can be thought of as representing the ratio of height to wavelength.) The spectral estimates S(n) were multiplied by frequency and divided by the square of friction velocity. Multiplication by n makes area proportional to energy on a semilog spectral plot, and since the total energy should be roughly proportional to u_*^2, spectra from different conditions can be more readily compared when normalized in this way. Printouts of F versus $nS(n)/u_*^2$ were provided both for the original 300 spectral estimates and for a smoothed spectrum where the estimates were block-averaged over five successive points.

To prepare for analysis, each of the smoothed spectra was plotted on semilogarithmic paper, and a smooth curve was drawn by eye through the plotted points. (Nonsmoothed spectral estimates were used at low frequencies to provide better resolution where points were further apart.) Since 31 cases were studied and six spectra (heights) were available for each case, nearly 180 individual spectra were plotted.

A. Spectral Variation with Height and Stability

Relatively little information appears in the literature on lateral turbulence spectra in the atmospheric boundary layer, at least in comparison with vertical and longitudinal components. One reason is that no theory has been proposed which accounts for observed features of the lateral spectrum. A summary of theory and observational evidence relative to atmospheric turbulence spectra is given by Lumley and Panofsky (5). They show that, according to similarity theory, it might be expected that atmospheric spectra would follow the relation

$$\frac{n\,S(n)}{u_*^2} = f(F, Rt) \qquad (3.1)$$

i.e., that the normalized spectrum will be a function only of dimensionless frequency and stability. While the theory has been adequately confirmed for vertical velocity spectra, it does not appear to apply to longitudinal and lateral components. Further, it cannot be expected to apply at heights above the constant-stress layer, which includes a maximum of 100 m. Fichtl (7) found, for longitudinal spectra at Cape Kennedy, that other parameters needed to be considered. Lumley and Panofsky summarize properties of lateral spectra by stating that they are nearly independent of height and strongly dependent on stability. The low-frequency portion of the spectrum (F less than, say, 0.5) increases rapidly with increasing instability, while the higher-frequency portions are not sensitive to stability but depend upon wind speed and surface roughness.

These conclusions tend to be confirmed by the lateral spectra from Merritt Island. The effect of stability on the low-frequency spectrum shows up clearly, and the variation of high-frequency spectral estimates with wind speed is well accounted for by the u_*^2 normalization. Though the measured spectra do not agree with similarity theory in the sense that a universal function exists, plotting in similarity coordinates does reduce the overall scatter and shows up systematic changes with stability and height.

The individual plotted spectra, even in smoothed form and similarity coordinates, showed quite wide variability. This variability was great enough that no clear trend with stability, wind speed or other parameters was apparent

from perusal of individual spectra. The cases were grouped according to Richardson number and averaged within each group, and the resulting mean spectra did then show clear trends. In classifying and averaging cases, three were eliminated from the sample because of either missing data at some heights or extreme scatter in the computed spectra that suggested irregularities in the wind records. The classification of the remaining 28 cases is indicated in Table 3.2.

Table 3.2

Classification and Averaging Of Merritt Island Spectra According to Low-Level Stability

Range of Ri_{30}	No. of Cases Averaged
$Ri < -2.0$	7
$-2.0 \leq Ri < -1.0$	8
$-1.0 \leq Ri < -0.3$	6
$-0.3 \leq Ri < 0.0$	4
$0.0 \leq Ri$	3
"neutral case" ($-0.3 \leq Ri < 0$)	4
"unstable case" ($Ri < -0.3$)	21

The change in spectral shape with changing stability is indicated clearly by comparison of the mean spectra for the different Richardson number classes. Figure 3.1 shows mean spectra for 18m height for all of the unstable classes. Plots for other heights showed very similar behavior. It can be seen that the energy at low frequency increases greatly with increasing instability. Unfortunately, the spectra do not extend to low enough frequency to show a peak in all cases, but there is a suggestion that the peak shifts toward smaller F as the atmosphere becomes more unstable. For F greater than about 0.4, stability seems to have virtually no effect on the normalized spectrum.

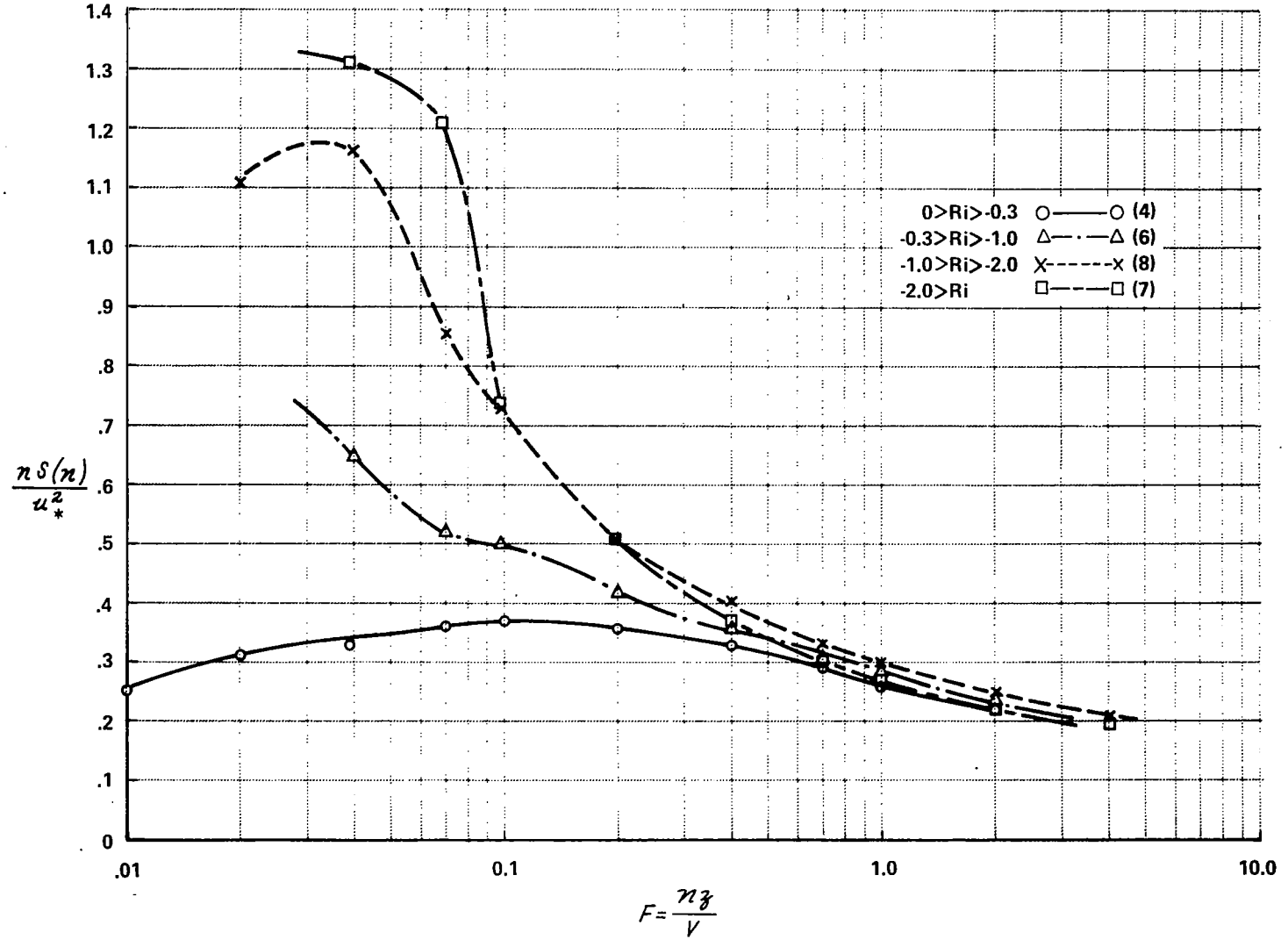

Figure 3.1 MEAN LATERAL SPECTRA AT 18 M HEIGHT FOR FOUR STABILITY CLASSES

A mean spectrum for stable conditions is not included in Figure 3. 1 since only three spectra were available for averaging. Two of the three showed surprisingly large values of $nS(n)/u_*^2$ for large F numbers, suggesting that the value of u_* used for normalization was incorrect or that the computed spectra were erroneous. However, one interesting feature appeared in each of the three stable spectra. A peak is present at intermediate F numbers (between F = 0. 10 and 0. 4 at 18 m) with a gap immediately below (F = 0. 05 to 0. 1) and another rise as F decreases further. On the high side $nS(n)/u_*^2$ decreases smoothly from the peak, though the spectra remain relatively high in two of the three cases, as already mentioned. This behavior suggests a maximum of energy from mechanical turbulence at wavelengths roughly five times the height and a suppression of longer wavelengths. The increase for very small F may be associated with the very large-scale "meanders" that have been observed elsewhere in stable conditions (5).

Change in the lateral spectrum with height is illustrated in Figure 3. 2. These spectra, labeled "unstable", are averages of the 21 cases for which Ri_{30} is less (more negative) than -0. 3. The curves are generally similar in shape but shift toward higher F number with increasing height. If these same spectra were plotted in dimensional form with frequency as the abscissa, there would be little systematic shift with height, confirming that height does not have a profound influence on the lateral spectrum.

The changes with height for the near-neutral cases are shown by Figure 3. 3. These spectra are averages of the four cases with Richardson number between zero and -0. 30. Since the peak in the neutral spectrum occurs at higher frequency than in the unstable case, a peak appears for all heights in Figure 3. 3. These make it clear that, as in the unstable case, the frequency shift which appears is primarily due to the z/V scale factor, and the peak frequency is essentially the same ($\sim$ 0. 025 cycles sec^{-1}) at all heights. However, in the neutral case the magnitude of the spectrum appears to decrease with height.

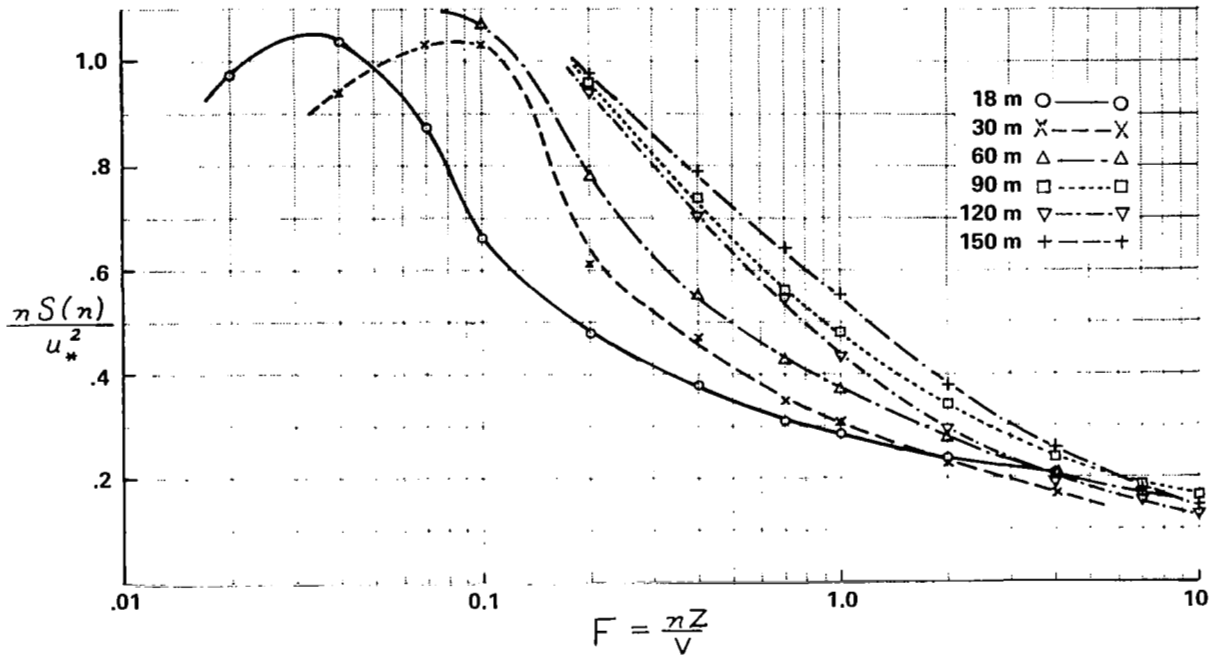

Figure 3.2 MEAN UNSTABLE LATERAL SPECTRA FOR SIX HEIGHTS

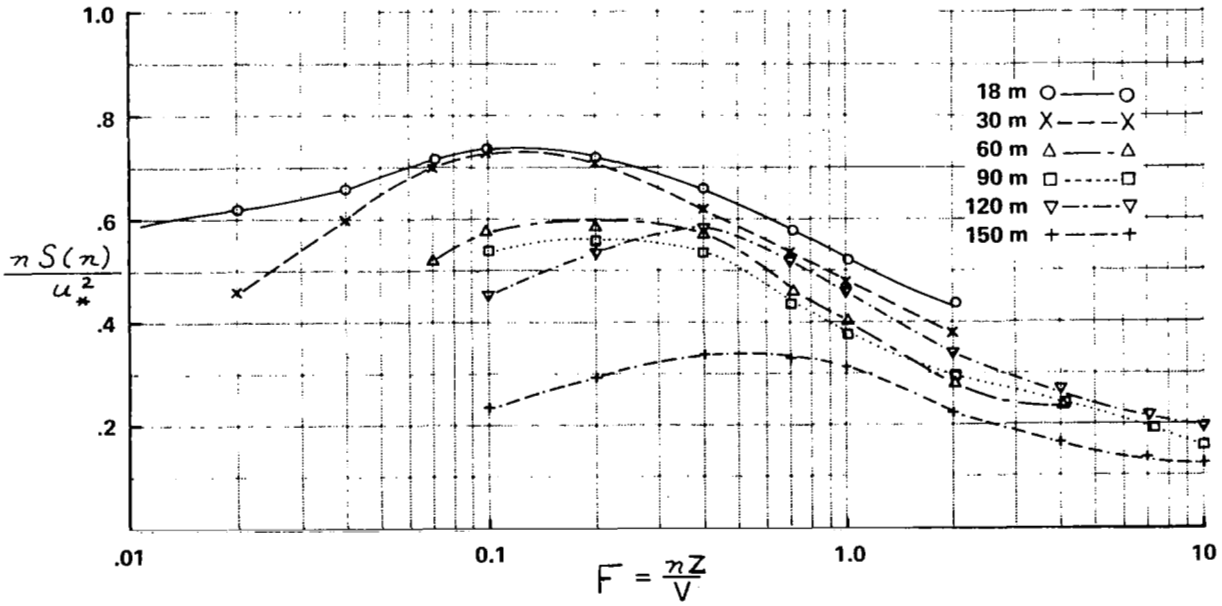

Figure 3.3 MEAN NEAR-NEUTRAL LATERAL SPECTRA FOR SIX HEIGHTS

It is of some interest to examine the slope of the spectrum at high F number. For F greater than, say, 1.0, the turbulence is expected to conform to the laws of the Kolmogoroff regime or inertial subrange, in which the spectra should vary as $(F)^{-2/3}$. It will be seen that the spectra in Figures 3.2 and 3.3 tend to have a smaller slope at high F. The reason for this result is unknown; the existence of a broad $F^{-2/3}$ range has been amply confirmed in numerous atmospheric spectra. It is worth noting that Fichtl (7) was able to fit a -2/3 law to longitudinal spectra from Cape Kennedy. It is possible that response of the wind vanes or the spectral computation procedures have introduced some error into the high frequency end of the lateral spectra.

B. Spectrum Models for Neutral and Unstable Conditions

The lateral spectra that have been presented show consistent behavior with changes in height and stability. It is useful to summarize these properties in a concise form that can be used by engineers to estimate spectral characteristics under any given conditions at Kennedy Space Center. Following a suggestion by G. Fichtl, two spectrum models have been devised by scaling the mean "neutral" and "unstable" spectra to account for variations with height.

The two model spectra are shown in Figure 3.4. They are given as plots of $nS(n)/\beta u_*^2$ versus F/F_m, where β is a parameter which scales the spectral intensity, and F_m, which represents the F number at which the peak occurs, is a scaling factor for the frequency coordinate. Both β and F_m are functions of height; their values for the KSC model are given by the curves in Figure 3.5. To estimate the lateral spectrum for a given situation, one requires values for the mean wind speed at the height of interest and the friction velocity u_*. (Statistics on these parameters are given in Chapter II.) Values of β and F_m are taken from Figure 3.5 for the appropriate height and stability condition, and then used with the spectra in Figure 3.4. Since all parameters are now known, spectral estimates S(n) may be obtained as desired for the given height and meteorological conditions.

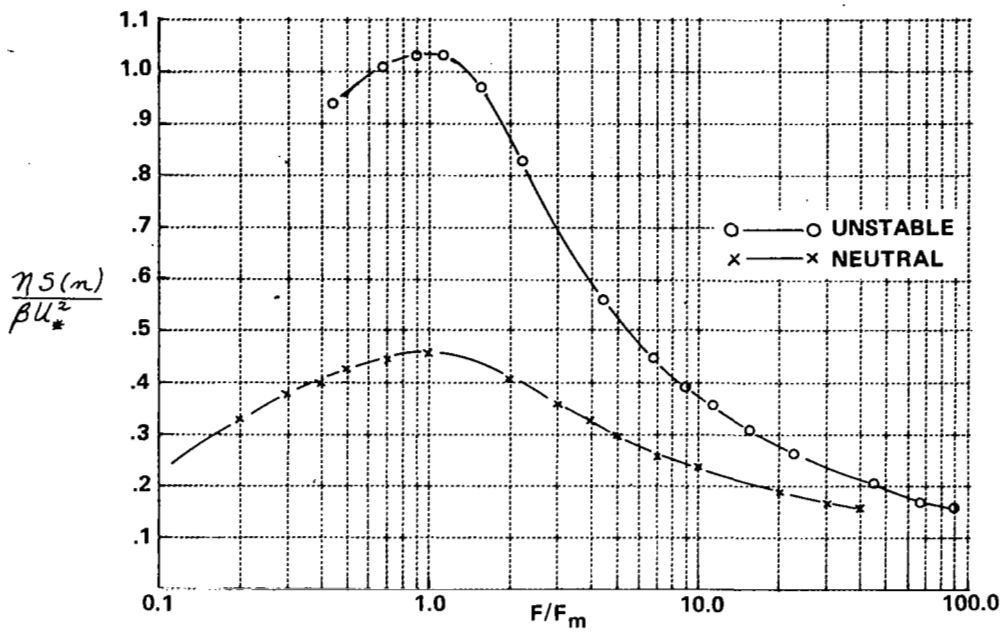

Figure 3.4 MODEL LATERAL SPECTRA DEVELOPED FROM MERRITT ISLAND TOWER DATA FOR NEUTRAL AND UNSTABLE CONDITIONS

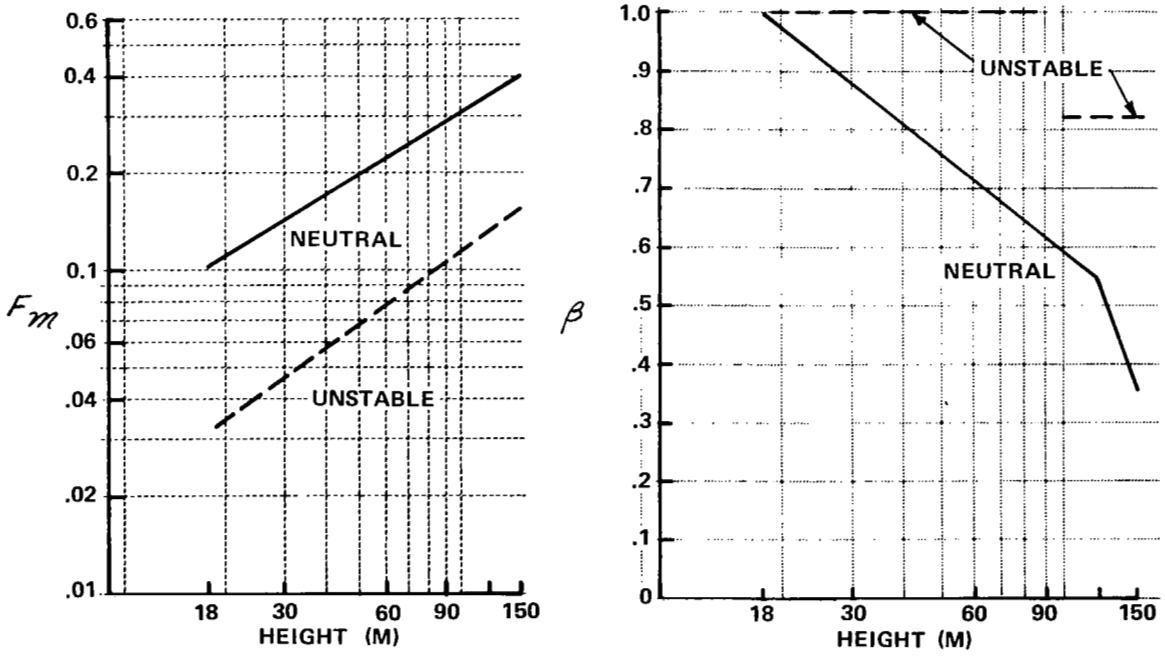

Figure 3.5 VALUES OF THE PARAMETERS F_m AND β FOR USE IN LATERAL SPECTRUM MODEL

The model spectra were obtained by graphically scaling the individual spectra in Figures 3.2 and 3.3 to determine the best overall fit to a single curve for each stability class. First, the individual spectra for each height were shifted with respect to F (the individual curves in Figures 3.2 and 3.3 can be thought of as being moved left or right) until the peaks were lined up at the same point on the abscissa. (For the unstable case where peaks are not present the curves were shifted until their slopes agreed as nearly as possible at all values of F. The value of F_m for each height was that value which would bring that spectrum into alignment with the 18m spectrum when both were plotted on a scale of F/F_m.) Then a factor for the ordinate scaling was determined by computing a value of $1/\beta$ for each height such that when the spectrum was multiplied by $1/\beta$ it would fall as closely as possible on top of the 18m spectrum. The values of F_m and β so determined were plotted as functions of height and represented for the model by the straight lines shown in Figure 3.5. Note that little scaling of intensity was required for the unstable case; β is unity for all heights except 120 and 150 m.

The fit of the original spectra to the final models is shown in Figures 3.6 and 3.7. The final β and F_m values for the model were used to calculate $nS(n)/\beta u_*^2$ and F/F_m for a number of points on each of the mean observed spectra. These points have all been plotted in the figures, along with the smooth curves adopted for the spectral models. It can be seen that though individual spectra depart slightly from the model spectrum they all agree within the experimental scatter, and the overall agreement is quite good.

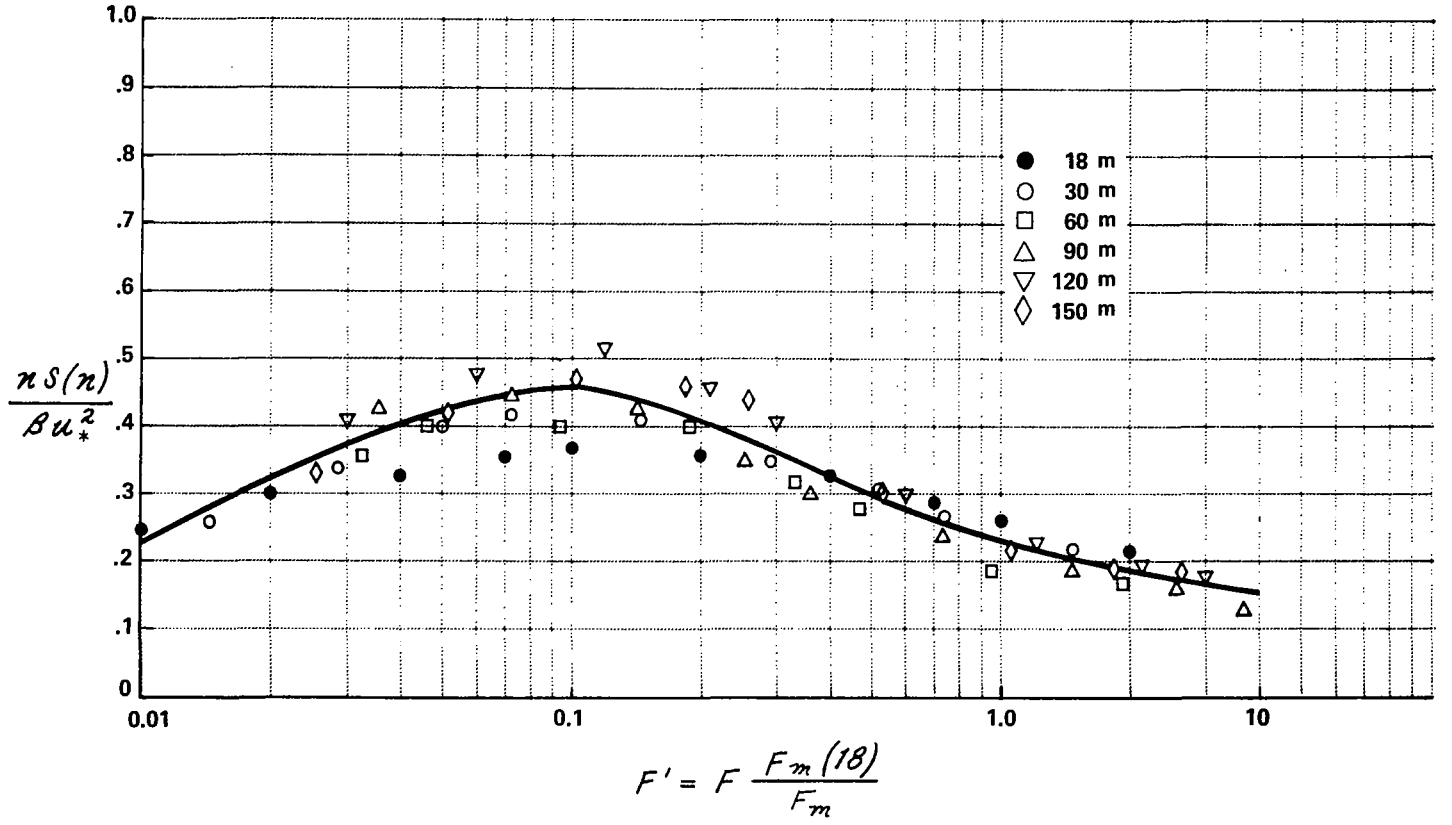

Figure 3.6 LATERAL SPECTRUM MODEL FOR NEUTRAL CONDITIONS WITH DATA FROM AVERAGE NEAR-NEUTRAL MERRITT ISLAND SPECTRA

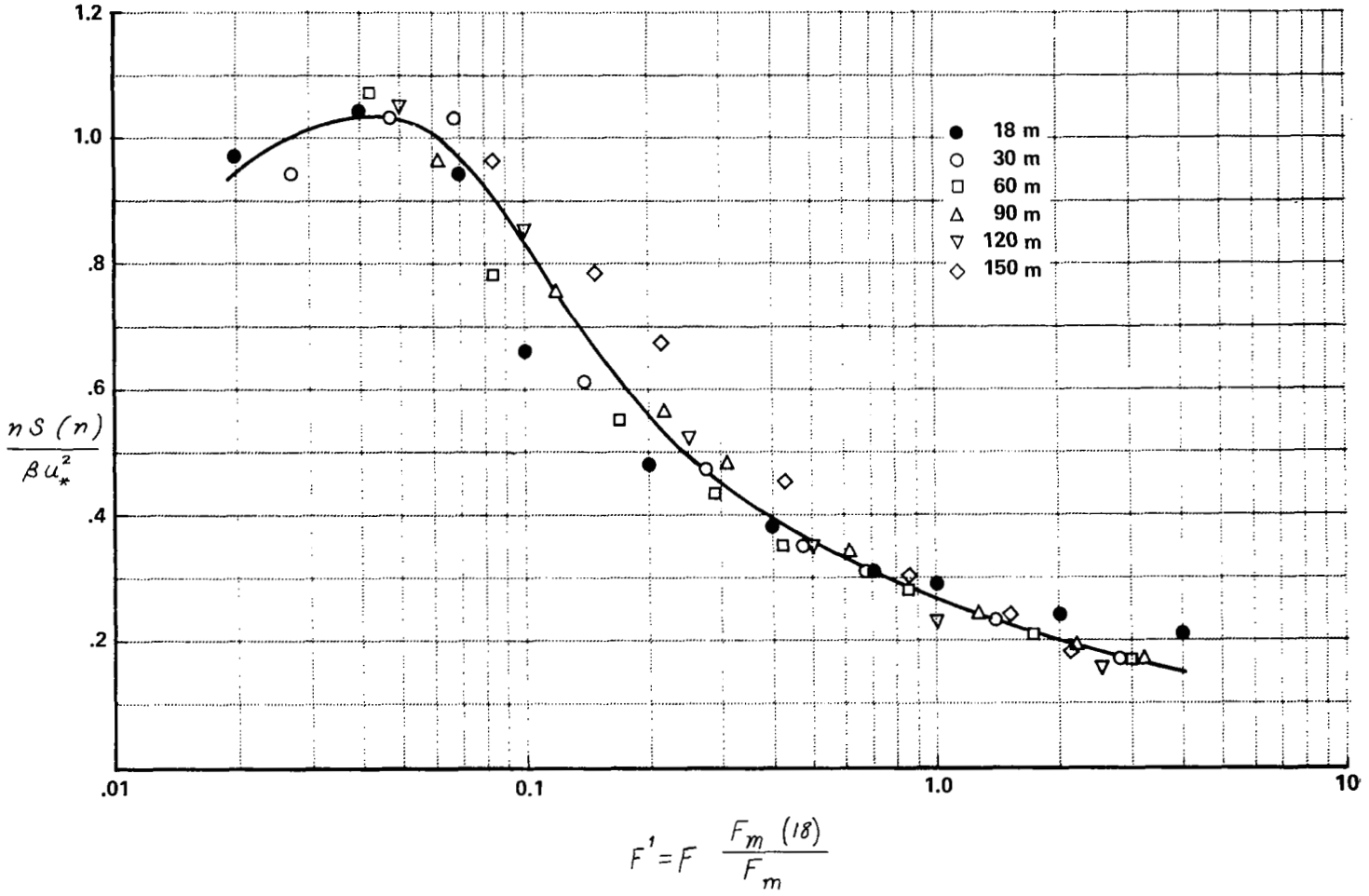

Figure 3.7 LATERAL SPECTRUM MODEL FOR UNSTABLE CONDITIONS WITH DATA FROM AVERAGE UNSTABLE MERRITT ISLAND SPECTRA

IV. CHARACTERISTICS OF GUSTS

A. Data Processing and Preliminary Calculations

Merritt Island tower data in the ten-point-per-second form were used by MSFC for computation of power spectra as discussed in the preceding Chapter. It was desired to also utilize these data to investigate properties of the wind that are not directly available from spectra, for example the duration of individual gusts, and the rate-of-change of wind speed during a gust. Some information on such characteristics has been presented (9), but the results so far have been based on relatively small data samples.

Computations related to the statistics of gusts have been made from the ten-point-per-second wind data tapes. Specifically, the following statistics have been computed:

a) frequency distributions of mean wind speed for nine given sampling intervals between 2.5 sec and 480 sec;

b) frequency distributions of peak wind speeds for the same sampling intervals;

c) frequency distributions of gust factors, again for the same set of nine sampling intervals;

d) frequency distributions of instantaneous wind speeds;

e) frequency distributions of the time intervals between successive positive-slope level crossings for selected wind speed levels;

f) frequency distributions of the time intervals between successive positive-slope and negative-slope level crossings for selected wind speed levels;

g) frequency distributions of wind speed which are conditional on the wind speed having a specified value at a time which is earlier by a specified interval.

Items (a) to (c) provide information on the sampling time dependence of peak and mean wind speed and gust factor; item (e) provides information on gust frequencies (at various wind speed levels) without regard for gust durations; item (f) provides information on mean frequencies of occurrence of gusts of specified duration without regard for the distribution of time intervals between successive gusts; and item (g) provides information on gust accelerations. No attempt will be made here to provide a complete discussion of all of the distributions listed above. Rather, only those statistics will be discussed that appear to have, on the basis of our analyses, a direct bearing on the determination and interpretation of gust characteristics.

Before computing the frequency distributions from the raw data tapes, several preliminary steps were taken. After the magnetic tapes were converted to a format suitable for processing on the CAL IBM 360 computer, each tape was used to make calculations of some fundamental statistical properties and to compute correlations between wind components at different heights and in different coordinate directions. A computer program was written for this preliminary processing; output from the program included:

mean and variance of wind speed,

magnitude and direction of the mean vector wind,

mean and variance of North-South and East-West components,

variance of lateral and longitudinal components,

each for successive 100 sec and longer periods over the total length of record, and for averaging times increasing in 100 sec steps from 100 sec to the total record length. In addition, the program gave zero-lag correlations between values of wind components (both lateral and longitudinal) at different heights, and cross-correlations between lateral and longitudinal components. The correlations were computed for 5-minute and longer periods.

This program was used for all data samples that were to be processed for determination of gust characteristics. In addition to providing data for study of vertical scales and correlations, the program gave complete statistics on the lateral and longitudinal components, so that records could be examined for gross turbulence properties and degree of stationarity before performing detailed analysis. In this way, it was possible to select cases for analysis that provided some variety in turbulence intensities and scales, while eliminating from further consideration anomalous cases where wind direction, speed, or turbulence intensity showed systematic trends or abrupt changes during the observation period.

1. Vertical Correlations

Considerable research on the correlations between winds at different heights has been performed, using Merritt Island data, by Marshall Space Flight Center and Penn State University (results unpublished at this time). Their analyses were made by consideration of coherence functions, which indicate the correlation between heights as a function of frequency and time lag. The present results are restricted to instantaneous correlations with zero time lag. Typical examples of the results obtained are shown in Figures 4.1 and 4.2.

The Figures indicate the degree to which instantaneous winds between the ground and 150 m height are correlated in conditions of moderate wind and unstable lapse rate. The two situations represented in the figures along with one other provided the basic data for most of the numerical results presented in this Chapter. Certain average wind speed characteristics for these three cases are given in Table 4.1. These data are useful in comparisons of the statistics for the individual cases.

Each line in the Figures connects points representing the correlation between a wind component (u or v) at one height and the same component at all other observation heights. Thus, the straight line segments in effect give the correlation function $\rho_u(z)$ or $\rho_v(z)$. For example, in the top portion of Figure 4.1, the line starting at $\rho = 1$, $z = 18$ is the correlation between u at 18 m and u at other heights. Of course u_{18} is perfectly

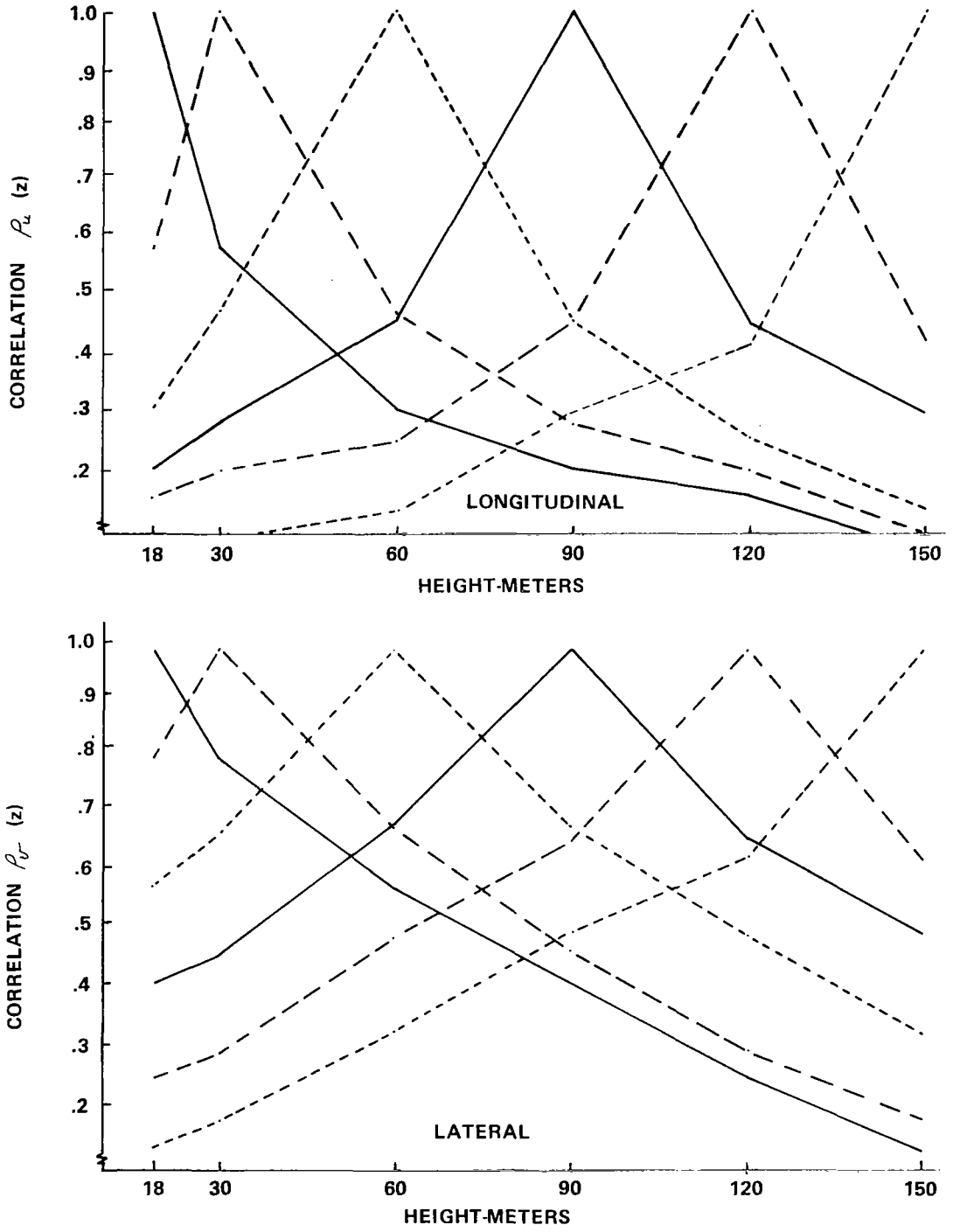

Figure 4.1 ZERO-LAG CORRELATIONS BETWEEN LONGITUDINAL (TOP) AND LATERAL (BOTTOM) WIND COMPONENTS AT VARIOUS HEIGHTS. CASE 150067

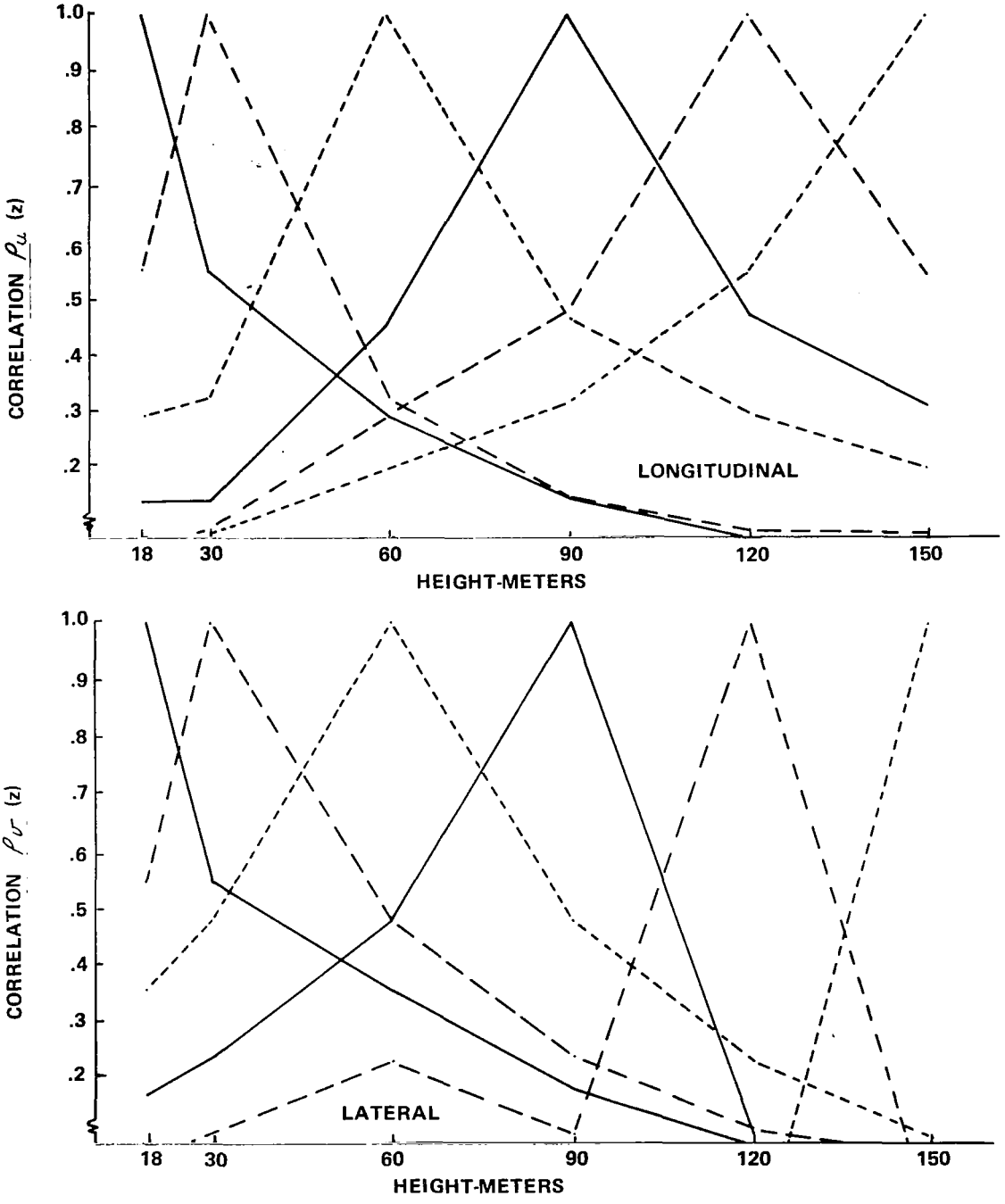

Figure 4.2 ZERO-LAG CORRELATIONS BETWEEN LONGITUDINAL (TOP) AND LATERAL (BOTTOM) WIND COMPONENTS AT VARIOUS HEIGHTS. CASE 150096

Table 4.1
STATISTICS FOR THREE WIND RECORDS

CASE NO.	TOWER HEIGHT (m)	MEAN WIND SPEED (m SEC^{-1})	SIGMA (WIND SPEED)	SAMPLE LENGTH (SECONDS)	DATE	STARTING TIME	τ_o* (SEC.)
150096	3	6.08	1.29	2470	5/11/67	1630	
"	18	7.10	1.23	2470	"	1630	26
"	30	7.82	1.12	2470	"	1630	26
"	60	8.45	0.92	2470	"	1630	26
"	90	7.42	0.68	2470	"	1630	24
"	120	8.56	0.75	2470	"	1630	23
"	150	8.89	0.78	2470	"	1630	23
150067	3	5.75	1.35	2380	4/20/67	1800	
"	18	7.43	1.22	2380	"	1800	35
"	30	7.85	1.12	2380	"	1800	35
"	60	8.19	1.00	2380	"	1800	31
"	90	8.34	0.91	2380	"	1800	26
"	120	8.37	0.91	2380	"	1800	
"	150	8.46	0.87	2380	"	1800	26
150089	3	2.19	0.88	2200	5/5/67	1510	
"	18	2.79	0.66	2200	"	1510	70
"	30	2.91	0.67	2200	"	1510	67
"	60	3.00	0.71	2200	"	1510	65
"	90	3.15	0.57	2200	"	1510	62
"	120	3.04	0.73	2200	"	1510	64
"	150	3.24	0.60	2200	"	1510	60

* FOR CASES 096 AND 067 τ_o WAS DETERMINED FROM THE AUTOCORRELATION FUNCTION. FOR CASE 089 τ_o WAS DETERMINED TO GIVE AGREEMENT WITH GUST FACTOR DISTRIBUTIONS FROM THE OTHER TWO CASES, AS EXPLAINED IN THE TEXT.

correlated with itself, so $\rho = 1$ at $z = 18$. It is seen that the correlation between u_{18} and u_{30} is 0.59, that between u_{18} and u_{60} is 0.32, etc.

The results indicate that correlation functions for both lateral and longitudinal components are roughly symmetric above and below any given height on the tower. This implies that the vertical correlation is dependent on the distance between anemometers, but not on the absolute height above ground. In other words, the vertical scale of the turbulence appears to be relatively constant between 18 and 150 m height. A similar conclusion is given by Lumley and Panofsky (5).

For case 150067 the lateral component is more highly correlated than is the longitudinal for given vertical separation. The converse is true for case 150096. In the latter case the lateral component shows zero or even negative correlation between adjacent levels near the top of the tower. This is in contrast to the general symmetry noted above. In terms of mean wind speed and stability, cases 067 and 096 are very similar, and there is no obvious reason to expect different vertical turbulence scales. The mean wind profile for 096 shows a speed minimum at 90 m with slight increases above and below; this feature is the only possible irregularity that might be related to the marked decorrelation in the lateral component above 90 m. In any event, it is clear that very small-scale lateral eddys existed at the higher levels on this occasion. With the exception of such irregularities, the general conclusion from all cases that have been seen is that vertical scales tend to be relatively constant and correlation functions well-behaved, but that there can be substantial differences between the lateral and longitudinal scales.

B. Dependence of Gust Factor on Sample Duration

To compute the frequency distribution of gust factor for a given sampling interval T, the data run was divided into N successive samples of length T with the largest possible value of N. The gust factor was computed for each interval by dividing the peak wind speed for the interval by the mean wind speed over the interval. The frequency distributions of gust factor (together with the means and rms deviations of gust factor) for sampling

period T were then computed from the set of gust factors for the interval T. In the following discussion the term mean gust factor in the case of a given sample duration refers to the average of gust factor over the frequency distribution for that sampling period.

1. Mean Gust Factor

Plots of mean gust factor versus sampling period for two cases and various tower levels are given in Figure 4.3. Due to the necessity for removing the influence of unrepresentative data points on the computed means, it was found necessary in many cases to recompute the means by hand calculation instead of employing computer values. Since these hand calculations required appreciable time and labor only a portion of the computer results were employed in preparing the plots. For this reason most of the plots in Figure 4.3 do not contain data on some tower levels.

In Figure 4.3 the mean gust factor was computed only for the nine sampling periods indicated by markers on the scale.* The joined-line-segment plots help to visualize the trends in each case. It is apparent that to a first approximation the mean gust factor for each tower level varies linearly with the logarithm of the sampling period. In the following the factors influencing the magnitude and variation of the gust factor are investigated.

Since the mean wind speeds do not vary appreciably with sampling interval for periods greater than two seconds, and their variances are relatively small, the expectation value of the peak wind speed in a sample of duration T is given to a good approximation by the product of the mean gust factor for duration T and the mean wind speed over a very long interval. For example, from Figure 4.3, in case 150096 the mean gust factor is 1.25

*In those cases in which there were no nonrepresentative points in the frequency distribution for gust factor, it is clear that the number of points contributing to the computed mean is the largest integer not greater than T_{max}/T, where T is the exposure period and T_{max} is the entire length of record. Thus, from Table 4.1 we conclude that the greatest number of contributing points for T = 480 sec is 5.

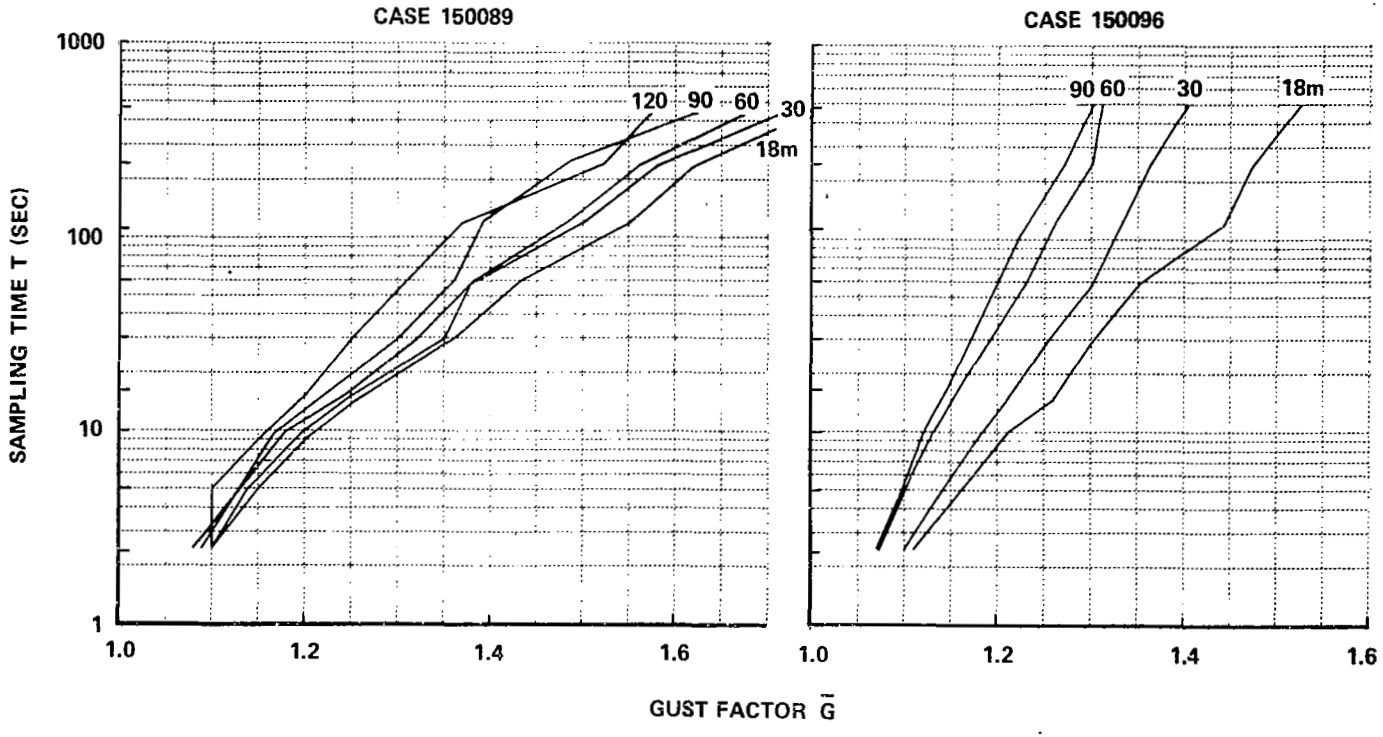

Figure 4.3 MEAN GUST FACTOR FOR VARIOUS HEIGHTS AS A FUNCTION OF SAMPLING PERIOD, CASES 089 AND 096

for a tower level of 30 meters and sampling period of 30 seconds. Multiplying this mean gust factor by the appropriate mean wind speed from Table 4.1 yields the value 9.8 for the expectation value of the peak wind speed. This value agrees to two significant places with that computed directly from the sampling-interval-dependent distribution of peak wind speed for this particular case. Calculations in other cases likewise yield agreement to two significant places.

As a first step in investigating the factors which influence the variation of mean gust factor with sample duration it is desirable to replot the data for each case in a form which removes (or at least reduces) any dependence on the means and variances of wind speed. The gust factor for sampling duration T is defined by

$$G_T = \frac{V_{T\,max}}{V_{T\,ave}}$$

where $V_{T_{max}}$ is the peak wind speed for sample duration T and $V_{T_{ave}}$ is the mean wind speed over T. Then we can write, as an approximation

$$\bar{G}_T = \frac{\bar{V}_{T\,max}}{\bar{V}_T} \cong \frac{\bar{V}_T + f_T\,\sigma_v}{\bar{V}_T} = 1 + f_T\,\frac{\sigma_v}{\bar{V}} \qquad (4.1)$$

where $\overline{V}_{T_{max}}$ = expectation value of peak wind speed for sample duration T.

$\overline{V}_T$ = expectation value of average of wind speed over an interval T = $\overline{V}$

$\overline{V}$ = mean wind speed for very long sample duration

σ_V = standard deviation of wind speed for very long sample duration

f_T = form factor dependent on sample duration and higher order statistics of the process

$\overline{G}_T$ = mean gust factor for sample duration T.

Thus, the mean gust factor should depend directly on the ratio of standard deviation of wind speed to mean wind speed, and on the form factor. It is our intention to normalize the gust factor so as to remove the dependence on $\sigma_V/\bar{V}$.

From eq. (4.1):

$$f_T = (\bar{G}_T - 1)\ \frac{\bar{V}}{\sigma_V}$$

Therefore, we can define a normalized gust factor dependent only on f_T by

$$\bar{G}_r = 1 + C f_T = 1 + \frac{1}{C}(\bar{G}_T - 1)\ \frac{\bar{V}}{\sigma_V} \qquad (4.2)$$

where C is a constant, arbitrarily taken as 1/6 so that $G_r = G_T$ when $\bar{V}/\sigma_V = 6$.

Since the variation of $\bar{G}_T$ with T depends not only on the form factor f_T but on the ratio $\bar{V}/\sigma_V$ whereas $\bar{G}_r$ depends only on f_T, one would generally expect the differences between $\bar{G}_r$ in two cases to be less than the differences between the corresponding $\bar{G}_T$'s. To test this hypothesis $\bar{G}_r$ was plotted for certain tower levels in the three cases considered. The results for the two cases shown in Figure 4.3 are presented in Figure 4.4. The third case gave a reduction in scatter intermediate between the two shown.

Comparing Figures 4.3 and 4.4 it is apparent that in case 096 the variation of $\bar{G}_r$ with tower level is considerably less than the corresponding variation in $\bar{G}_T$. All of the curves are represented very well by the relation

$$\bar{G}_r = 1.05 + .165 \log_{10} T \qquad (4.3)$$

From (4.2), $\bar{G}_T$ is given by

$$\bar{G}_T = 1 + 6\ \frac{\sigma_V}{\bar{V}}\ (\bar{G}_r - 1) \qquad (4.4)$$

The relation (4.4) in conjunction with (4.3) and the appropriate values of $\bar{V}/\sigma_V$ in Table 4.1 provide an excellent parametric representation of $\bar{G}_T$ for Case 096.

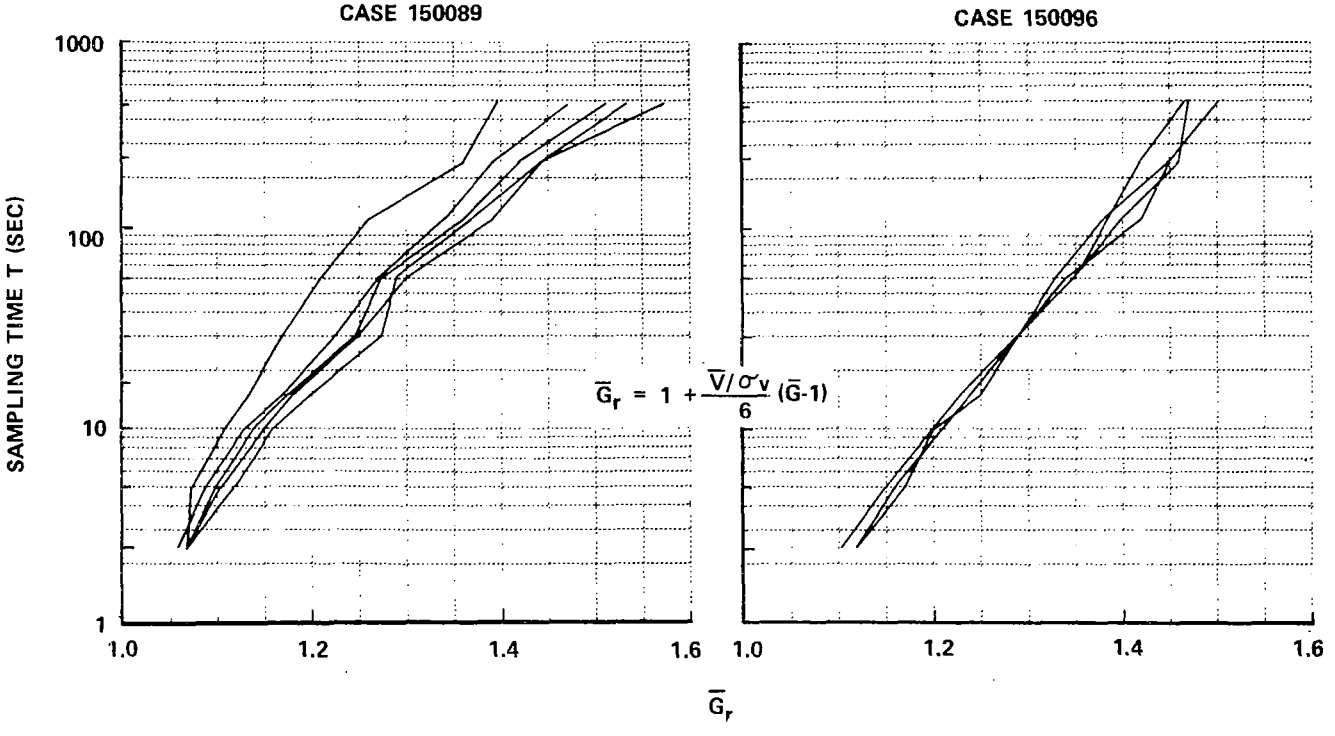

Figure 4.4 SCALED MEAN GUST FACTOR $\bar{G}_r$ FOR VARIOUS HEIGHTS AS A FUNCTION OF SAMPLING PERIOD, CASES 089 AND 096

Referring again to Figures 4.3 and 4.4, it is apparent that in Case 089 only part of the differences between the plots of $\bar{G}_\tau$ can be ascribed to variations in $\bar{V}/\sigma_V$. Those differences which are not due to variations in $\bar{V}/\sigma_V$ are reflected in the diversity of the $\bar{G}_\tau$ plots in Figure 4.4 and must be the result of differences in the statistical scales and forms of the wind speed variations at the various heights.

Of the statistical scales upon which $\bar{G}_\tau$ depends, the most important are the time scales. We turn our attention next to the choice of an appropriate time scale to characterize the behavior of $\bar{G}_\tau$. To start, we shall show that $\bar{G}_\tau$ is sensitive to the behavior of the autocorrelation, $\rho_V(\tau)$ of the wind speed at relatively small values of τ but not at large values of τ . Whatever the wind speed level considered there are far more gusts per hour with short durations (of the order of seconds in the cases for which we have gust duration data) than long durations (of the order of tens of seconds). It follows that $\bar{G}_\tau$ is very sensitive to the statistics of the short duration gusts and relatively insensitive to the statistics of the long duration gusts. Since $\rho_V(\tau)$ at small τ is very sensitive to the durations of the short term gusts and relatively insensitive to long duration gusts, that time scale which best characterizes $\rho_V(\tau)$ at small τ should best characterize $\bar{G}_\tau$.

Experimental data on the autocorrelation function $\rho_L(\tau)$ of the longitudinal component were available for two of the cases studied. Since the statistics of wind speed and longitudinal velocity are approximately the same (Lumley and Panofsky, pg. 154), these data for $\rho_L(\tau)$ were utilized for determination of time scales. For small values of τ , $\rho_L(\tau)$ can be represented by

$$\rho_L(\tau) = 1 - \left(\frac{\tau}{\tau_o}\right)^{2/3} \qquad (4.5)$$

where the time scale τ_o completely characterizes $\rho_L(\tau)$ for the region in which the equation is valid.* Values of τ_o in Cases 096 and 067 are

*Since the Obukhov inner time scale is apparently less than the response time of the anemometers employed, the relation (4.5) fits the experimental data for the shortest measured lags.

listed in Table 4.1. These values were obtained by fitting (4.5) at small τ to small photographic reproductions of the autocorrelation plots, and it is estimated that they are only accurate to about ±10 percent.

The influence of the time scale τ_0 on $\bar{G}_T$ or $\bar{G}_\tau$ can be removed by scaling the sampling duration T by τ_0. Thus, a set of plots of $\bar{G}_\tau$ versus T/τ_0 should display noticeably less spread than the corresponding set of plots of $\bar{G}_\tau$ versus T if the time scale is significant in determining the variation of gust factor with sampling time. Values of $\bar{G}_\tau$ are shown plotted against $26\,T/\tau_0$ in Figure 4.5. The numerical constant is arbitrary; it was chosen to facilitate comparison between this and previous figures. Each data point represents the mean gust factor for one height and one sampling period. Because of the large number of points, those points for various times from the same case and height have not been connected by line segments as in previous figures.

Figure 4.5 contains data from Cases 067, 096, and 089. Since τ_0 values were not available for the latter case, a mean τ_0 was chosen to give the best overall agreement with the other two cases, and τ_0 was varied for the different observation heights according to the inverse of mean wind speed. The values of τ_0 used are given in Table 4.1.

It can be seen that the line given by Equation (4.3), generalized for any τ_0 in the form

$$\bar{G}_\tau = 1.05 + .165 \log_{10}\left(\frac{26T}{\tau_0}\right) \qquad (4.6)$$

gives a good approximate fit to all data points. It follows that the expression for $\bar{G}_\tau$ in (4.6) in conjunction with the expression for $\bar{G}_T$ in (4.4) provides a good parametric representation of $\bar{G}_T$ in all the cases studied. Combining the two equations,

$$\bar{G}_T = 1 + 6\,\frac{\sigma_V}{\bar{V}}\left[.05 + .165 \log_{10}\left(\frac{26T}{\tau_0}\right)\right] \qquad (4.7)$$

On the basis of the limited evidence available, it appears that estimates of $\bar{G}_T$ based on this equation should be approximately valid for many cases.

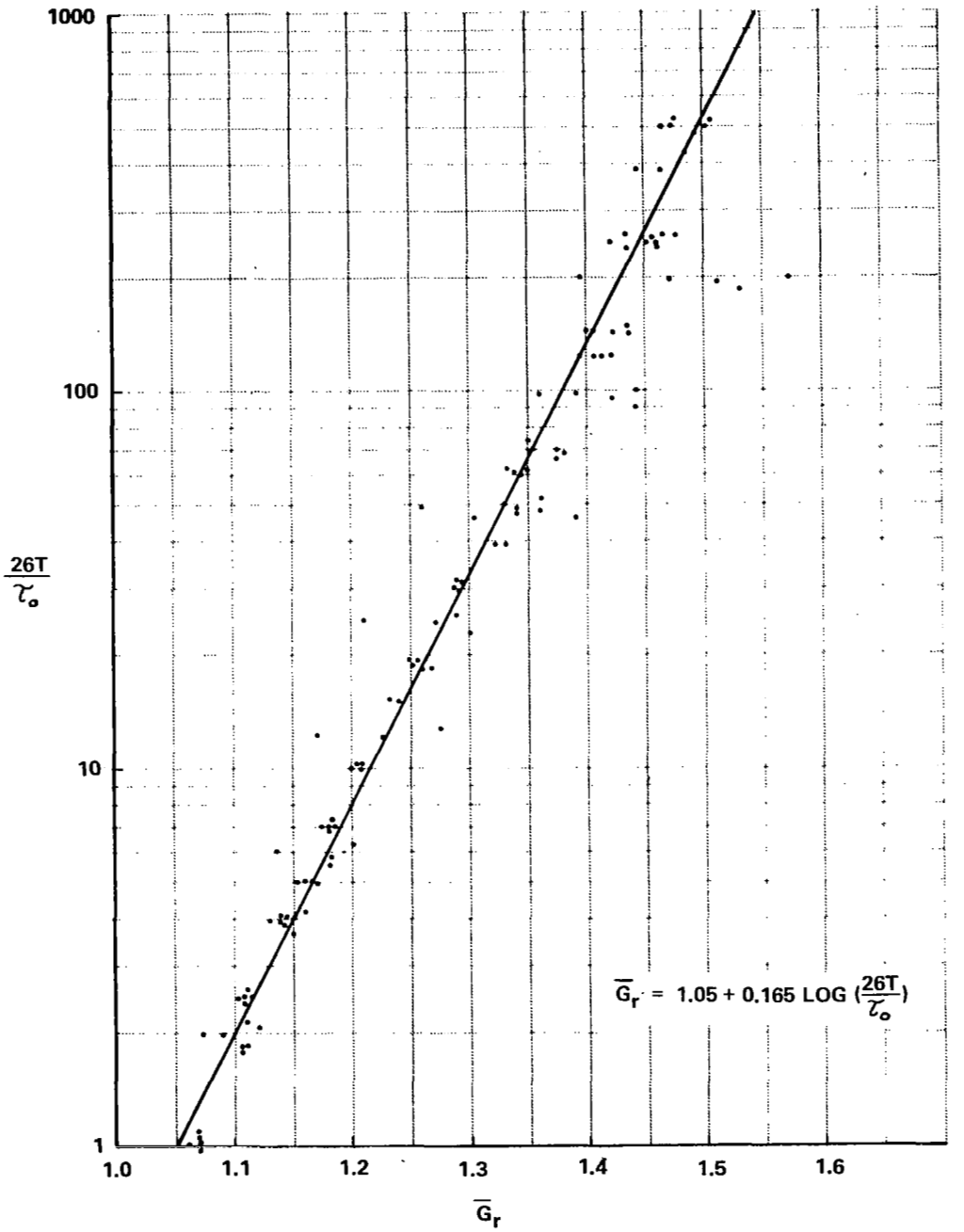

Figure 4.5 OBSERVED MEAN GUST FACTORS PLOTTED IN SCALED COORDINATES. SCALED GUST FACTOR $\overline{G}_r$ COMPUTED AS FOR FIGURE 4.4, SAMPLING TIME SCALED BY $26/\tau_o$. EQUATION GIVES STRAIGHT-LINE FIT TO THE DATA

2. Frequency Distribution of Gust Factor

In closing our discussion of the dependence of gust factor on sample duration, we discuss briefly the shape and spread of the frequency distributions of gust factor. Observations of the shapes of these distributions in various cases chosen at random reveal that they are approximately Gaussian and quite symmetric for sample durations of 15 seconds and less. For sample durations from 30 to 60 seconds the distributions are skewed in such a manner that the mean is up to 10% greater than the most probable value. For durations of 120 seconds and greater there were not enough points to obtain good estimates of the shapes.

To obtain an assessment of the dependence of spread of the gust factor distributions on sample duration, the 25% and 75% percentile values in the cumulative distributions of G_r were computed for all six tower levels (18 m to 150 m) and each of the nine sample durations in Case 096. These results are summarized in Figure 4.6, which indicates upper and lower bounds on the computed 25% and 75% percentiles as a function of sample duration. As an example of the significance of the plots in Figure 4.6, consider a sample duration of 15 seconds. From the figure the 75% percentile values for all tower levels and this sample duration were between $G_r = 1.28$ and $G_r = 1.33$ while the 25% percentile values were between $G_r = 1.16$ and 1.20. The plots have a similar interpretation for other sample durations.

It will be observed from Figure 4.6 that for sample durations less than 120 seconds there is only a gradual increase in the spread of the distributions of G_r with sample duration. The large values of the upper bounds on the 75% percentile values at durations of 240 and 480 seconds, apparent in the figure, are the result of untypically large (and therefore perhaps statistically improbable) 75% percentile values at the 90-meter level. We can approximate each of the four plots in Figure 4.6 by straight lines. Those straight lines which best fit the upper bounds on the 75% percentile values and the lower bounds on the 25% percentile values can be employed as pessimistic averages for the variations of the 75% and 25% percentile values with sample duration. They are given by

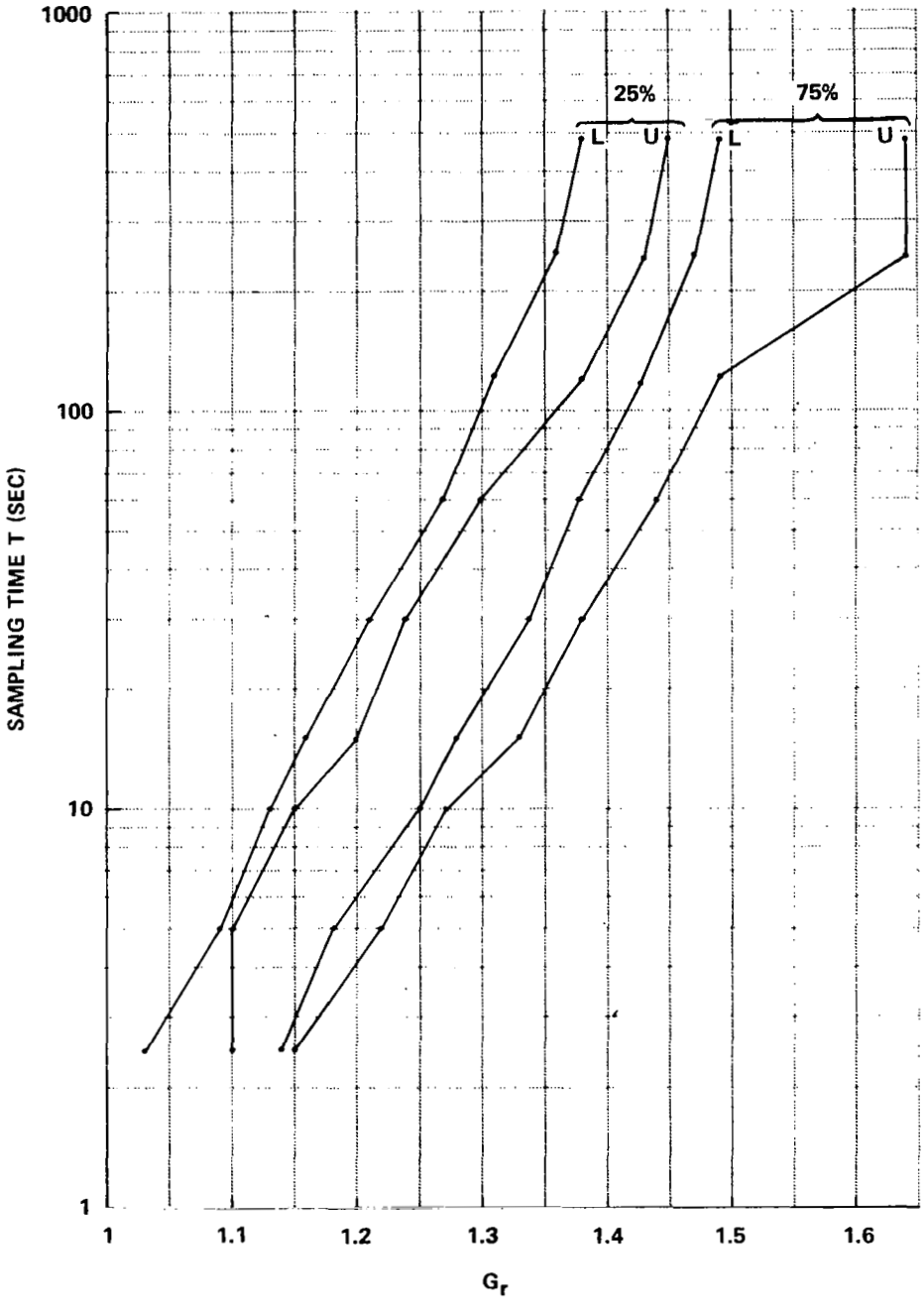

Figure 4.6 UPPER AND LOWER BOUNDS ON 25 AND 75 PERCENTILES OF SCALED GUST FACTOR DISTRIBUTIONS (FOR VARIOUS HEIGHTS) AS FUNCTIONS OF SAMPLING PERIOD. CASE 150096

$$25\% \text{ percentile value of } G_r = .97 + .16 \log_{10} (26T/\tau_o) \qquad (4.8)$$

$$75\% \text{ percentile value of } G_r = 1.07 + .20 \log_{10} (26T/\tau_o) \qquad (4.9)$$

These expressions in conjunction with the expression

$$G_T = \frac{6}{(\bar{V}/\sigma_V)} (G_r - 1) + 1$$

constitute tentative relations for quantitative estimation of probabilities of occurrence of values of the gust factor G_T for given $\bar{V}/\sigma_V$, τ_o and sample duration T, where $26T/\tau_o$ lies in the range from 2.5 to 480.

C. Duration of Gusts

1. Distributions of Gust Duration

Of particular interest in the description of gusts is information pertaining to how often the wind speed rises to a given level and how long it may be expected to exceed this level. This information is contained in the frequency distributions of time intervals between successive positive-slope and negative-slope level crossings for selected wind speed levels. In discussing these statistics it is convenient, with regard to a given wind speed level, to refer to the wind speed variation between any pair of successive positive-slope and negative-slope level crossings as a gust, and to the time difference between the level crossings as the gust duration. With these definitions, we will, without fear of misunderstanding, employ the term frequency distribution of gust durations at a given wind speed level.

Frequency distributions have been computed for Cases 150096, 150067, and 150089. In each case the computations included all tower heights and wind speed levels spaced by increments of 0.5 m sec^{-1}. The statistical data chosen for discussion are presented in Figures 4.7, 4.8, and 4.9. Figure 4.7 contains data on frequency distributions of gust duration for the wind speed levels from 5 to 11 m/s in Case 096 - 18 m height. It will be observed that there are two different ordinate scales in the figure. The scale to the left indicates the wind speed in m sec^{-1} and the scale to the right indicates values of $(V-\bar{V})/\sigma_V$. The abscissa gives the gust duration, Δ, in seconds. All gust durations except zero are marked on a logarithmic

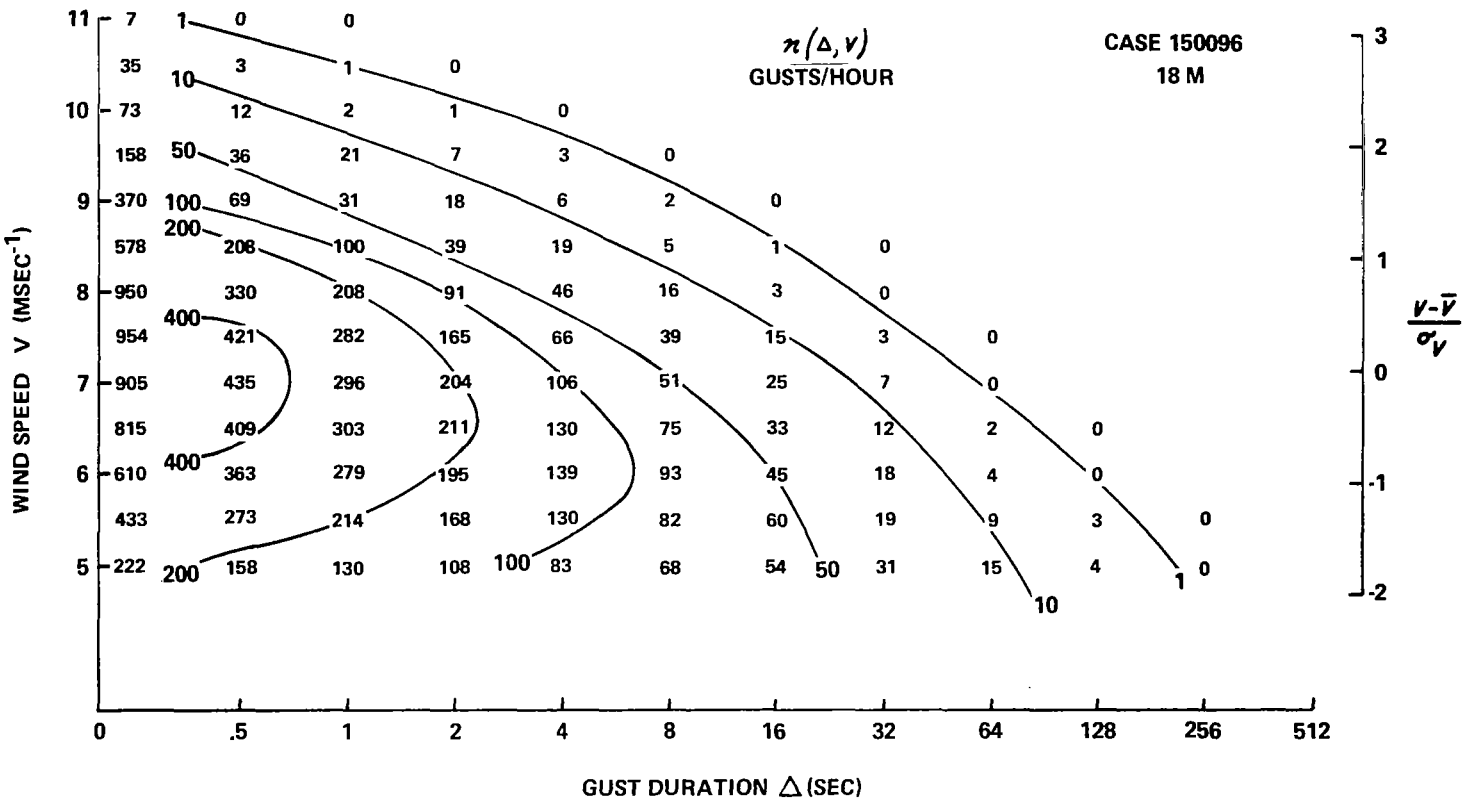

Figure 4.7 CUMULATIVE DISTRIBUTIONS OF GUST DURATION, CASE 096, 18 M. PLOTTED VALUES GIVE NUMBER OF GUSTS PER HOUR EXCEEDING SPEED V AND LASTING LONGER THAN Δ

scale. Each numeral in the body of the plot indicates the (average) number of gusts per hour for which the gust duration indicated by the coordinate on the abscissa is exceeded in the case of the wind speed level indicated by the numeral on the ordinate. For example, referring to the 9 m sec^{-1} wind speed level in Figure 4.7, we conclude that there were 31 gusts per hour with gust durations greater than one second in the case of the 9 m sec^{-1} wind speed level.

The curves in Figure 4.7 are smoothed contours of constant gust frequency. It will be observed that the high-gust-frequency contours bend back so that the wind speed is not a single-valued function of gust duration on a high-gust-frequency contour. This behavior can be understood by consideration of a somewhat oversimplified model in which the wind speed variations consist of a superposition of low-amplitude, short-duration gusts at a roughly constant repetition frequency on top of more gradual, longer duration wind variations.

Figures 4.8 and 4.9 contain gust-duration data for Cases 067-60m and 089-18m, respectively. Note that the same scale for $(V - \bar{V})/\sigma_V$ is employed in all three gust-duration figures. This choice of ordinate scale offsets the effects of the different values of $\bar{V}$ and σ_V in the three cases, and thus provides a more meaningful basis for comparison. In order to partially offset the effects of an approximate factor of two difference between the time scale τ_o in Case 089 and the other two cases, in Figure 4.9 the numerals in the body of the plot are gusts per two hours (rather than gusts per hour) and the abscissa indicates half the gust duration in units of seconds.* With these exceptions, all three figures have the same interpretation.

While the agreement between Figures 4.7 and 4.9 is poorer than that between Figures 4.7 and 4.8, it is clear that Figure 4.7 is roughly

*Since the τ_o scales are approximately equal in Cases 096-18m and 067-60m no attempt has been made to compensate for their difference in Figures 4.7 and 4.8.

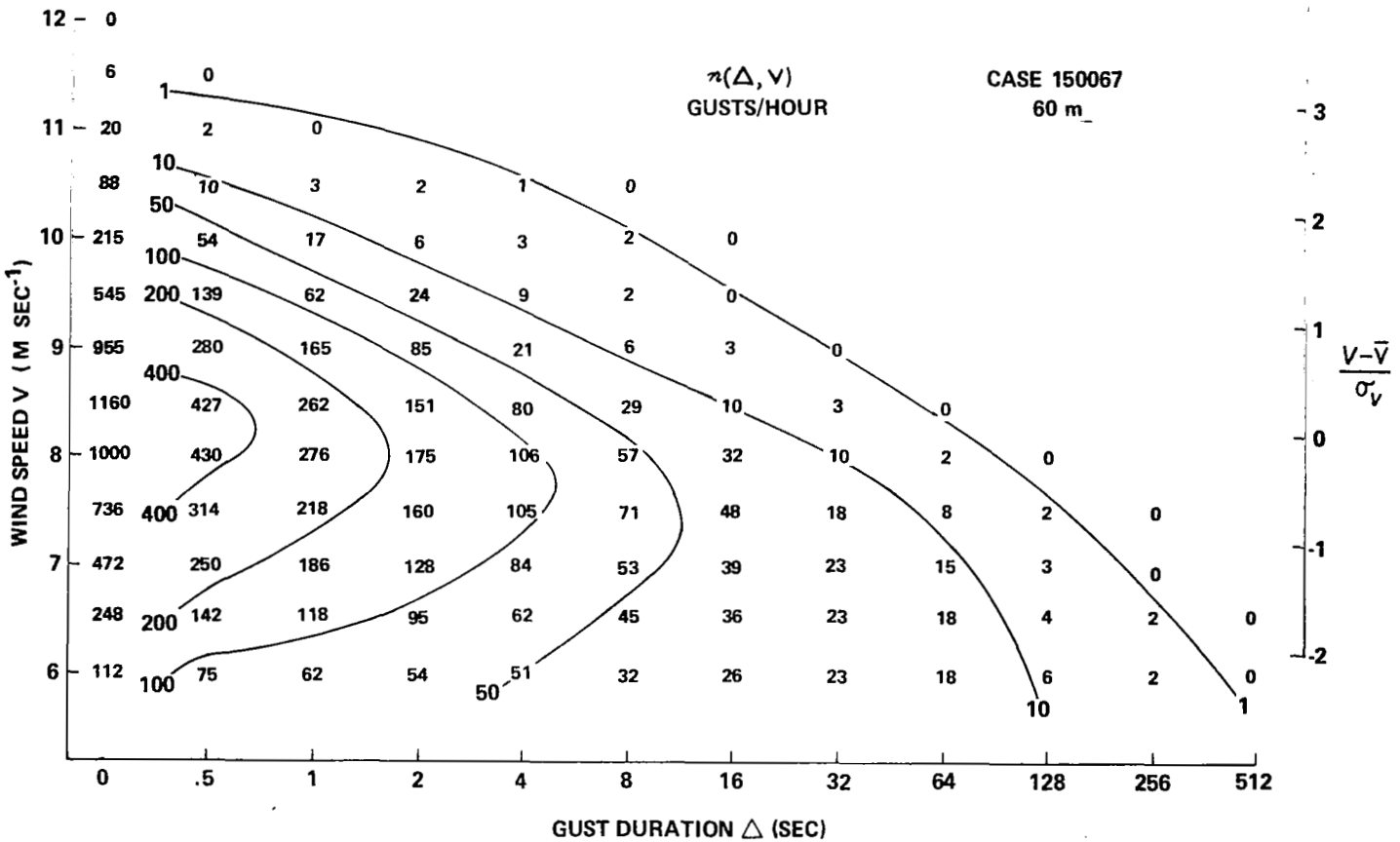

Figure 4.8 CUMULATIVE DISTRIBUTIONS OF GUST DURATION, CASE 067, 60 M.PLOTTED VALUES GIVE NUMBER OF GUSTS PER HOUR EXCEEDING SPEED V AND LASTING LONGER THAN Δ

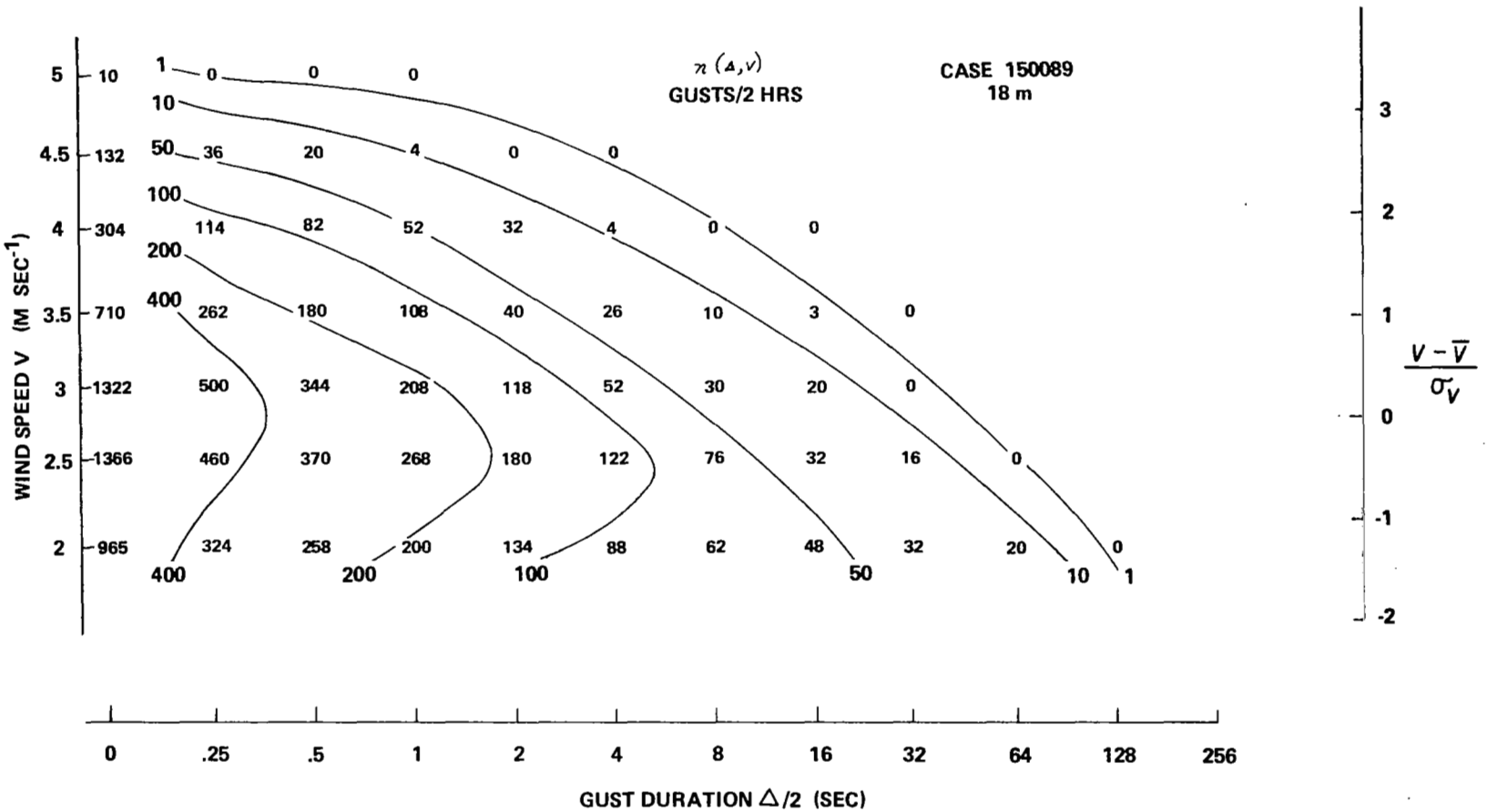

Figure 4.9 CUMULATIVE DISTRIBUTIONS OF GUST DURATION, CASE 089, 18 M.PLOTTED VALUES GIVE NUMBER OF GUSTS PER TWO HOURS EXCEEDING SPEED V AND LASTING LONGER THAN Δ

representative of all three of these rather diverse cases. Accordingly, it is reasonable to assume that useful estimates of gust durations for other values of $\bar{V}$, σ_V and τ_o can be obtained by scaling the data in Figure 4.7.

2. Gust Duration Probabilities

In discussing the explicit information given in the gust-duration plots it is convenient to employ the symbol $n(\Delta, V)$ to denote the number of gusts per hour at the wind speed level V with durations greater than Δ. While the general trends of $n(\Delta, V)$ as a function of both V and Δ are obvious from perusal of the gust-duration plots, certain characteristics merit special attention. Of particular interest is the sparsity of long-duration gusts, particularly at the higher wind speed levels. For example, Figure 4.7 indicates only 51 gusts per hour with durations greater than 8 seconds, as compared to over 800 gusts per hour with durations less than 8 seconds in the case of the 7 m sec^{-1} wind speed level.

The gust-duration data can be employed to answer such questions as: If a time point is chosen at random within a very long sample of wind speed variations, what is the probability that this time point lies within a gust of duration greater than Δ at the wind speed level V? The answer is clearly equal to the combined fractional duration of all gusts with durations greater than Δ at the wind speed level V. This fractional duration is given by

$$D(\Delta, V) = -\frac{1}{3600}\int_{\Delta}^{\infty} \bar{\Delta}\ \frac{\partial n(\bar{\Delta}, V)}{\partial \bar{\Delta}}\, d\bar{\Delta} \qquad (4.10)$$

where Δ is in seconds and $n(\Delta, V)$ is the number of gusts per hour. If $P(\Delta, V)d\Delta$ denotes the probability that a time point chosen at random lies within a gust with duration between Δ and $\Delta + d\Delta$ at the wind speed level V it is clear that*

$$D(\Delta, V) = \int_{\Delta}^{\infty} P(\bar{\Delta}, V)\, d\bar{\Delta} \qquad (4.11)$$

*Observe that $D(0, V) < 1$ for $V > 0$ so that $P(\Delta, V)$ is not normalized in the usual manner.

whence

$$P(\Delta, V) = -\frac{\Delta}{3600} \frac{\partial n(\Delta, V)}{\partial \Delta} \tag{4.12}$$

Various other probabilities can be determined from the gust-duration data. Of particular interest is the probability distribution for gust durations at the wind speed level V. In a very long sample of duration T hours the total number of gusts with durations greater than Δ at the wind speed level V is given by $Tn(\Delta, V)$. Therefore, if a single gust is chosen at random from those with durations greater than zero in this sample, the probability that this gust will have a duration greater than Δ at the wind speed level V is given by

$$\frac{n(\Delta, V)}{n(0, V)} \tag{4.13}$$

The probabilities in (4.11) and (4.13) provide separate measures of the characteristics of gusts at a given wind speed level. The probability in (4.13) provides no indication of whether the wind speed is likely to be greater than V at a randomly chosen time t. However, if it is assumed that a gust is incident on a structure at time t (i.e., given that a gust is beginning at the level V at time t) the probability in (4.13) provides the likelihood for various durations of the gust. The probability in (4.11) provides not only the likelihood that the wind speed is greater than V at a randomly chosen time t but also the likelihood that at time t a physical structure is in the process of subjection to a gust of duration greater than Δ at the wind speed level V.*

*Clearly D(0, V) is equal to the unconditional probability that the wind speed is greater than V at a randomly chosen time. The probability in (4.11) should not be confused with the joint probability that the wind speed is both greater than V at a randomly chosen time and will continue to be greater than V throughout an additional time interval of duration greater than Δ. This latter probability is equal to $[D(\Delta, V) - \Delta n(\Delta, V)/3600]$.

A consideration of the functions $n(\Delta, V)$ and $D(\Delta, V)$ for the wind speed level $V = 7$ m sec^{-1} in Case 096-18m provides an informative application of the probability analysis. For convenience, the functions in (4.11) and (4.13) for this case have been plotted in Figure 4.10 to indicate their shape. $D(\Delta, 7)$ was computed by graphical differentiation and integration employing the formulas in 4.11 and 4.12. The abscissa in Figure 4.10 is $\log_2 \Delta$ with Δ in seconds.

The median gust duration is that value of Δ for which $n(\Delta, 7)/n(0, 7) = 1/2$. From Figure 4.10 we conclude that the median gust duration is less than 0.5 sec for Case 096-18m. From (4.10) the mean gust duration is given by

$$\text{Mean gust duration at level V} = \frac{3600\, D(0, V)}{n(0, V)}$$

so that for this case the mean gust duration at the 7 m sec^{-1} level is 2.2 sec. The small values for the median and mean gust durations are not surprising in view of the trend of $n(\Delta, V)$ with Δ.

Turning to a consideration of the probability density $P(\Delta, V)$ defined in the context of (4.12), we conclude that the median for this distribution is that value of Δ for which $D(\Delta, V) = D(0, V)/2$. Employing Figure 4.10 we obtain a median value of 8 seconds. The significance of this median is as follows: If a time point is chosen at random within a very long sample displaying the statistics of Case 096-18 m, then there is a 45% probability that the wind speed is less than 7 m sec^{-1} at this time point; a 27.5% probability that the time point lies within a gust with duration greater than 8 seconds at the 7 m sec^{-1} level and a 27.5% probability that the time point lies within a gust of duration less than 8 seconds (but greater than zero seconds) at the 7 m sec^{-1} level. Since $D(\Delta, V)$ is equal to the combined fractional duration of all gusts with durations greater than Δ at the wind speed level V, we can also conclude that the fixed point at which the wind speed is measured will be subjected to gusts of duration greater than 8 seconds at the level 7 m sec^{-1} for 27.5% of the time. This result indicates that gusts with duration greater than 8 seconds at the 7 m sec^{-1} level constitute an important fraction of the

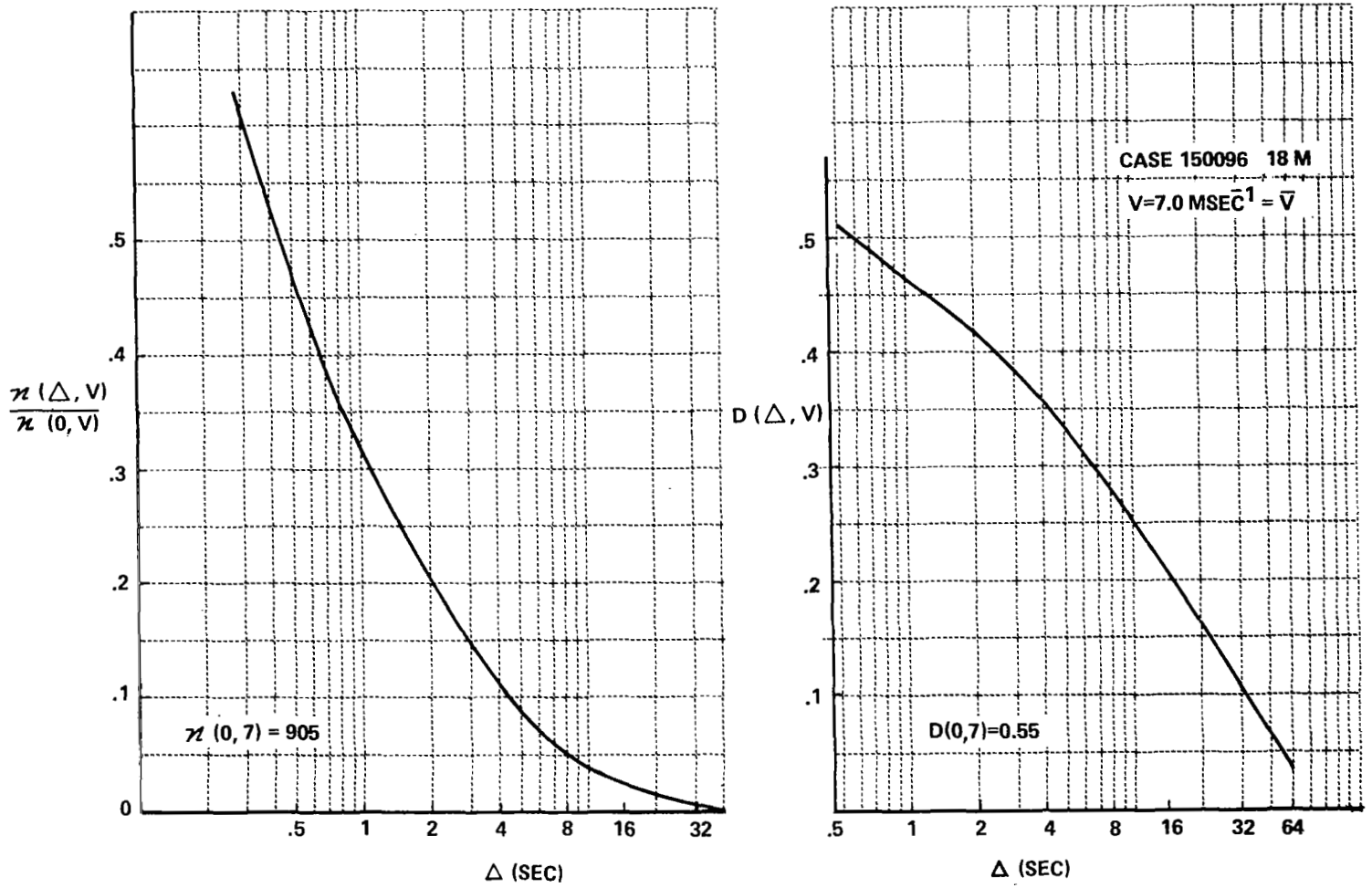

Figure 4.10 PROBABILITY FUNCTIONS IN EQUATIONS 4.11 AND 4.13 DERIVED FROM GUST DURATION DATA FOR CASE 096, 18 m, 7 M SEC^{-1} WIND SPEED LEVEL

structure of the wind speed variations in spite of their relatively low frequencies as compared to the shorter duration gusts.

For comparison, Figure 4.11 shows curves of $n(\Delta, V)/n(0, V)$ and $D(\Delta, V)$ for the same wind speed record but for $V = 9.5$ m sec^{-1}. This wind speed level is approximately 2σ above the mean. As would be expected, the probabilities are substantially lower in both distributions. For example, given that a gust is occurring, there is only a 13% chance that the gust will have a duration greater than one second (from $n(\Delta, V)/n(0, V)$ curve). Picking a time at random, there is only a 0.9% chance that a gust exceeding one second duration is occurring, and less than a 3% chance that any gust is occurring at the 9.5 m sec^{-1} level (from $D(\Delta, V)$ curve). Thus, at this relatively high wind speed level, there are few long gusts (as at 7 m sec^{-1}), and gusts longer than one second occupy a very small fraction of the total time (unlike gusts at the 7 m sec^{-1} level).

D. Gust Acceleration Statistics

In the preceding sections data have been presented on the magnitude of wind gusts (gust factor) and on the time duration of gusts at various wind speed levels. One further gust characteristic, of particular importance to the vehicle design engineer, is the rate of change of wind speed, especially during the onset of a strong gust. The rate of change of wind speed, which will be referred to as gust acceleration, was investigated by computing distributions of wind speed for various times after the wind crossed a given level.

1. Conditional Wind Speed Distributions

The statistics on gust accelerations provide information on the dependence of the average gust acceleration over a given time interval on the duration of the interval, and also the dependence on the wind speed at the beginning of the interval. These statistics are contained in, and readily derivable from, frequency distributions of wind speed which are conditional on the wind speed having a given value at a time which is earlier by a specified interval. For brevity in the following discussion we shall refer to these distributions by the term "conditional wind speed distributions."

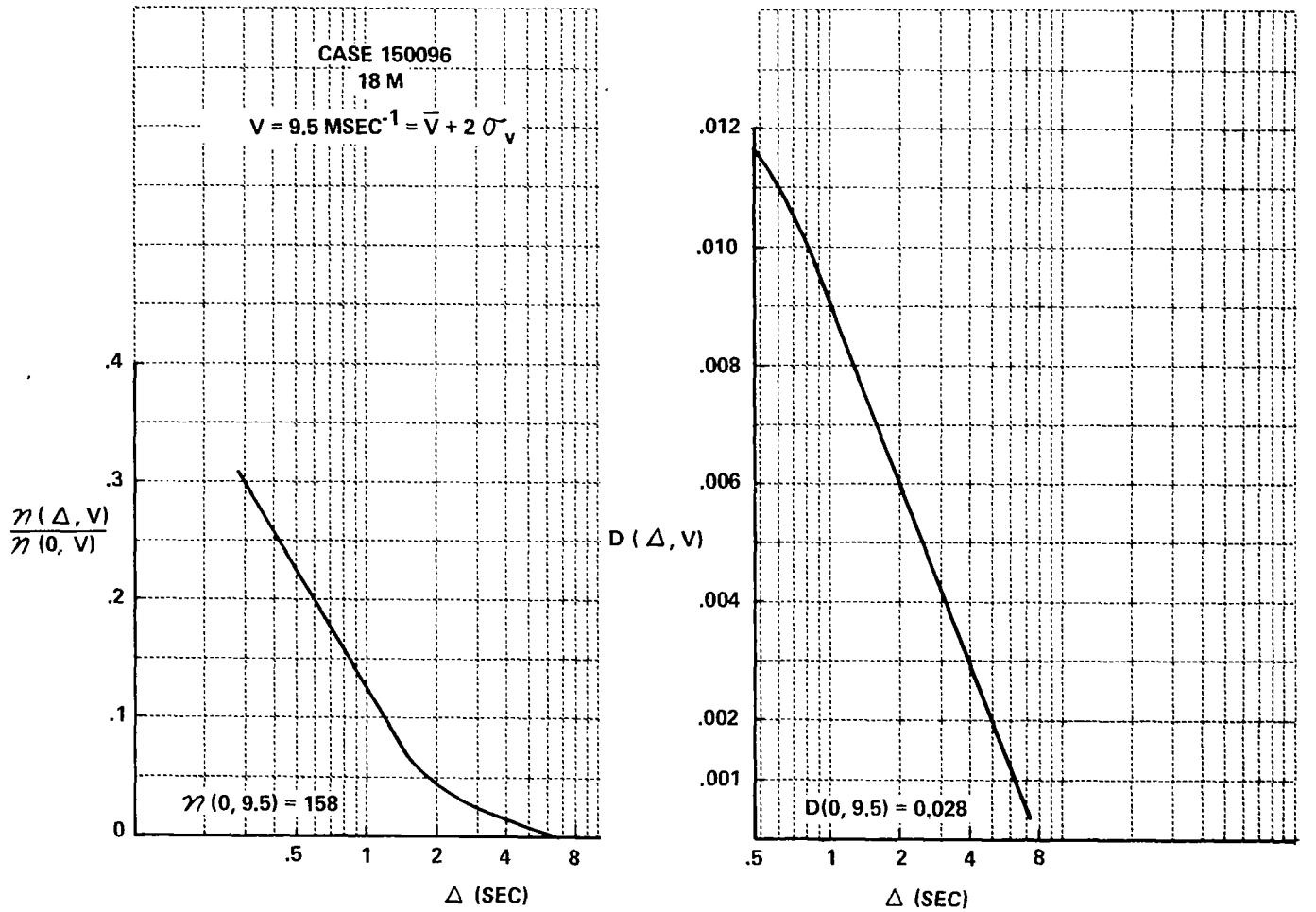

Figure 4.11 PROBABILITY FUNCTIONS IN EQUATIONS 4.11 AND 4.13 DERIVED FROM GUST DURATION DATA FOR CASE 096, 18 m, 9.5 M SEC^{-1} WIND SPEED LEVEL

Figure 4.12 shows some conditional wind speed distributions for Case 096-18m. All of the distributions in Figure 4.12 have been computed for an initial (or conditional) value of wind speed of 7 m sec^{-1}. As an example of how to interpret the plot we refer to the intersection of the 1-second lag abscissa value and the 8 m sec^{-1} ordinate value, obtaining the numeral 90. This value indicates that 1 second after the wind speed was 7 m sec^{-1} there was a 90% probability that the wind speed was less than 8 m sec^{-1}. Similarly, we see from the plot that 10 seconds after the wind speed was 7 m sec^{-1} there was an 81% probability that the wind speed was less than 8 m sec^{-1}.

The cumulative probability contours in Figure 4.12 were not constructed from the plotted numerals, but from an approximate mathematical model which is described below. Since the contours are not accurate for small lags, cumulative probability values should be obtained from the numerals rather than the contours.

Conditional wind speed distributions may be employed to determine the quantitative dependence of gust acceleration on initial wind speed. Referring to Figure 4.12 we see that there is a 5% probability of finding a wind speed greater than 8.5 m sec^{-1} (representing an increase of 1.5 m sec^{-1} or more above the initial value) after a lag of 2 seconds. This means that there is a 5% probability of observing an average gust acceleration of 0.75 m/sec^2 or greater over an interval of 2 seconds when the initial value of wind speed is 7 m sec^{-1}. To determine the variation of the probability with initial wind speed, we employ the plots in Figures 4.13 and 4.14, which show conditional distributions for Case 096-18 m for initial speeds of 5 and 9 m sec^{-1} respectively. From Figure 4.13 there is a 24% probability of finding an increase of 1.5 m sec^{-1} or greater in wind speed after a lag of 2 seconds and from Figure 4.14 there is a 1% probability of finding an increase of 1.5 m sec^{-1} or greater in wind speed after a lag of 2 seconds. From these figures it can be concluded that in Case 096-18m the probability of observing an average gust acceleration of 0.75 m/sec^2 or greater over a 2-second interval is 24% for an initial wind speed of 5 m/s, 5% in the case of an initial wind speed of 7 m/s, and only 1% for an initial wind speed of 9 m/s. This dependence of

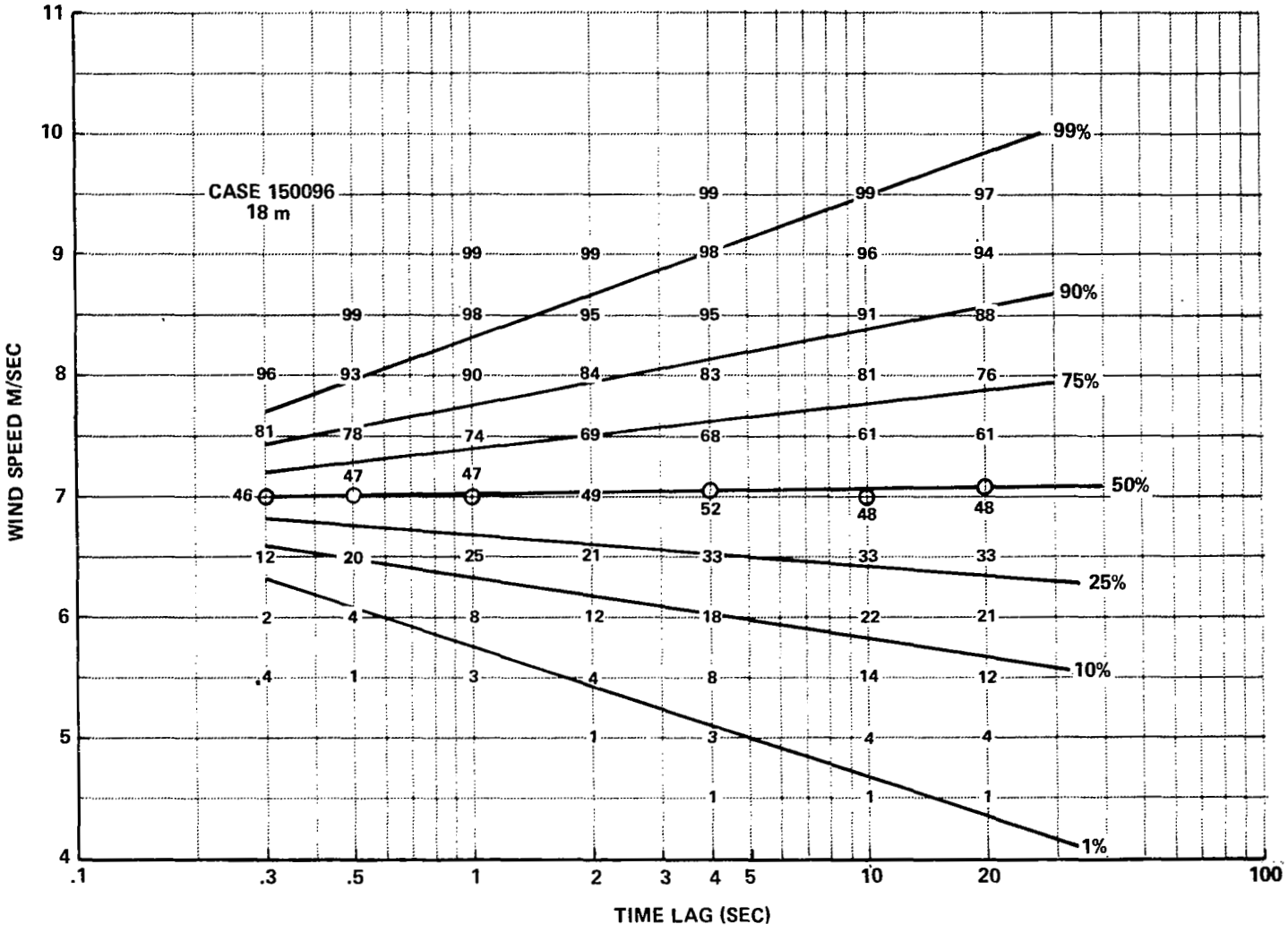

Figure 4.12 CONDITIONAL WIND SPEED DISTRIBUTIONS FOR VARIOUS TIME LAGS, CONDITIONAL ON A SPEED OF 7 M SEC^{-1} AT LAG ZERO. CASE 096, 18 M HEIGHT. NUMBERS ARE FROM WIND MEASUREMENTS, CONTOURS FROM MATHEMATICAL MODEL

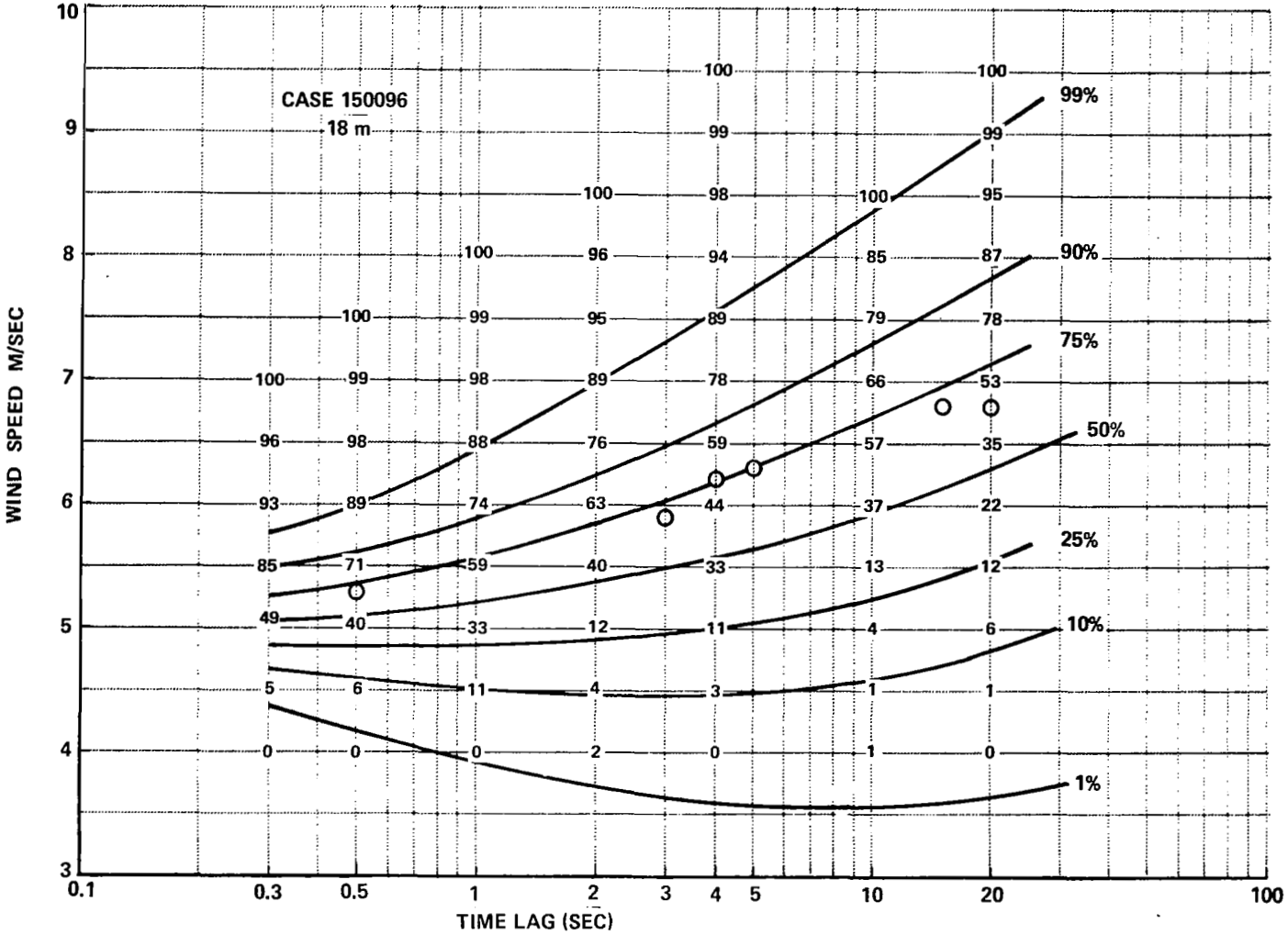

Figure 4.13 CONDITIONAL WIND SPEED DISTRIBUTIONS FOR VARIOUS TIME LAGS, CONDITIONAL ON A SPEED OF 5 M SEC^{-1} AT LAG ZERO. CASE 096, 18 M HEIGHT. NUMBERS ARE FROM WIND MEASUREMENTS, CONTOURS FROM MATHEMATICAL MODEL

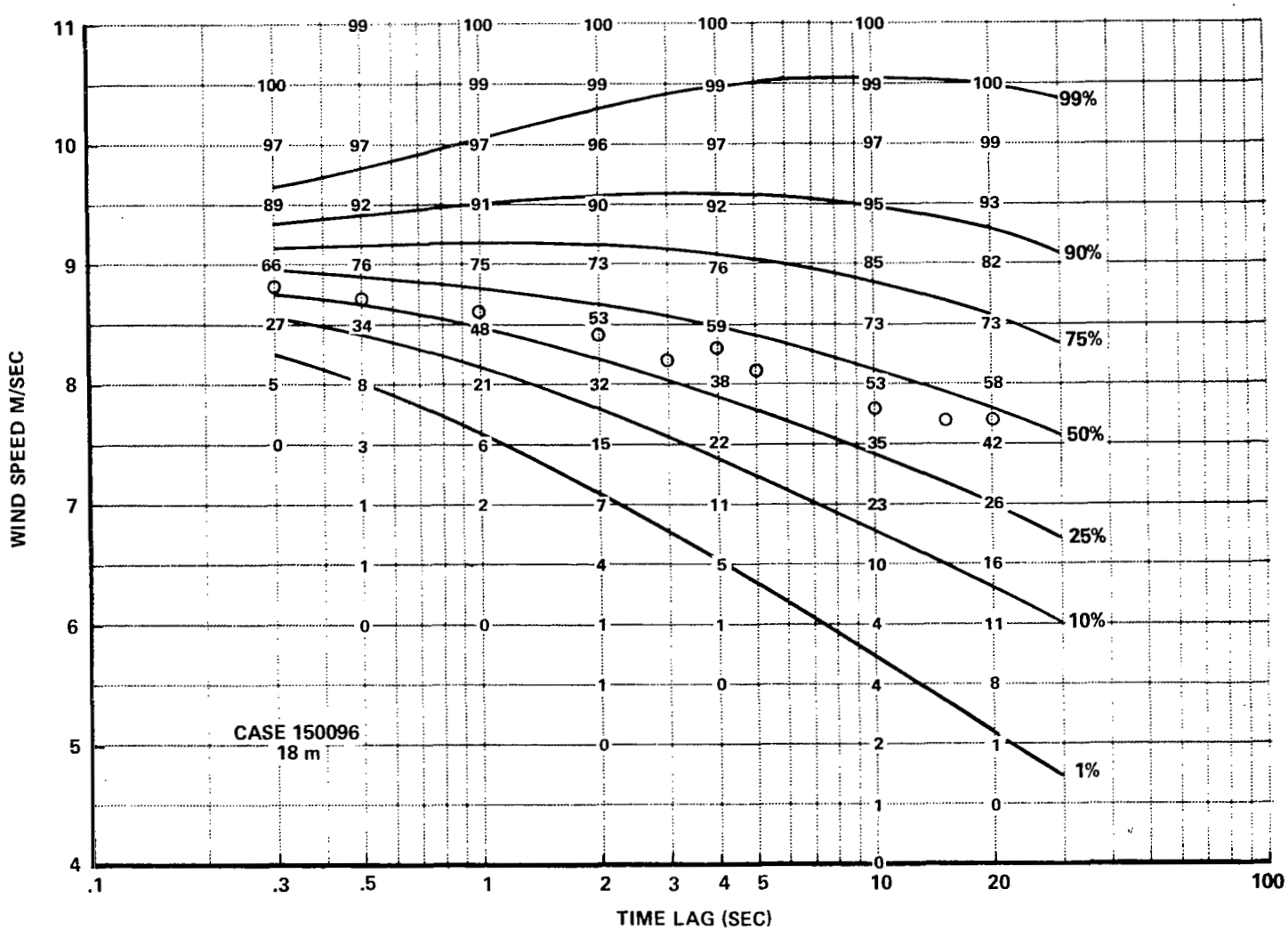

Figure 4.14 CONDITIONAL WIND SPEED DISTRIBUTIONS FOR VARIOUS TIME LAGS, CONDITIONAL ON A SPEED OF 9 M SEC^{-1} AT LAG ZERO. CASE 096, 18 M HEIGHT. NUMBERS ARE FROM WIND MEASUREMENTS, CONTOURS FROM MATHEMATICAL MODEL

probability of occurrence of a given average gust acceleration on the initial value of wind speed is of course expected since the wind speed is more likely to increase if it has a small value than if it has a large value.

By combining data from the conditional distributions with gust duration data one can obtain quantitative information on the frequencies of occurrence of gusts with large accelerations. As an example, from Figure 4.7 there were 905 gusts/hr at the 7 m sec^{-1} level in Case 096-18m. From Figure 4.12 the wind speed exceeded 9 m sec^{-1} about 1% of the time following 1 second after a 7 m sec^{-1} level crossing. Therefore, there are expected to be 1810/100 or about 18 occurrences per hour in which the wind speed rises from 7 to 9 m sec^{-1} or greater in 1 second or less. This method of computing may be employed for various lags and average accelerations. However, for long lags and small accelerations the prediction does not necessarily refer to a discrete gust in which the wind speed rises from the initial to the final value without further crossings of the initial level at intermediate times.

Since the accelerations under discussion are large and the time intervals small, it is appropriate to consider whether the response of the Merritt Island tower anemometers is adequate to measure the actual wind changes which occur. Camp (9) has calculated theoretical maximum accelerations which can be measured by the anemometers, on the basis of experimentally determined instrument response. Comparing Camp's maximum measurable acceleration with the maximum accelerations calculated here, it is found that the two are essentially the same for time intervals of 0.5 sec and less. This suggests that the observed accelerations are limited by anemometer response, and that in fact greater accelerations may occur. However, for all time periods longer than 0.5 sec, the experimental average accelerations are substantially less than the maximum observable, and so are believed to be correct.

2. A Mathematical Model for Conditional Wind Distributions

There is a conditional wind speed distribution for each time lag, so that Figure 4.12, for example, contains data on seven different conditional

distributions with time lags from 0.3 to 20.0 seconds. Fundamental parameters of each distribution are the mean and the standard deviation. To distinguish these parameters from the corresponding ones for the unconditional wind speed distributions we shall refer to them as the conditional mean and the conditional standard deviation (or conditional sigma).

Both the conditional mean and conditional sigma vary with time lag. Since the wind speed decorrelates for long lags, the conditional wind speed distribution will be the same as the unconditional wind speed distribution after very long lags. The gradual increase of conditional sigma with time lag is quite apparent in Figure 4.12. Since the wind speed is almost completely decorrelated after about 100 seconds in this case, the difference between the unconditional and conditional wind speed distributions should be quite small for lags greater than 100 seconds. Indeed, the distribution for a time lag of 20 seconds in Figure 4.12 differs by only 1 to 2% from the unconditional distribution.

The conditional mean will be equal to the initial (or conditional) wind speed at lag zero and equal to the unconditional mean after long lags. Since the unconditional wind speed is about 7.1 m sec^{-1} in Case 096-18 m the conditional mean in Figure 4.12 should vary gradually from 7 m sec^{-1} at short lags to 7.1 m sec^{-1} at long lags. This behavior is apparent in the 50% contour in Figure 4.12 though it is not so apparent in the conditional means computed from the data. The latter are indicated by circles and are all equal to 7 m sec^{-1} except for the value 7.1 m sec^{-1} at 20 seconds. The variation of conditional mean with time lag shows up more clearly when the initial wind speed differs appreciably from the unconditional mean, as in Figures 4.13 and 4.14.

The probability contours in Figures 4.12 through 4.14 were computed from the well-known multivariate Gaussian conditional distribution. This particular mathematical distribution was chosen because it is simple and it accounts for the observed qualitative trends with time lag in the conditional means and variances. To define the mathematical distribution let

$$P(V_2 \mid V_1) \propto V_2$$

denote the probability of finding the wind speed at time $t + \tau$ in an increment dV_2 about V_2, given that the wind speed is V_1, at time t. Then

$$p(V_2 \mid V_1) = \frac{1}{\sqrt{2\pi}\,\sigma_c} \; e^{\frac{-(V_2 - \bar{V}_2)^2}{2\sigma_c^2}} \tag{4.14}$$

where

$$\bar{V}_2 = \bar{V} + (V_1 - \bar{V})\,\rho(\tau) \tag{4.15}$$

$$\sigma_c = \sigma\sqrt{1 - \rho^2} \tag{4.16}$$

In (4.15) and (4.16) $\bar{V}$ denotes the unconditional mean wind speed, σ denotes the standard deviation of the unconditional wind speed distribution, and $\rho(\tau)$ denotes the time-lag autocorrelation of wind speed. From the mathematical expression for $P(V_2 \mid V_1)$ we see that it is simply Gaussian with standard deviation σ_c and mean $\bar{V}_2$. Since $\rho(\tau)$ is one for zero lag and zero for infinite lag, σ_c is zero at zero lag and after long times it increases to the standard deviation of the unconditional wind speed distribution. The conditional mean $\bar{V}_2$ is equal to the initial wind speed V_1 at zero lag and approaches the unconditional mean wind speed as the time lag increase. It will be observed that whatever the time lag, the multivariate Gaussian conditional distribution is symmetric about the conditional mean. We shall see that the experimental conditional distributions are noticeably skewed when the initial wind speed is appreciably less than the unconditional mean.

The cumulative distribution is given by

$$p(V_2 < \xi \mid V_1) = \int_{-\infty}^{\xi} p(V_2 \mid V_1)\, dV_2 \tag{4.17}$$

Substituting from (4.14) and employing the definition of the error function, erf(x) we obtain

$$P(V_2 < \xi \mid V_1) = 1/2 + 1/2\ erf\left[\frac{\xi - \bar{V}_2}{\sqrt{2}\ \sigma_c}\right] \qquad (4.18)$$

In order to plot the conditional distribution as a function of time lag in various cases, we need the unconditional mean and standard deviation, and ρ as a function of time lag τ . The autocorrelation of the longitudinal component of the wind velocity has been employed as an approximation to the autocorrelation of the wind speed since the latter were not readily available. The autocorrelation function for Case 096-18m is shown in Figure 4.15. The function is smoothly varying and apparently decorrelates substantially for time lags greater than 100 seconds (the first null or zero crossing is at 120 seconds).

The conditional wind speed distribution for an initial wind speed of 5 m sec^{-1} in Case 096-18m was shown in Figure 4.13. The qualitative trends of the distributions with time lag are as would be expected and as predicted by the mathematical model. As before, the conditional means computed from the experimental data are indicated by circles. It can be observed that the conditional mean is 5 m sec^{-1} for small lag and approaches the unconditional mean of 7.1 m sec^{-1} as lag increases. The experimentally determined distributions for this initial speed, in marked contrast to the theoretical ones, are noticeably skewed, the upper tails being appreciably longer than the lower tails. It is not clear at this time what significance is in this skewness, though it can certainly be stated that the distributions are not multivariate Gaussian to good approximation in the second-order statistics.

It is apparent that the theoretical model not only fails to account properly for the skewed-character and the spreads in the experimental distributions of Figure 4.13 but it also fails to predict the correct conditional mean. The model fits the data much better when the initial wind speed is greater than the unconditional mean wind speed, as shown in Figure 4.14 for the initial speed 9 m sec^{-1}.

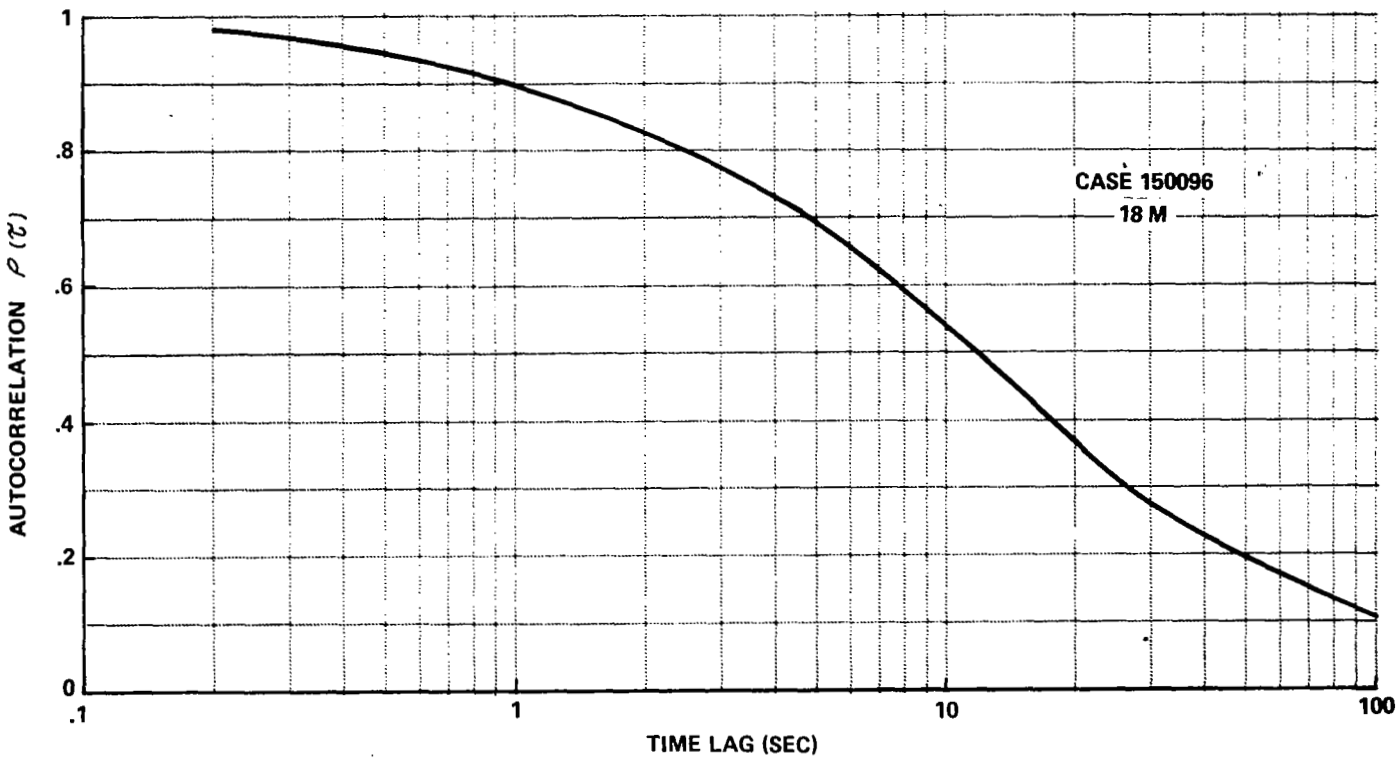

Figure 4.15 AUTOCORRELATION FUNCTION FOR LONGITUDINAL WIND COMPONENT, CASE 096, 18 M HEIGHT

In Figure 4.14 it is observed that the experimental distributions are much more symmetric than they were for the case of Figure 4.13, and the theoretical model fits much better. Indeed, the model should be quite good for this case if the predicted conditional variances are altered to agree with the experimental data. On the basis of the three cases examined it appears that such a modified model will provide reasonably good fits in cases in which the initial wind speed is not less than the unconditional mean.

In order to determine how the model should be modified to provide more realistic spreads (or conditional sigmas) the variation of conditional sigma with autocorrelation ρ was examined. Figure 4.16 shows mean experimental values of the ratio of the conditional sigma to the unconditional sigma, σ_c / σ , versus ρ for a number of cases. The vertical spread bar for each data point encloses over 80% of the experimental points except for $\rho = 0.71$, in which case 67% of the experimental points are enclosed. There did not appear to be any definite overall correlation of σ_c/σ values with either tower level or initial wind speed. The smooth solid curve shows the variation according to the multivariate Gaussian model, which, it may be recalled, is simply $\sigma_c/\sigma = \sqrt{1-\rho^2}$.

It is apparent that the experimental mean values of σ_c/σ differ by almost a factor of 2 from the theoretical ones in the case of ρ close to one. Therefore, the mathematical model may be modified and improved by utilizing the broken curve in Figure 4.16 to determine the value of σ_c/σ to employ in calculations based on the Gaussian conditional wind speed model.

The modified model has been employed in conjunction with the appropriate autocorrelation function to compute the conditional wind speed distributions for initial wind speeds of 8 m sec^{-1}, 9 m sec^{-1}, and 10 m sec^{-1} in Case 067-150m. These distributions are shown in Figures 4.17, 4.18 and 4.19. The numerals in the bodies of the plots were obtained from the experimental data, and the cumulative probability contours were computed from the modified model. Since the mean wind speed is 8.46 m sec^{-1} in Case 067-150m, the distribution means equal the initial wind speeds at zero lag and approach 8.46 m sec^{-1} at long lags.

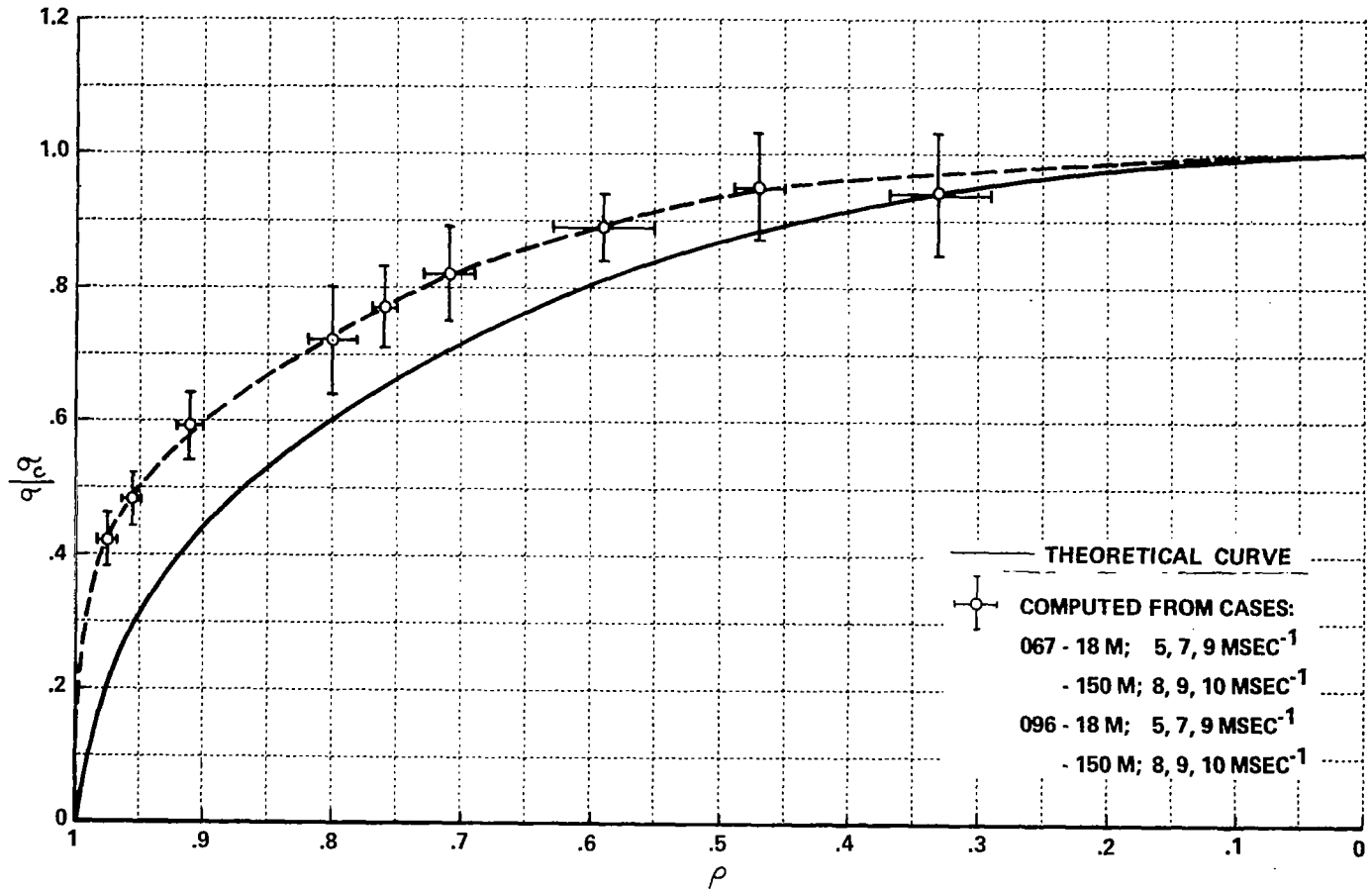

Figure 4.16 RATIO OF CONDITIONAL DISTRIBUTION σ TO UNCONDITIONAL DISTRIBUTION σ AS A FUNCTION OF AUTOCORRELATION. POINTS COMPUTED FROM WIND DATA FOR CASES LISTED, SOLID CURVE FROM MATHEMATICAL MODEL

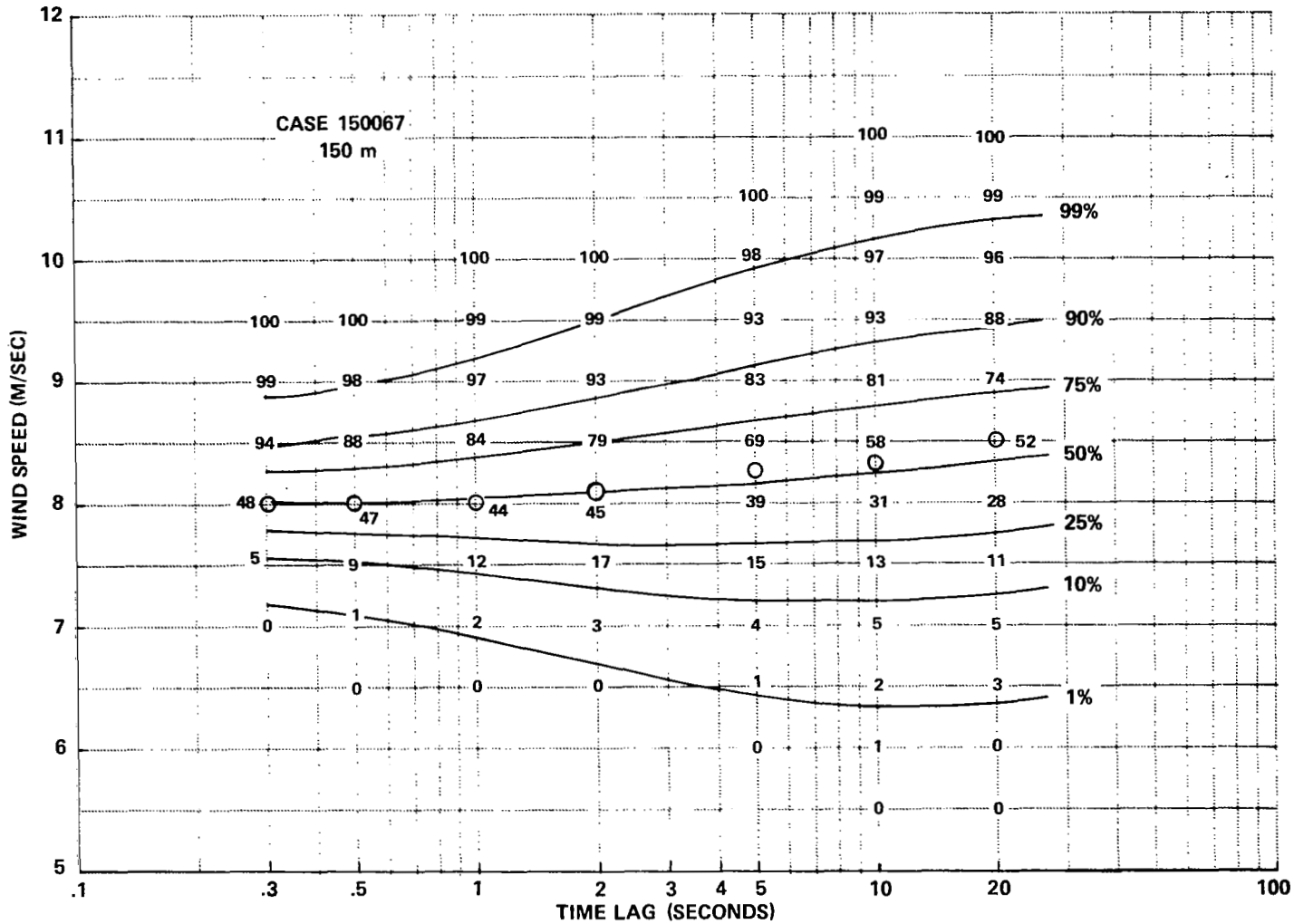

Figure 4.17 CONDITIONAL WIND SPEED DISTRIBUTIONS FOR VARIOUS TIME LAGS, CONDITIONAL ON A SPEED OF 8 M SEC^{-1} AT LAG ZERO. CASE 067, 150 M HEIGHT. NUMBERS ARE FROM WIND MEASUREMENTS, CONTOURS FROM MODIFIED MODEL

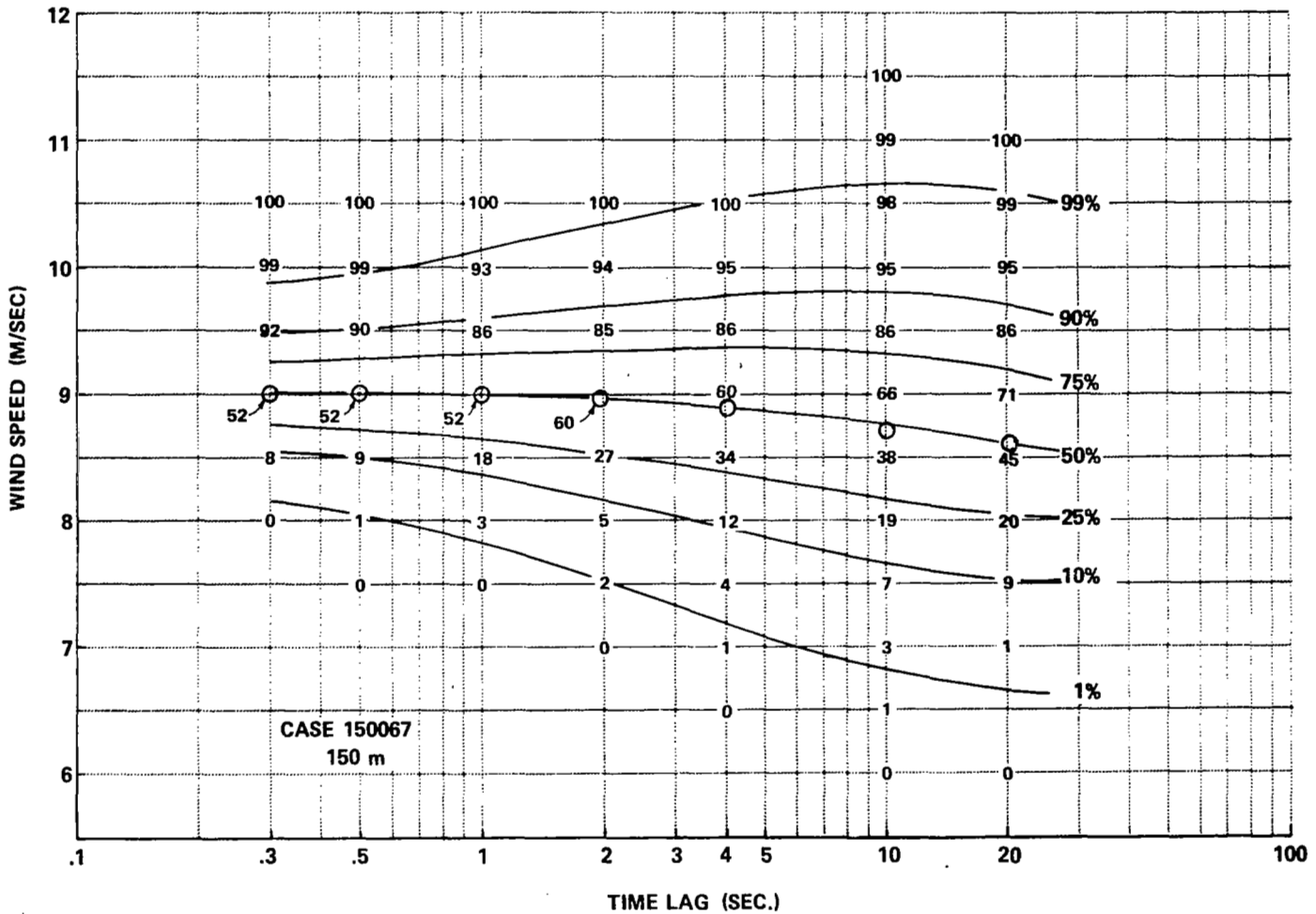

Figure 4.18 CONDITIONAL WIND SPEED DISTRIBUTIONS FOR VARIOUS TIME LAGS, CONDITIONAL ON A SPEED OF 9 M SEC^{-1} AT LAG ZERO. CASE 067, 150 M HEIGHT. NUMBERS ARE FROM WIND MEASUREMENTS, CONTOURS FROM MODIFIED MODEL

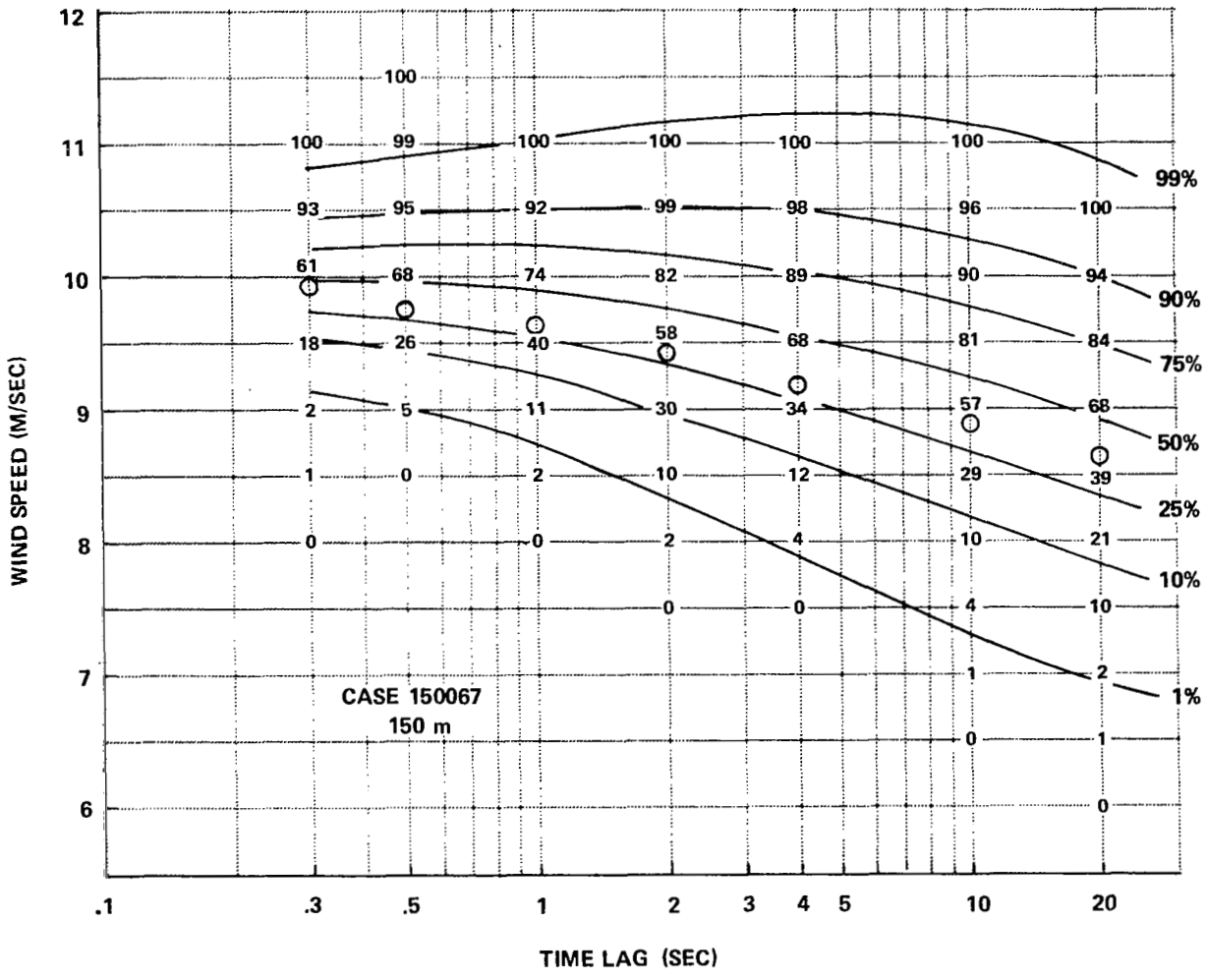

Figure 4.19 CONDITIONAL WIND SPEED DISTRIBUTIONS FOR VARIOUS TIME LAGS, CONDITIONAL ON A SPEED OF 10 M SEC^{-1} AT LAG ZERO. CASE 067, 150 M HEIGHT. NUMBERS ARE FROM WIND MEASUREMENTS, CONTOURS FROM MODIFIED MODEL

Quite clearly, the modified model provides an excellent fit to the data in Figures 4.17 and 4.18. In the case of Figure 4.19 the model fails to provide a correct account of the distribution mean though it does provide the correct variances. Indeed, it is clear from the various figures that the mean computed from the mathematical model is too low (high) when the initial wind speed is less than (greater than) the mean wind speed. It may, therefore, be desirable to empirically modify the mathematical model further so that it provides a correct account of the conditional means. With such modification the model may be employed to estimate the conditional wind speed distributions for any case in which σ, $\overline{V}$ and $\rho(\tau)$ are known.

V. SUMMARY AND CONCLUSIONS

Three aspects of the ground-wind environment at Kennedy Space Center have been investigated. The results of these studies are listed below and the principal conclusions summarized.

A. Statistics on Seasonal and Annual Distributions of Wind

Frequency distributions were compiled from one year of hourly observations for mean wind speed, 10 min peak wind speed, one-hour peak wind speed, gust factor, power-law exponent and friction velocity. By use of conditional frequency distributions, relationships between these wind parameters and wind direction, mean wind speed, and Richardson number were investigated. The relationships between variables have been discussed in the light of current knowledge of atmospheric turbulence structure. Observed features at KSC are found to be consistent with available theory and empirical knowledge; however, some characteristics of the annual statistics are the result of meso and synoptic scale weather characteristics rather than microscale turbulence. The numerical results presented will be useful in estimating the probability of occurrence of mean wind speeds, gust speeds, etc.

B. Spectrum of the Lateral Turbulence Component

The spectrum of the lateral component was studied as a function of height, Richardson number, and wind speed. It is shown that the low-frequency portion of the spectrum ($F = 0.01$ to $F = 0.4$) is highly dependent on stability; energy in this range may be three times as great in moderately unstable conditions as in neutral conditions. The spectrum shape changes relatively little with height. For Richardson numbers near zero, the spectral intensity decreases by approximately one-half at 150m height relative to the values at 18m. For unstable lapse rates, the intensity is nearly the same at all heights from 18 to 150m.

Two model spectra have been presented for Kennedy Space Center, one for neutral stability and one for unstable conditions. To use these models, estimates of mean wind speed and friction velocity only are required. Given these parameters and the spectrum models, the spectrum can be estimated for any height in the ground-wind regime. It has been shown that the spectrum models provide an excellent representation of average lateral spectra observed at KSC.

C. Characteristics of Gusts

Detailed wind records were analyzed to obtain information on the intensity, frequency and duration of gusts.

1. Gust Factor

It has been found that the mean gust factor is approximately proportional to the logarithm of sampling time for times between three and 400 seconds. By taking account of variations in mean wind speed, standard deviation of wind speed, and time scale of the turbulence, a single equation for the proportionality between gust factor and the logarithm of sampling time was derived which fits data from all heights and all cases studied. Similar relationships were obtained for the spread of gust factor distributions as a function of sampling time.

2. Duration of Gusts

A technique was developed for computing and presenting statistical data on the frequency and duration of gusts. For the limited number of cases analyzed, all gust duration distributions were of similar form after scaling for mean wind speed, wind variance, and time scale. It has been shown how the probability of gusts of various durations and speeds can be estimated from the derived frequency distributions.

3. Gust Accelerations

Frequency distributions of wind speed were derived which give the conditional probability of various wind speeds for various times after the wind crosses a given level. These distributions give, in effect, the probability of various average accelerations as a function of initial wind speed and averaging time.

A modified multivariate Gaussian model has been proposed to represent the distributions of gust acceleration. Under a fairly wide range of circumstances the model, as empirically modified, appears to give an excellent description of conditional wind speed distributions.

It is believed that both the statistical data and the empirical models that have been presented should be useful in providing inputs for a wide range of vehicle design and operational problems. It is recommended that additional data be processed and analyzed to confirm, refine, and extend the models, particularly with regard to detailed gust characteristics.

VI. REFERENCES

1. Kaufman, J.W., and L.F. Keene, 1968: NASA's 150-meter Meteorological Tower Located at the Kennedy Space Center, Florida. NASA TM X-53699, Marshall Space Flight Center, Huntsville, Alabama.

2. "Research Achievements Review," Vol. II, No. 10, NASA TM X-53706, Marshall Space Flight Center, Huntsville, Alabama.

3. Fichtl, G.H., 1968: An Analysis of the Roughness Length Associated with the NASA 150-meter Meteorological Tower. NASA TM X-53690, Marshall Space Flight Center, Huntsville, Alabama.

4. Davis, F.K., and H. Newstein, 1968: The variation of gust factors with mean wind speed and with height. J. App. Met., 7, 372-8.

5. Lumley, J.L., and H.A. Panofsky, 1964: The Structure of Atmospheric Turbulence, Interscience Publishers, New York, 239 pgs.

6. McVehil, G.E., 1964: Wind and temperature profiles near the ground in stable stratification. Quart. J. Royal Met. Soc., 90, 136-46.

7. Fichtl, G., 1968: Characteristics of turbulence observed at the NASA 150-m Meteorological Tower. J. App. Met., 7, 838-44.

8. Blackman, R.B., and J.W. Tukey, 1958: The Measurement of Power Spectra. Dover Publications, New York, 190 pgs.

9. Camp, D.W., 1968: Low Level Wind Gust Amplitude and Duration Study. NASA TM X-53771, Marshall Space Flight Center, Huntsville, Alabama.

APPENDIX A*

WIND LOAD CONSIDERATIONS IN LAUNCH VEHICLE DESIGN AND OPERATION

The overriding factor in design and selection of launch vehicles for manned space missions is the "man-rating" of the vehicle. It is well established that wind loads are a primary design input for such vehicles. Ground wind considerations have established certain ground handling requirements. Winds and turbulence above the ground are critical factors in operational considerations. It is impossible to design the Saturn V launch vehicle, for example, so that it can perform its mission with sufficient structural margin to insure integrity under all conceivable combinations of wind velocity, wind shear and turbulence. Hence, a major consideration in the decision to launch is the ambient wind, both near the ground and aloft.

The following discussion is not intended to be an exhaustive survey of the static and dynamic response of launch vehicles to wind loads. Emphasis is on the ground wind environment, with but brief mention of winds aloft. The survey is intended only as an indication of the current state of the art, and includes certain recommendations for additional research needed in this area.

A. Wind Environment Effects

1. Prelaunch and Launch

There are three primary sources of wind loads in the prelaunch and launch regimes - steady drag loads resulting from the mean steady wind,

*This survey was prepared by Mr. W. G. Brady, Applied Mechanics Department, Cornell Aeronautical Laboratory, Inc.

unsteady drag loads, both fore-and-aft and lateral (in terms of the mean steady wind direction) arising from wind gusts and turbulence, and lateral unsteady loads associated with vortex shedding. The principal differences between the prelaunch and launch categories result from changes in boost vehicle mass distribution (empty to fully fueled), physical constraints on the boost vehicle (tied down at the base, attached to the gantry), or operation or nonoperation of the vehicle control system, and, immediately following launch, changes in wind environment as the ground wind boundary layer (atmospheric surface layer) is penetrated.

2. Boost

During boost, vehicle mass properties vary as fuel is burned. Mach number and boundary layer Reynolds number change, and most generally, wind velocities increase with altitude. The wind loads are primarily quasi-steady and unsteady, arising from the quasi-steady (slowly varying) wind and the wind turbulence, respectively; vortex shedding and the associated lateral bending loads do not appear to be a significant factor.

A major source of dynamic loading during boost is transonic buffeting (Reference 1); several boost vehicle failures have been attributed to this cause. However, the primary phenomenon is a separated flow shock interaction, and the modifying effects of cross-flow due to wind (steady or unsteady) are most likely of secondary importance. Hence, no further consideration will be given to transonic buffet in this review.

In summary, the ground wind environment in the atmospheric surface layer results in (1) lateral oscillations of the launch vehicle associated with (steady wind) vortex shedding, (2) quasi-steady drag loading, and (3) unsteady loading arising from wind gusts (turbulence). At altitude, unsteady vortex shedding is no problem, but the remaining two types of wind loadings are correspondingly more critical.

B. Modeling

The launch vehicle designer needs to know the effects of the wind environment on control, stability, structural loads and ground handling requirements. Of the three major ways of establishing design and operational requirements, namely (1) on the basis of past experience, (2) by means of tests with physical models, and (3) by means of mathematical models, we will here be concerned primarily with the third.

It is noted in passing that, currently, the only practical approach to obtaining dynamic loads data on the response of launch vehicles (or any tall structure) to vortex shedding in a steady wind is by means of wind-tunnel model tests, or by semi-empirical analytical approaches based on experimental tests.

1. Mathematical Models for Dynamic Analysis

The two principal elements of a mathematical model to treat the dynamic response of a structure are the representations of the structure and of the time-dependent loading involved. The specific forms assumed for these two elements depend on the type and complexity of the structure, the complexity of the loading, the types of computing facilities available, and the specific information desired.

The launch vehicles under consideration are long, relatively slender bodies. Most have a degree of axial symmetry structurally, although TITAN III is an exception. The most obvious approach is to treat the vehicle as a nonuniform beam, or as an assemblage of nonuniform beams. For a flexible beamlike structure such as a typical launch vehicle, the most obvious generalized coordinates to use in setting up equations of motion for dynamic analyses are the normalized beam-bending modes. That is, the time-dependent fore-and-aft deformation, y(x, t), is written

$$y(x, t) = \sum_{n=1} f_n(x) q_n(t) \qquad (1)$$

where $f_n(x)$ is the nth bending modal deflection normalized to unity at some convenient reference station, and $q_n(t)$ is the generalized coordinate in the nth mode, a function of time only, and is the displacement in the nth mode at the reference station.

The use of beam normal-mode generalized coordinates and the assumptions of "small" deflections lead to the equations of motion for these modes in the form

$$\ddot{q}_n(t) + \omega_n^2 \; q_n(t) = \frac{1}{M_{nn}} \; Q_n \qquad (2)$$

for n = 1, 2, 3, ..., where ω_n is the nth mode natural frequency, M_{nn} is the generalized mass in the nth mode, and Q_n is the generalized force in the nth mode, generally a function of all mode - generalized coordinates, including control and rigid body modes for example.

If true zero air speed normal modes are used, there is no mass coupling.

The determination of the mode shapes $f_n(x)$ and the corresponding frequencies can be made by one of a number of standard techniques; Reference 2 is typical.

2. Treatment of Aerodynamic Forces

Consider first of all the ground wind environment. Even for a rigidly fixed launch vehicle, the ground winds result in an unsteady pressure distribution acting on the vehicle. The interaction of the wind and the vehicle is an extremely complicated process in which the aerodynamic boundary layer plays a crucial part. The launch vehicle is a bluff body, and the flow of air around the vehicle separates from the surface. The location of these separations on the vehicle depends on the Reynolds number, the Mach number (for flight conditions), the roughness of the vehicle skin, and the wind turbulence (scale and frequency), among other things.

For a launch vehicle on the launch pad, the simplest assumption to make as regards the wind-induced aerodynamic force is that this force is a

pure drag acting on the vehicle in the direction of the relative wind. It is normally assumed that this drag is proportional to the product of a drag coefficient and the square of the local wind velocity, i.e.,

$$\text{Drag} \sim C_D \left[V(x,t)\right]^2 \tag{3}$$

where C_D, the drag coefficient, is the two-dimensional drag coefficient for steady flow about a two-dimensional cylinder of the same diameter as the local diameter of the launch vehicle at height x, and V is the wind velocity. A refinement would be to determine experimentally the variation of drag coefficient along the height of the launch vehicle in a uniform steady cross-flow or in a vertically sheared cross-flow by means of wind-tunnel tests, and use this distribution, $C_D(x)$, in analyses. This approach can be used to account for local Reynolds number variation as well as vehicle skin roughness.

The use of such a drag coefficient is straightforward, and, if derived from properly scaled wind tunnel tests, should permit reasonably accurate representation of steady aerodynamic loads. Extension of Equation (3) to the unsteady drag loading due both to the unsteady wind (turbulence) and motion of the vehicle is straightforward (see Reference 3, for example). However, it is not at all clear that this representation of the unsteady drag loading is, in fact, a reasonably accurate representation of the actual physical process.

Extension to the boost phase further complicates consideration of the unsteady aerodynamics. Again, the straightforward (and most often used) approach is a direct application of Equation (3) to the launch vehicle cross-flow. There have been many attempts to develop more refined analytical models of the mean steady flow around slender bodies (Reference 4 discusses some of these) to account for separation effects which persist into the supersonic regime. As yet, even these attempts at steady flow theory have not been particularly successful, although a basic understanding of the flow mechanisms is evolving.

The most obvious source of steady aerodynamic data for launch vehicles would be from wind tunnel tests. Empirical methods for applying

such steady test data to configurations other than those tested are available (Reference 5). An obvious extension of these static data is to use them in dynamic analyses on the basis of an assumption that the unsteady flow is quasi-steady and linear. The accuracy of this approach requires validation on the basis of a comparison of analytical results with experimental results.

Reference 6 is an analytical study of the dynamic response of the Saturn C-5 vehicle, including structural modes, rigid-body modes, and control-system dynamics, during the boost phase after the first 30 seconds of flight. Unsteady linear slender-body aerodynamic theory was used to develop the generalized aerodynamic forces. The results of the study showed that, on the basis of assumed wind profile inputs and linear slender-body theory, aerodynamic time lags and wind profile penetration time lags were relatively unimportant. However, the slender-body theory employed in Reference 6 does not account for separation effects which undoubtedly are of importance. The extent to which the above conclusions apply to physical reality is not apparent at this time.

It is evident that the unsteady aerodynamics of slender configurations is a critical component in both experimental modeling and analytical treatments of the response of slender flexible structures to turbulence. Once freed of ground-support structure and any damping external to the boost vehicle which may be provided via attached ground-support structure, the only system damping (other than that which may be provided through the control system) is the structural damping inherent to the boost vehicle, usually very small, and the aerodynamic damping. Hence, both in terms of the input aerodynamic loads (forcing function), and the response, it would appear that much more information on unsteady slender-body aerodynamics is required than is evidenced by available literature. This is not to infer that studies such as those reported in Reference 6 are not useful, and is stated in full recognition of the extremely difficult problems involved in treating separated flows analytically whether steady or unsteady. It is obvious that awareness of the limitations of analytical and experimental tools is an important element of the design process.

3. Types of Dynamic Analyses

Given a representation of the structure, and aerodynamic approximations such that a specific analytical form for Q_n, the generalized force in the nth mode (Equation (2)), and the aerodynamic damping and stiffness (if any) can be written down, then the required ingredients for dynamic analyses are in hand. The type of analysis performed depends, to a large extent, on the number of degrees of freedom involved, whether the control system is to be considered in whole, in part, or not at all, the coupling between degrees of freedom, the type of computer facilities available (digital or analog), whether the analytic system is linear or not, and the type of information desired. However, the nature of the input loading (wind with many random variables involved) suggests that some form of statistical approach is needed.

If statistical information as to the dynamic response is desired, it would be possible to run computer solutions for a whole series of wind profile samples as they vary with time, as was done in Reference 7. If enough runs are made, a large enough sample of the response in terms of, say, the displacement amplitudes, bending moment distributions or stress distributions, may be available on which to perform statistical analyses. Another approach if the equations of motion are linear, is to use the technique of generalized harmonic analysis.

A detailed discussion of generalized harmonic analysis techniques is beyond the scope of this survey. Reference 8 derives general equations applicable to the response of linear systems to random excitation which is Gaussian, stationary in time, but inhomogeneous in space. No specific calculations are reported on; however, Reference 9 presents developments directly in terms of the ground wind-launch vehicle response problem. In order to apply the techniques of generalized harmonic analysis, frequency response functions for the (linear) dynamic system, and power spectra (including, in general, cross-spectra) of the input random disturbances are required. The importance of the Gaussian random process is, of course, that output power spectral density completely specifies the statistics of the process. In view of the complications which arise in treating non-Gaussian random processes, it is a natural tendency for the analytical dynamicist to take recourse in the Central Limit Theorem and assume the process Gaussian.

a. Prelaunch Phase

The principal wind-related problems associated with the erected boost vehicle prior to launch (other than dynamic structural loads from "steady wind" vortex shedding) are dynamic drag loads due to wind turbulence superimposed on the static wind drag loading. Considerations of structural fatigue are required in addition to the structural integrity of the boost vehicle.

The structural configuration is that of the vehicle (assumed to be a slender beam) usually with structural constraints (tie downs) at the base and at intervals up the vehicle (viscous dampers to suppress vortex shedding response, for example). The vehicle control system is inoperative.

Reference 9 presents the results of calculations for the Saturn V fundamental bending mode based on single-mode-frequency response functions and on longitudinal and lateral wind gusts (turbulence), both fully correlated over the length of the launch vehicle (one-dimensional), and on theoretical cross-spectra derived from considerations including turbulence assumed frozen in the mean wind, and local homogeneity and isotropy (two-dimensional). Significant differences in response are shown between the one-dimensional and two-dimensional results.

It would appear that this approach (generalized harmonic analysis) is by far the most effective analysis technique for the ground wind response. The dynamic system is relatively simple (as compared to the boost phase) with no rigid-body degrees of freedom, or control system constraints. The only coupling which may be a problem, if normal structural modes are used as generalized coordinates (which modes must include the effects of ground tie-downs and other constraints exterior to the vehicle, such as dampers), would be aerodynamic damping coupling terms (not considered in the above-noted results of Reference 9).

b. Launch and Boost Phase

In this case, the dynamic system is far more complicated than for the prelaunch phase. Rigid-body degrees of freedom must be included, as well as control system constraints and coupling. The mass distribution

is time varying, and fuel sloshing becomes more and more significant as the fuel mass decreases, and fuel sloshing mode frequencies increase to values closer to the lowest bending mode frequencies. The equations of motion can be linearized to a reasonable degree of accuracy by perturbing from the nominal trajectory. The aerodynamics are now a function of Mach number, and the flow regime covers the complete range from non-incompressible to hypersonic.

Analytic studies reported in Reference 7 indicate the critical importance of the response to wind turbulence during the boost phase. It is noted that, under certain conditions, up to 30% of the critical stress loading near maximum dynamic pressure conditions can result from the wind turbulence loading. Reference 7 is also indicative of the nature of the design problem for the boost phase.

c. Operational Considerations

The results of the Reference 7 studies showed that magnitude of wind velocity and shear alone are not indicative of the severity of a wind environment in terms of launch vehicle structural loads. It was recommended that a continual monitoring of the winds-aloft environment prior to launch is required in order that rational decisions as to launch safety can be made. This monitoring presumably involves obtaining series of wind profiles prior to scheduled launch which are then used in computer simulation to determine whether safe loading limits are likely to be exceeded.

Analog computer simulation would be most desirable in such monitoring studies. It is fast, compared to digital simulation and its forte is accurate integration. However, function generator capability usually available to analog computer facilities is relatively limited. The flexibility and speed of integration of the analog computer and the computational virtuosity of the digital computer can sometimes be combined via hybrid computer techniques to provide a near-optimum computing capability.

C. Discussion

Certain aspects of the wind turbulence dynamic response problem of launch vehicles such as the Saturn V have been considered, with emphasis on analytical techniques. As far as dynamic analysis tools are concerned, the following observations are made.

1. Structural representation techniques are relatively well understood and reasonably well advanced insofar as the launch vehicle aeroelastic response problem is concerned. At worst, as structural complexity increases, (à la the Saturn I fuel and lox tank cluster, Reference 2) the necessary analytical techniques become relatively more involved and costly. Fuel sloshing simulation techniques also appear to be relatively well in hand.

2. Not all aspects of the unsteady aerodynamics of launch vehicles are very well understood. Questions exist particularly for the boost phase. At present, the use of simple cross-flow drag coefficients seems to be as good as any for pre-launch and launch phases. It would appear that there is a long road ahead insofar as research is required to improve this situation. The problem is complicated by the difficulties in obtaining experimental data to provide guidelines for analytical research, and to provide data to validate analyses. Note that inaccuracies in the aerodynamic simulation are reflected in the results, whatever the type of analytical solution, deterministic (integrate equations of motion for specific time-varying wind profile) or statistical (generalized harmonic analysis).

3. As an analytical design tool for studying response to wind turbulence, particularly in the ground wind environment, generalized harmonic analysis is extremely useful. Inevitably, approximations and assumptions must be made, particularly as to the statistics of the input, in order that results be obtained in reasonable fashion. The indications in the literature are that there is a dearth of information as to the validity of the various approximations. (Reference 7 and 10 are exceptions.) It is believed that considerably more research, such as that represented by the present report, is called for.

4. Finally, it is felt that serious consideration should be given to the potential of the hybrid computer as applied to complicated aeroelastic problems involving many degrees of freedom and random variable inputs.

As a final note, it is suggested in Reference 9 that wind-tunnel tests of dynamically scaled models in turbulent flows are not feasible as yet because of the marked differences in frequency characteristics of atmospheric and wind-tunnel turbulence. It is possible (Reference 11) that within a relatively short time period, more accurate simulation of ground wind turbulence in specially designed atmospheric wind tunnels will be a reality. The biggest limitation in evidence, currently, is a restriction as to model size. This size problem may make accurate scaling of the ground wind aeroelastic problem rather difficult. However, in terms of research application to ground wind dynamic response problems, the potential of such atmospheric wind tunnels is high.

REFERENCES

1. Rainey, A. Gerald, "Progress on the Launch Vehicle Buffeting Problem" Journal of Spacecraft and Rockets, Volume 2, Number 3, May-June 1965.

2. Loewy, Robert G. and Mukund, M. Joglekar, Matrix Holzer Analyses for Fully-Coupled Vibrations of Clustered Launch-Vehicle Configurations Including Applications to the Titan IIIC and Uncoupled Saturn I Cases, NASA CR-592, December 1966.

3. Etkin, Bernard, "Theory of the Response of a Slender Vertical Structure to a Turbulent Wind with Shear," presented at the Meeting on Ground Wind Load Problems in Relation to Launch Vehicles, NASA Langley Research Center, June 7-8, 1966.

4. Schindel, Leon H. and Chamberlain, Thomas E., Vortex Separation on Slender Bodies of Elliptic Cross Section, Technical Report 138, Massachusetts Institute of Technology Aerophysics Laboratory, August 1967.

5. Muraca, Ralph J., An Empirical Method for Determining Static Distributed Loads on Axisymmetric Multistage Launch Vehicles, NASA TN D-3283, March 1966.

6. Blackburn, Robert R. and A. D. St. John, Effects and Importance of Penetration and Growth of Lift on Space Vehicle Response, NASA CR-326, November 1965.

7. Ryan, Robert S., and Alberta W. King, "The Influential Aspects of Atmospheric Disturbances on Space Vehicle Design Using Statistical Approaches for Analysis, NASA Technical Memorandum X-53565, January 13, 1967.

8. Botman, M., The Response of Linear Systems to Inhomogeneous Random Excitation, IAS Paper No. 61-32, IAS 29th Annual Meeting New York, New York, January 23-25, 1961.

9. Reed, Wilmer H., III, Models for Obtaining Effects of Ground Winds in Space Vehicles Erected on the Launch Pad, Presented at the Conférence on the Role of Simulation in Space Technology, Virginia Polytechnic Institute, Blacksburg, Virginia, August 17-21, 1964.

10. Campbell, A. C., and B. Etkin, The Response of a Cylindrical Structure to a Turbulent Flow Field at Subcritical Reynolds Number, UTIAS, Technical Note No. 115, Institute for Aerospace Studies, University of Toronto, Toronto, Canada, July 1967.

11. McVehil, G. E., G. R. Ludwig, T. R. Sundaram, "On the Feasibility of Modeling Small Scale Atmospheric Motions," CAL Report No. ZB-2328-P-1, Cornell Aeronautical Laboratory, Inc., Buffalo, N. Y., April 22, 1967.